2010-03

Dynamic fluidic nozzles for pulse detonation engine applications

McClure, James R. III

Monterey, California. Naval Postgraduate School

NAVAL POSTGRADUATE SCHOOL

MONTEREY, CALIFORNIA

THESIS

DYNAMIC FLUIDIC NOZZLES FOR PULSE DETONATION ENGINE APPLICATIONS

by

James R. McClure III

March 2010

Thesis Advisor:	Christopher M. Brophy
Second Reader:	Garth V. Hobson

Approved for public release; distribution is unlimited

THIS PAGE INTENTIONALLY LEFT BLANK

REPORT DOCUMENTATION PAGE			Form Approved OMB No. 0704-0188
Public reporting burden for this collection of information is estimated to average 1 hour per response, including the time for reviewing instruction, searching existing data sources, gathering and maintaining the data needed, and completing and reviewing the collection of information. Send comments regarding this burden estimate or any other aspect of this collection of information, including suggestions for reducing this burden, to Washington headquarters Services, Directorate for Information Operations and Reports, 1215 Jefferson Davis Highway, Suite 1204, Arlington, VA 22202-4302, and to the Office of Management and Budget, Paperwork Reduction Project (0704-0188) Washington DC 20503.			
1. AGENCY USE ONLY ***(Leave blank)***	**2. REPORT DATE** March 2010	**3. REPORT TYPE AND DATES COVERED** Master's Thesis	
4. TITLE AND SUBTITLE Dynamic Fluidic Nozzles for Pulse Detonation Engine Applications		**5. FUNDING NUMBERS** **N0001409WR20022**	
6. AUTHOR(S) James R. McClure III			
7. PERFORMING ORGANIZATION NAME(S) AND ADDRESS(ES) Naval Postgraduate School Monterey, CA 93943-5000		**8. PERFORMING ORGANIZATION REPORT NUMBER**	
9. SPONSORING /MONITORING AGENCY NAME(S) AND ADDRESS(ES) Office of Naval Research (ONR) Code 33 Ballstone Tower One 800 N. Quincy St Arlington, VA 22203-1995		**10. SPONSORING/MONITORING AGENCY REPORT NUMBER**	
11. SUPPLEMENTARY NOTES The views expressed in this thesis are those of the author and do not reflect the official policy or position of the Department of Defense or the U.S. Government. IRB Protocol number _____.			
12a. DISTRIBUTION / AVAILABILITY STATEMENT Approved for public release; distribution is unlimited		**12b. DISTRIBUTION CODE**	

13. ABSTRACT (maximum 200 words)

An efficient nozzle design is critical for enhancing the benefits of Pulse Detonation Engines (PDEs) and enabling their use as future propulsion or power generation systems. Due to the inherent variation in chamber pressure for Pulse Detonation Combustors, it has been difficult to design a nozzle, which has the capability to provide an appropriate exit-to-throat area ratio suited for both the detonation blow-down event and refresh pressures associated with the cyclic operation of a PDE. A two-dimensional PDE exit nozzle was designed, modeled, and constructed in an attempt to increase the overall efficiency of converting thermal energy to kinetic energy by providing a fluidic method to dynamically vary the effective nozzle area ratio. A fluidic nozzle configuration was evaluated, which had the ability to inject a small amount of air into the diverging section of the nozzle in order to dynamically create a more desirable exit-to-throat area ratio. Experimental testing was conducted on various injection flow rates, and a shadowgraph system was used to observe the fluid flow characteristics within the nozzle. Computer simulations were used to analyze the fluid flow properties within the nozzle. A comparison of the computer simulations and the experimental results was performed and demonstrated good agreement.

14. SUBJECT TERMS Pulse Detonation Engines, PDE, Dynamic Fluidic Nozzles, Nozzles, Dynamic, Fluidic, Schlieren			**15. NUMBER OF PAGES** 189
			16. PRICE CODE
17. SECURITY CLASSIFICATION OF REPORT Unclassified	**18. SECURITY CLASSIFICATION OF THIS PAGE** Unclassified	**19. SECURITY CLASSIFICATION OF ABSTRACT** Unclassified	**20. LIMITATION OF ABSTRACT** UU

NSN 7540-01-280-5500 Standard Form 298 (Rev. 2-89)
Prescribed by ANSI Std. 239-18

THIS PAGE INTENTIONALLY LEFT BLANK

Approved for public release; distribution is unlimited.

DYNAMIC FLUIDIC NOZZLES FOR PULSE DETONATION ENGINE APPLICATIONS

James R. McClure III
Lieutenant, United States Navy
B.S., Auburn University, 2003

Submitted in partial fulfillment of the
requirements for the degree of

MASTER OF SCIENCE IN MECHANICAL ENGINEERING

from the

NAVAL POSTGRADUATE SCHOOL
March 2010

Author: James R. McClure III

Approved by: Christopher M. Brophy
Thesis Advisor

Garth V. Hobson
Second Reader

Knox T. Millsaps
Chairman, Department of Mechanical and Aerospace Engineering

THIS PAGE INTENTIONALLY LEFT BLANK

ABSTRACT

An efficient nozzle design is critical for enhancing the benefits of Pulse Detonation Engines (PDEs) and enabling their use as future propulsion or power generation systems. Due to the inherent variation in chamber pressure for Pulse Detonation Combustors, it has been difficult to design a nozzle that has the capability to provide an appropriate exit-to-throat area ratio suited for both the detonation blow-down event and refresh pressures associated with the cyclic operation of a PDE. A two-dimensional PDE exit nozzle was designed, modeled, and constructed in an attempt to increase the overall efficiency of converting thermal energy to kinetic energy by providing a fluidic method to dynamically vary the effective nozzle area ratio. A fluidic nozzle configuration was evaluated, which had the ability to inject a small amount of air into the diverging section of the nozzle in order to dynamically create a more desirable exit-to-throat area ratio. Experimental testing was conducted on various injection flow rates, and a shadowgraph system was used to observe the fluid flow characteristics within the nozzle. Computer simulations were used to analyze the fluid flow properties within the nozzle. A comparison of the computer simulations and the experimental results was performed and demonstrated good agreement.

THIS PAGE INTENTIONALLY LEFT BLANK

TABLE OF CONTENTS

THIS PAGE INTENTIONALLY LEFT BLANK

LIST OF FIGURES

LIST OF TABLES

THIS PAGE INTENTIONALLY LEFT BLANK

LIST OF ACRONYMS, ABBREVIATIONS AND SYMBOLS

CEA	Chemical Equilibrium with Applications	
CFD	Computational Fluid Dynamic	
CJ	Chapman-Jouget	
DDT	Deflagration-to-Detonation Transition	
GUI	Graphical User Interface	
NASA	National Aeronautics and Space Administration	
NDF	Nozzle Deviation Factor	
NI	National Instruments	
PDE	Pulse Detonation Engine	
A_1	PDE chamber area	[m^2]
A_2	Nozzle exit area	[m^2]
A_t	Nozzle throat area	[m^2]
c	Speed of sound	[$m \cdot s^{-1}$]
C_F	Thrust coefficient	
ε	Nozzle area expansion ratio	
F	Thrust	[N]
g	Acceleration of gravity	[$m \cdot s^{-2}$]
I_c	Specific impulse of combustion chamber	[s^{-1}]
I_n	Specific impulse of nozzle	[s^{-1}]
I_s	Specific impulse	[s^{-1}]
k	Specific heat ratio	
L	Length	[m]

M	Mach number	
$\dot{m}$	Mass flow rate	[kg·s^{-1}]
Π	Shock factor	
p_1	PDE chamber pressure	[Pa]
p_2	Nozzle exit pressure	[Pa]
p_3	Atmospheric pressure	[Pa]
p_t	Nozzle throat pressure	[Pa]
t	Time	[s]
T_1	PDE chamber temperature	[K]
T_2	Nozzle exit temperature	[K]
τ	Non-dimensional time	
u_1	PDE chamber velocity	[m·s^{-1}]
u_2	Nozzle exit velocity	[m·s^{-1}]
u_t	Nozzle throat velocity	[m·s^{-1}]
V	Volume	[m^3]

ACKNOWLEDGMENTS

I would like to thank Professor Chris Brophy for his guidance and oversight throughout this challenging yet fulfilling process. Without his patience and wealth of knowledge, this work would not have been possible.

I would also like to thank Mr. Dave Dausen and Mr. George Hageman for their assistance, support, and friendship. Their understanding and selfless willingness to provide support were crucial in keeping the final goal insight.

Finally, I would like to thank my best friend and wife, Rebecca, and my four wonderful daughters, Kiley, Kinsey, Kennedy, and Kelsey, for their support and understanding throughout this milestone of my life. They are my life, and I would not be the person I am today without them.

THIS PAGE INTENTIONALLY LEFT BLANK

I. INTRODUCTION

There are many propulsion technologies currently available for various mission needs that include turbojet/turbofans, ramjets, and rockets. These technologies have reached a maturity level where future development will not likely produce significant gains in thermodynamic efficiency and performance. All of the current propulsion technologies have an associated range of flight Mach number where their performance is optimal. Figure 1 shows various propulsion concepts and how their specific impulse varies over a range of flight Mach numbers.

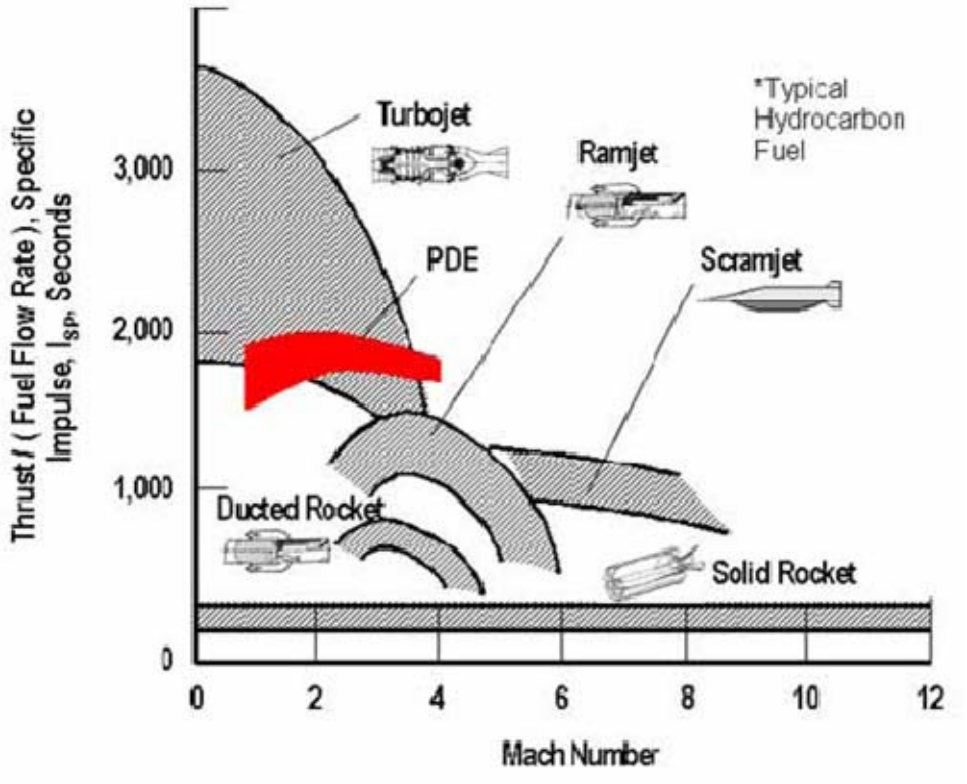

Figure 1. Comparison of High-speed Propulsion Technologies (From [1])

The primary advantage offered by pulse detonation engines (PDEs) is the high thermal efficiency due to the nearly constant-volume combustion process. The specific impulses of PDEs have been theorized to be greater than most supersonic air-breathing

engines currently in use with the exception of advanced turbofan/turbojet engines, which are extremely complex requiring hundreds of moving parts resulting in higher production and construction costs.

Figure 1 reveals that turbojet engines exhibit superior performance at Mach numbers below Mach 3. Above this value the technical challenges of the required advanced materials needed for these turbines increases dramatically and the thermodynamic advantages of these propulsion systems diminishes rapidly. Above Mach 2, ramjet engines approach the performance level of turbojet engines, but these engines do not have the ability to operate at low Mach numbers since the inlet air is compressed by a diffuser, and a booster is required to attain the initial flight speed necessary for engine start. As the flight Mach number increases past Mach 5, scramjets become the preferred air breathing system.

Detonation-based propulsion systems, such as PDEs, have the capability of operating from the high subsonic region through high flight Mach numbers. The PDE combines high thermodynamic performance, efficiency, and relative simplicity, thus making it a viable mode of propulsion for supersonic tactical missile applications. Other concepts incorporating detonation-based propulsion are hybrid PDE-gas turbine systems and a combined-cycle PDE for single stage to orbit launch vehicles.

In order to improve the delivered performance benefits of detonation-based propulsion, a nozzle that is designed to perform efficiently during both the detonation and blow-down portions of the PDE cycle is critical. Due to the vastly differing pressures associated with each of these portions of the PDE cycle, a fixed nozzle cannot be designed to operate efficiently at both associated pressures. This research examines the possibility of using air injection to dynamically vary the effective exit-to-throat area ratio at the lower pressure associated with the blow-down portion of the PDE cycle, thereby increasing both nozzle and PDE efficiency. A proposed source of the injection air would come from the normally unused air taken from the inlet bleed system to minimize boundary layer effects at the entrance of the inlet.

II. BACKGROUND

A. BASIC PULSE DETONATION ENGINE OPERATION

A PDE operates in a cycle consisting of four distinct phases commonly referred to as the fill, detonation, blow-down, and purge phases. Figure 2 shows the basic PDE cycle and helps to visualize what is occurring during each of the phases. Steps one and two represent the fill phase, step three represents ignition, the detonation phase is shown in steps four and five, step six represents the blow-down phase, and step seven represents the purge phase. This cycle repeats at a frequency generally between 60 and 100 Hz with higher frequencies more desirable as long as flow losses are not excessive.

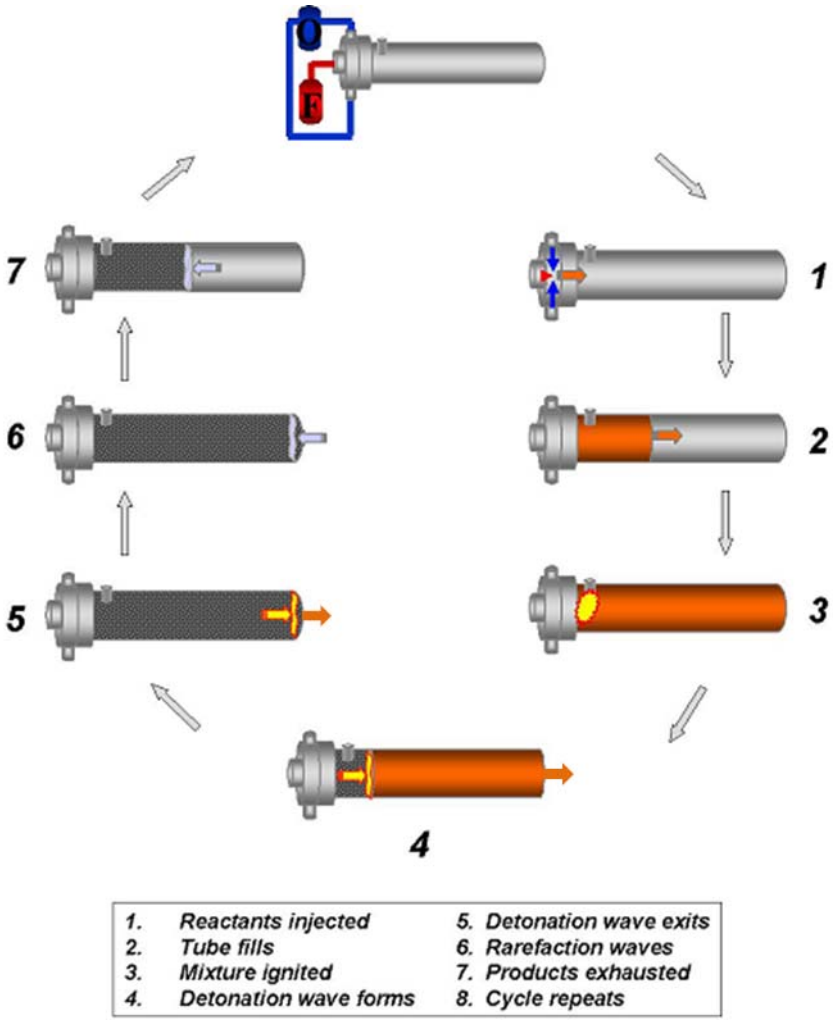

Figure 2. Simplified Ideal PDE Operation Cycle (From [2])

During the fill phase, the combustor is filled with the fuel/oxidizer mixture. The mixture is then ignited at the closed, upstream end of the combustor, and the resulting flame travels for some distance before experiencing a deflagration-to-detonation transition (DDT). The resulting Chapman-Jouget (CJ) detonation wave then travels down the tube and exits into the atmosphere. The resulting high pressure and high temperature combustion products are then expelled out of the tube resulting in thrust generation.

The remaining exhaust gases are now at lower pressure but are still at relatively high temperature. It is now necessary to insert a slug of purge gas (typically air) into the combustor to prevent the next cycle's fuel/oxidizer mixture from pre-igniting due to the exhaust gas high temperature during the purge phase. Once the purge phase is complete, the cycle repeats beginning with the fill phase once again.

Adding a nozzle to a PDE is beneficial for two primary reasons. The first reason is to provide sufficient back pressure during the fill phase to ensure the fuel/oxidizer mixture remains at a favorable pressure for a sufficient length of time in the combustor for detonation to occur. This is especially important when the system would be operating at high altitudes. The second is to allow a means for converting the high enthalpy combustion products created during the detonation event to high exit velocities, which is the driving mechanism for thrust.

As the pressure and temperature increase in the combustor due to the detonation event, the combustion products are forced through the nozzle. The products are first forced through the converging section of the nozzle where the area is decreasing resulting in an increase in velocity and a decrease in pressure. A choked condition is then experienced at the throat of the nozzle where the velocity of the reactants undergoes a change from subsonic to supersonic flow. The products then pass through the diverging section of the nozzle where area is increasing, and this results in a further increases of velocity as the static pressure continues to decreases back to ambient pressure at the nozzle exit. Kinetic energy therefore increases throughout the nozzle as the velocity of the products increase throughout the nozzle.

B. NOZZLES

Nozzles are well known to expand the exhaust flow in steady devices resulting in higher velocity and momentum flux, thus, substantially increasing the thrust. The PDE application of an effective nozzle faces the same problem as other propulsion technologies concerning the exhaust pressure ratio of the nozzle. While most air breathing propulsion technologies face the problem of varying atmospheric pressures when flight altitude is changed, the PDE also experiences this phenomenon but with a widely varying chamber pressure as well. This varying chamber pressure is due to the cyclic nature of the pulse detonation devices. Extremely high pressures are experienced during the detonation phase, while much lower pressures are experience during the blow-down phase of the cycle making it very difficult to design a fixed area ratio nozzle that operates efficiently at both extremes.

There have been advances in nozzle design in the past to correct for pressure changes associated with changes in flight altitude. Some of these designs include the aerospike, plug nozzle, and expansion-deflection nozzle to list a few. These designs offer increased efficiency for altitude compensation, but the chamber pressure within a PDE changes on the order of microseconds rather than seconds normally associated with altitude change. Another consideration is that the changes in pressure occur between 80 and 100 times per second instead of gradually over the entire flight of a tactical missile.

1. Nozzle Configuration

This thesis focused on a convergent-divergent nozzle with a bell shaped divergent section, which is often referred to as a De Laval nozzle after its inventor. Figure 3 shows the basic geometry and nomenclature associated with nozzle analysis.

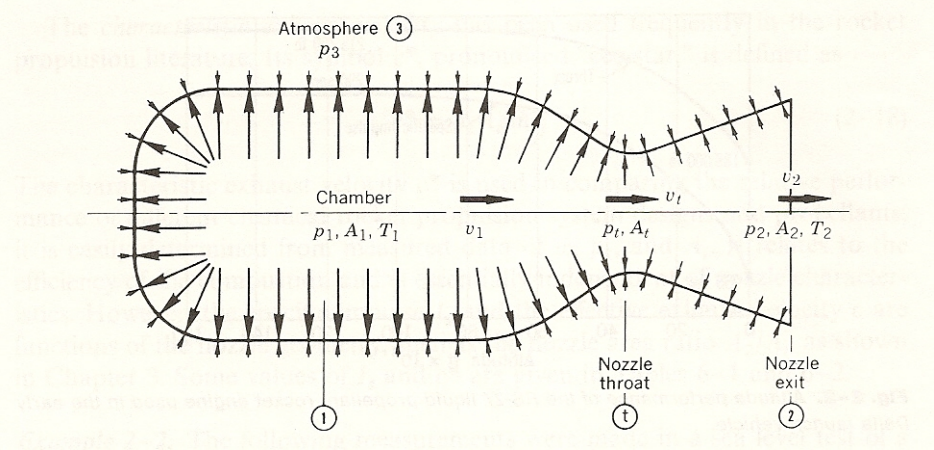

Figure 3. General Nozzle Configuration and Abbreviations (From [5])

Subscripts of 1, t, 2, and 3 refer to conditions existed at the combustion chamber, nozzle throat, nozzle exit, and atmosphere respectively. The minimum nozzle area is called the throat area, and the nozzle area expansion ratio (ε) refers to ratio of the nozzle exit area (A_2) to the nozzle throat area (A_t).

$$\varepsilon = A_2 / A_t \qquad (1)$$

2. Thrust and Expansion

The thrust (F) on the structure is caused by the action of the pressure of the combustion gases against the rocket chamber, injector, and nozzle surfaces. Through a control volume analysis, it can also be shown that the thrust of a steady-state device can also be related to the net momentum and pressure forces across boundaries. Equation 2 shows how thrust can be calculated for steady-state devices.

$$F = u_2 \dot{m} + (p_2 - p_3) A_2 \qquad (2)$$

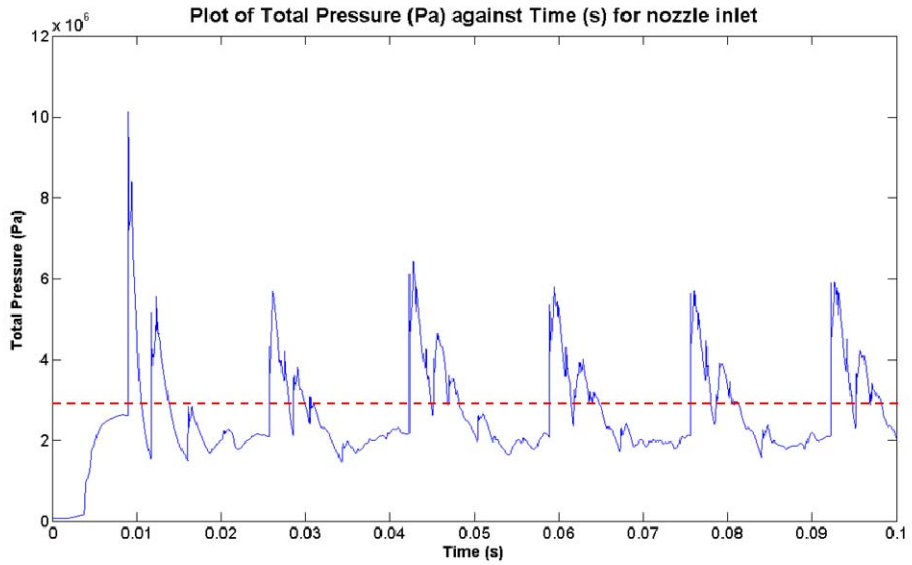

Figure 4. PDE Chamber Pressure versus Time for Hydrogen/Air Reaction at 60 Hz (From [3])

A PDE is far from a steady-state device as can be seen in Figure 4 and concluded from the previous section discussing the basic PDE operation. Due to this dynamic change in pressure, fixed nozzles for PDE applications have previously been designed for optimal operation about an average chamber pressure as represented by the dashed, red line of Figure 4. The utilization of an average chamber pressure was an attempt to simply the very complex problem associated with PDE nozzle applications.

The thrust calculation is much more complex than shown in Equation 2 above due to this greatly varying chamber pressure with respect to time. Because the thrust varies with time, it is more appropriate to discuss the specific impulse rather than the thrust of a PDE. The specific impulse is the total impulse per unit weight of the propellant and can generally be written as seen in Equation 3.

$$I_s = \frac{\int_0^t F dt}{g \int \dot{m} dt} \quad (3)$$

For a PDE, the total specific impulse is determined by adding the specific impulse contribution of the combustion chamber (I_c) and the specific impulse of the nozzle (I_n).

The specific impulse of the combustion chamber is beyond the scope of this thesis, and further information can be found in Ethan Barbour's Doctoral Dissertation [4]. The specific impulse of the nozzle is comprised of the specific impulse from the Taylor Wave / steady flow and the blow-down.

$$I_s = I_c + I_n \qquad (4) \text{ (From [4])}$$

$$I_n = I_{n,Taylor/steady} + I_{n,blowdown} \qquad (5) \text{ (From [4])}$$

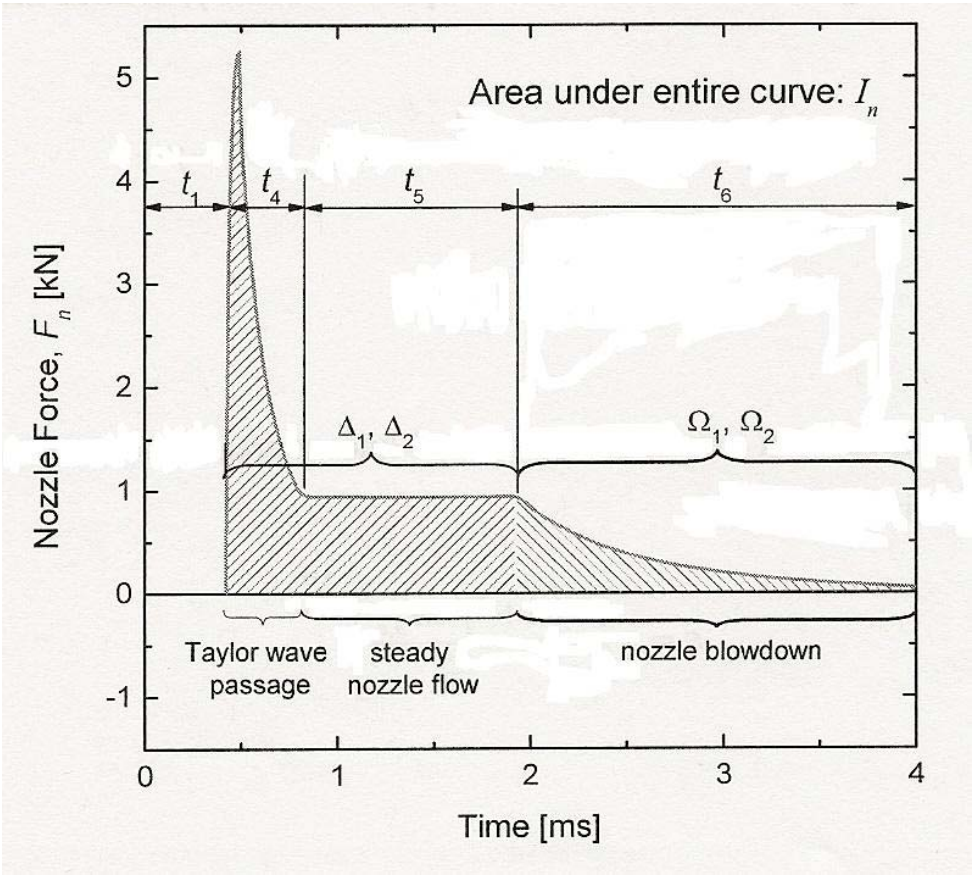

Figure 5. Subdividing Nozzle Force History for a Single Detonation Cycle (From [4])

A general description to show the complexity of the specific impulse calculation for a PDE nozzle is found in the following equations. Figure 5 represents a single detonation cycle of the PDE operation previously seen in Figure 4. The plateau refers to the period encompassed by t_5 of Figure 5. Further details and a complete derivation can be found in [4]. The subscripts of n, c, p, i, and e refer to the nozzle, combustion

chamber, plateau of Figure 5, inlet, and exit respectively in the following equations. All other subscripts remain the same as discussed previously. Equations 6 through 9 and their supporting equations were taken from [4].

$$I_{n,Taylor/steady} = \int_{t_1}^{t_1+t_4+t_5} F_n dt \qquad (6)$$

$$I_{n,Taylor/steady} = \frac{A_{n,i}L_c}{c_p}\left(p_p G_1 \int_{\tau_1}^{\tau_1+\tau_4+\tau_5} \frac{p_{1,e}(\tau)}{p_p} d\tau - p_3 G_2 \int_{\tau_1}^{\tau_1+\tau_4+\tau_5} d\tau \right) \qquad (7)$$

$$\tau = \frac{tc_p}{L}$$

$$G_1(\varepsilon,k) = kM_2(\varepsilon M_2)^{-\left(\frac{k-1}{k+1}\right)} + \varepsilon(\varepsilon M_2)^{-\left(\frac{2k}{k+1}\right)} - k - 1$$

$$G_2(\varepsilon) = \varepsilon - 1$$

$$I_{n,Taylor/steady} = \frac{V_c}{c_p}\left(p_p G_1 \Delta_1 - p_3 G_2 \Delta_2 \right) \quad (8)$$

$$\Delta_1 = \int_{\tau_1}^{\tau_1+\tau_4+\tau_5} \frac{p_{1,e}(\tau)}{p_p} d\tau$$

$$\Delta_2 = \int_{\tau_1}^{\tau_1+\tau_4+\tau_5} d\tau = \tau_4 + \tau_5$$

$$I_{n,blowdown} = \frac{V_s}{c_p}\left(p_p G_1 \Omega_1 - p_3 G_2 \Omega_2 \right) \qquad (9)$$

$$\Omega_1 = \left(\frac{2}{k+1}\right)^{\left(\frac{2k}{k-1}\right)} \left[1 - \left(\Pi \frac{p_3}{p_p} \right)^{\left(\frac{k+1}{2k}\right)} \right]$$

$$\Omega_2 = \frac{k+1}{k-1}\left[\left(\Pi \frac{p_3}{p_p} \right)^{-\left(\frac{k-1}{2k}\right)} - 1 \right]$$

$$\Pi(\varepsilon,k)=\left(\frac{k+1}{2}\right)^{\left(\frac{2k}{k-1}\right)}(\varepsilon M_2)^{\left(\frac{2k}{k+1}\right)}\frac{k+1}{2kM_2^2-k+1}$$

Another term often used is the thrust coefficient (C_F). The thrust coefficient is a function of the specific heat ratio, the ratio of the chamber pressure to the nozzle exit pressure and the ambient pressure, and the nozzle area ratio and is written as equation 11. The thrust coefficient has a maximum value when optimum expansion is reached ($p_2 = p_3$). The equation for thrust can then be written as equation 12 for a steady-state device.

$$C_F=\frac{u_2^2A_2}{p_1A_1V_2}+\frac{p_2A_2}{p_1A_t}-\frac{p_3A_2}{p_1A_t} \qquad (10)\ (\text{From [5]})$$

$$C_F=\sqrt{\frac{2k^2}{k-1}\left(\frac{2}{k+1}\right)^{\left(\frac{k+1}{k-1}\right)}\left[1-\left(\frac{p_2}{p_1}\right)^{\left(\frac{k-1}{k}\right)}\right]}+\frac{(p_2-p_3)A_2}{p_1A_t} \qquad (11)\ (\text{From [5]})$$

$$k=\frac{c_p}{c_v}$$

$$F=C_FA_tp_1 \qquad (12)$$

A nozzle area expansion ratio that is too small results in an underexpanded condition. This means the exit pressure of the nozzle is greater that the atmospheric pressure at the current flight condition resulting in further expansion outside the nozzle and exhaust plume expansion, which does not increase thrust. Figure 6 illustrates various degrees of underexpansion with severity increasing from top to bottom.

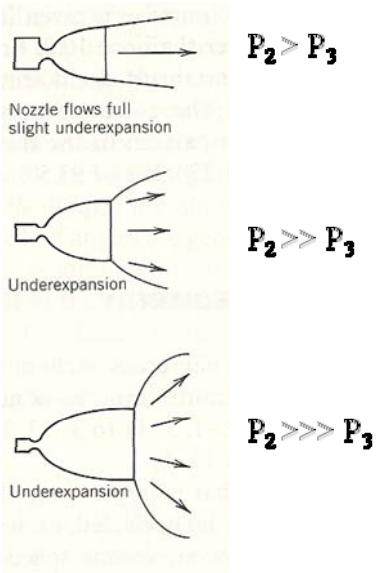

Figure 6. Various Degrees of Underexpansion (From [5])

Conversely, a nozzle area expansion ratio that is too large results in an overexpansion condition. This means the exit pressure of the nozzle is lower than the atmospheric pressure at the current flight condition resulting in a sudden pressure rise at the nozzle exit and possible flow separation from the walls of the nozzle. Figure 7 shows an optimally expanded nozzle at the top of the figure with the severity of overexpansion increasing from top to bottom. Flow separation that occurs in severe cases of overexpansion is depicted in the bottom right corner of Figure 8.

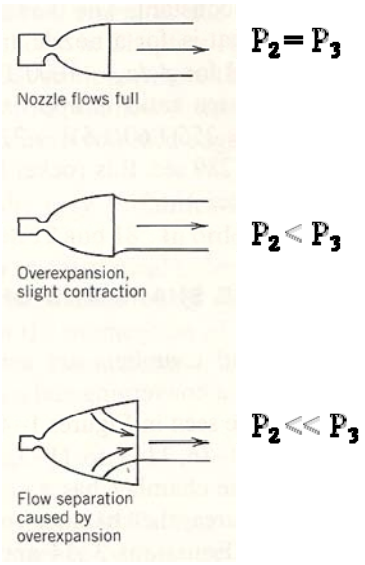

Figure 7. Optimum Expansion and Various Cases of Overexpansion (From [5])

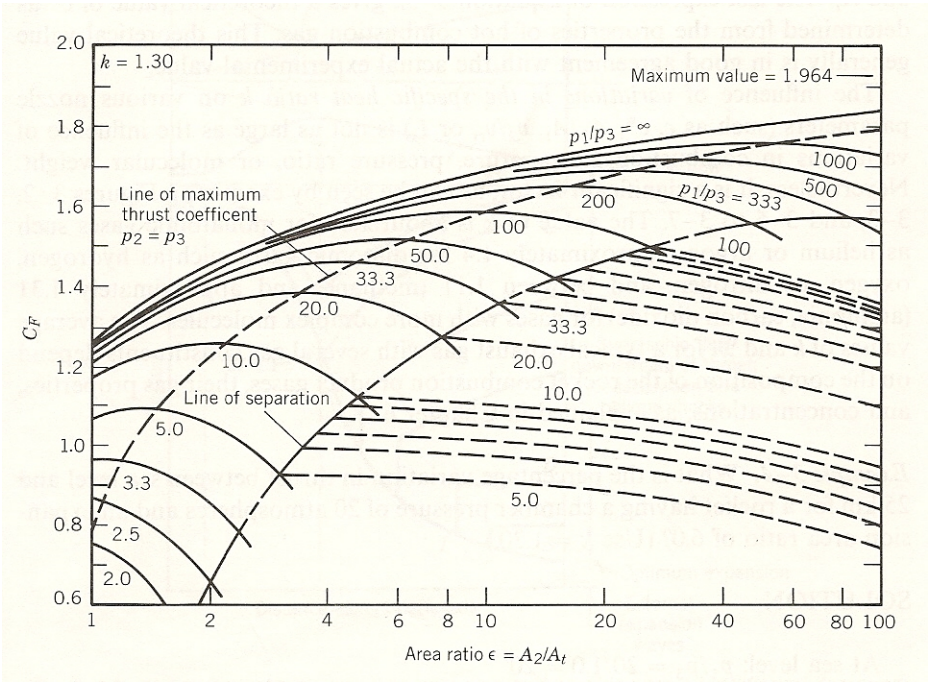

Figure 8. Thrust Coefficient Versus Nozzle Area Ratio for k = 1.30 (From [5])

Figure 8 shows that for a given pressure ratio, a maximum thrust coefficient exists, and therefore a maximum thrust exists at a particular nozzle area expansion ratio, ε. Underexpansion exists to the left of the optimum expansion curve, and overexpansion

exists to the right of the optimum expansion curve. Flow separation will eventually occur when the conditions are far enough to the right of the optimum expansion curve. This is highly undesirable, not only because of poor performance, but also due to severe structural side loads that can occur.

In a PDE, a nozzle designed for an efficient nozzle area expansion ratio for the higher pressures associated with detonation would result in an extremely overexpanded condition at the lower pressures associated with the blow-down and refresh portions of the cycle. At the same time, a nozzle designed for an efficient nozzle area expansion ratio for the lower pressures associated with blow-down would result in an extremely underexpanded condition at the higher pressures associated with the detonation. Both of these cases result in a loss of performance.

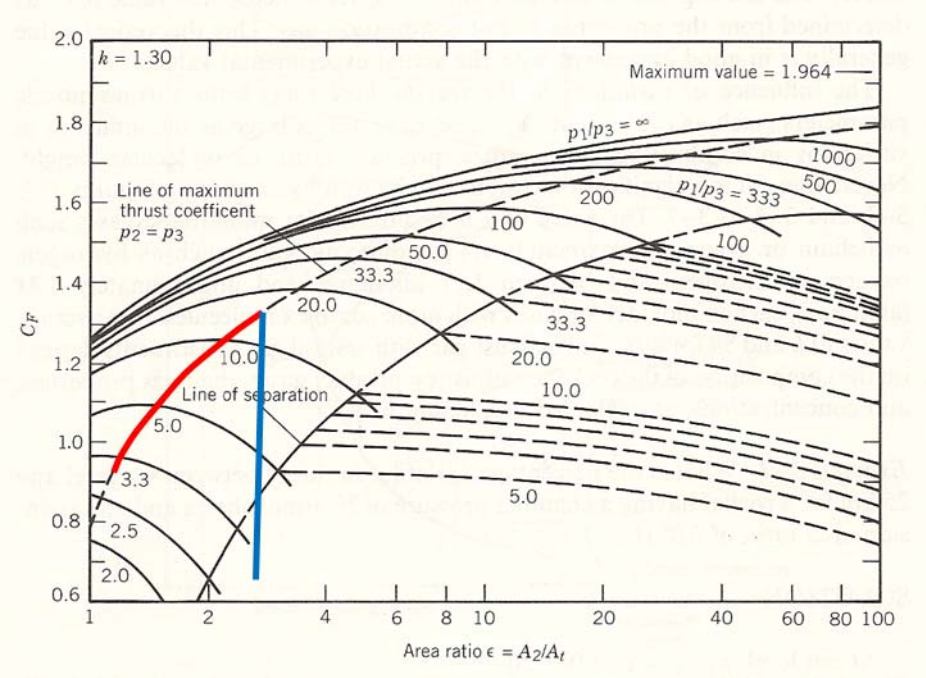

Figure 9. Thrust Coefficient for Fixed Nozzle Versus Dynamic Fluidic Nozzle

Figure 9 illustrates a possible PDE scenario where pressure ratios of 15:1 are experienced during the detonation portion of the cycle followed by a pressure ratio of 3:1 experienced during the blow-down/refresh portion of the cycle. A blue and red line have

been added to the original thrust coefficient figure to illustrate how a fixed nozzle and a dynamic fluidic nozzle would behave after being designed for optimum expansion at a 15:1 pressure ratio.

The blue line represents a fixed nozzle. Because the nozzle cannot vary its associated area ratio (ε), the thrust coefficient changes vertically as the pressure changes. This results in an extremely overexpanded nozzle condition and is in the flow separation region at the lower 3:1 pressure ratio. The extreme overexpansion and flow separation result in poor performance of the nozzle. As can be seen in Figure 9, the thrust coefficient decreases from approximately 1.3 to 0.65.

The red line represents a dynamic fluidic nozzle. Because the dynamic fluidic nozzle has the ability to vary its associated area ratio, the thrust coefficient would change along the optimum expansion curve where $p_2 = p_3$. This results in a much more efficient nozzle and maintains the nozzle at an optimum expansion condition. As seen in Figure 9, the thrust coefficient decreases over a much smaller range, from 1.3 to 0.95.

The ultimate objective of this work was to obtain near-ideal expansion in a supersonic nozzle operating under widely varying pressure ratios by utilizing secondary air injection at various injection angles and mass flow rates. By doing so, the intention was for the nozzle performance to effectively track the red line of Figure 9 throughout the complete engine cycle.

C. SHADOWGRAPH

A Schlieren visualization method translates phase differences into amplitude and sometimes color differences that we can see resulting in what is known as a schliere, the German word for streak. Schlieres occur in solids, liquids, and gases and may result from temperature changes, high-speed flows, or the mixing of dissimilar materials. Some schlieres are complicated in structure, while others are simple. Some refract light strongly, others barely at all. Some are sharply defined, while others are more gradual.

Another method for viewing density gradients, and the one chosen for this thesis, is the shadowgraph method. The main difference between the two methods is that the

illuminance level of the schlieren method responds to the first spatial derivative of the density gradient while the shadowgraph method responds to the second spatial derivative of the density gradient. This means that the schlieren image displays the deflection angle while shadowgraphy displays the ray displacement resulting from the displacement. Another difference is that the schlieren method requires a knife-edge or some other cutoff of the refracted light where this is not required in the shadowgraph method resulting in the shadowgraph method being easier to setup and utilize [6].

THIS PAGE INTENTIONALLY LEFT BLANK

III. DESIGN/EXPERIMENTAL SETUP

The experimental testing was performed at the Naval Postgraduate School, in Test Cell #1 of the Rocket Propulsion Laboratory. The test equipment was comprised of a combustor section, shock formation tube, test section, optical viewing section, and exhaust tube. Gaseous ethylene (C_2H_4) and air (O_2 + 3.76 N_2) were used as reactants and were premixed prior to injection into the combustion section. The ignition of the fuel/air mixture was initiated by a high capacitance igniter mounted in the forward flange of the combustion section. The instrumentation used during testing included high-speed pressure data acquisition sensors integrated with a DRS Hadland Lightning RDT 2000 high-speed digital camera that captured the shadowgraph images in the optical test section. The entire test assembly was supported by a Newport Research Corporation optical table. The actuation and instrumentation for the test cell was accomplished remotely in the control room via a National Instruments GUI. Operation of the camera was also controlled from the control room from a separate computer.

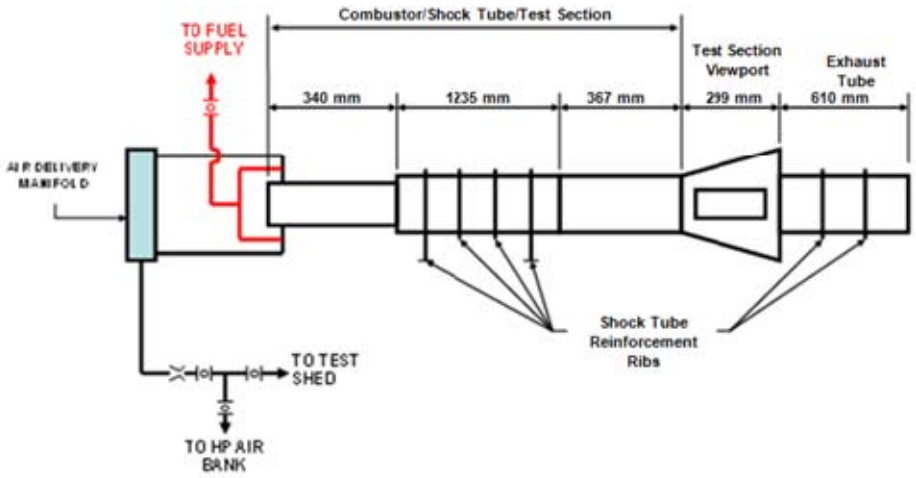

Figure 10. Diagram of the Experimental Assembly (From [7])

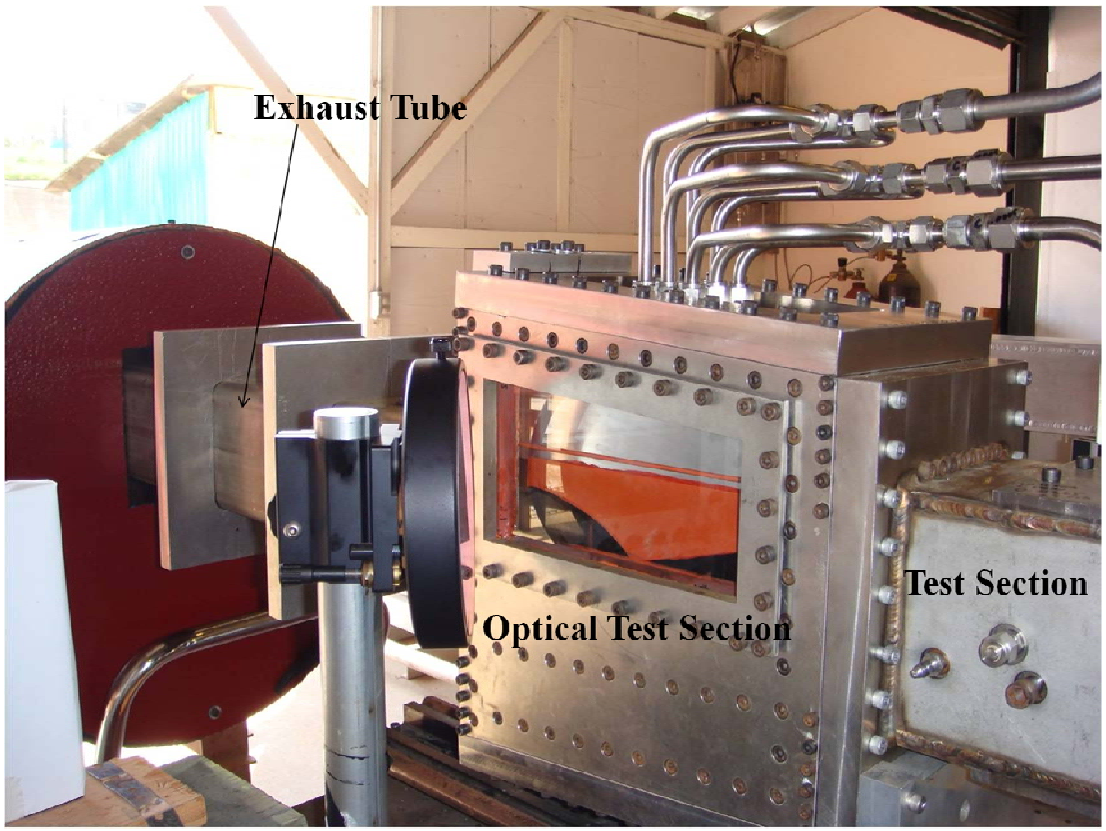

Figure 11. Experimental Setup

A. DESCRIPTION OF THE EXPERIMENTAL ASSEMBLY

1. Combustor

The purpose of the combustor section was to generate a fully developed detonation wave. The combustor section was made of 112.71 mm diameter stainless steel tube that was 340 mm in length as seen in Figures 12 and 13. The inlet for the fuel/air mixture was located 25.4 mm from the combustor head and entered through two 25.4 mm tubes welded to the steel tube 180 degrees apart. An igniter flange was located on the upstream wall of the combustor for the high capacitance igniter, and it was shielded by a cone shaped shroud as seen in Figure 14. The purpose of the shroud was to protect the nascent flame from being extinguished during high flow rate testing. The shock formation tube was attached to the downstream end of the combustion section.

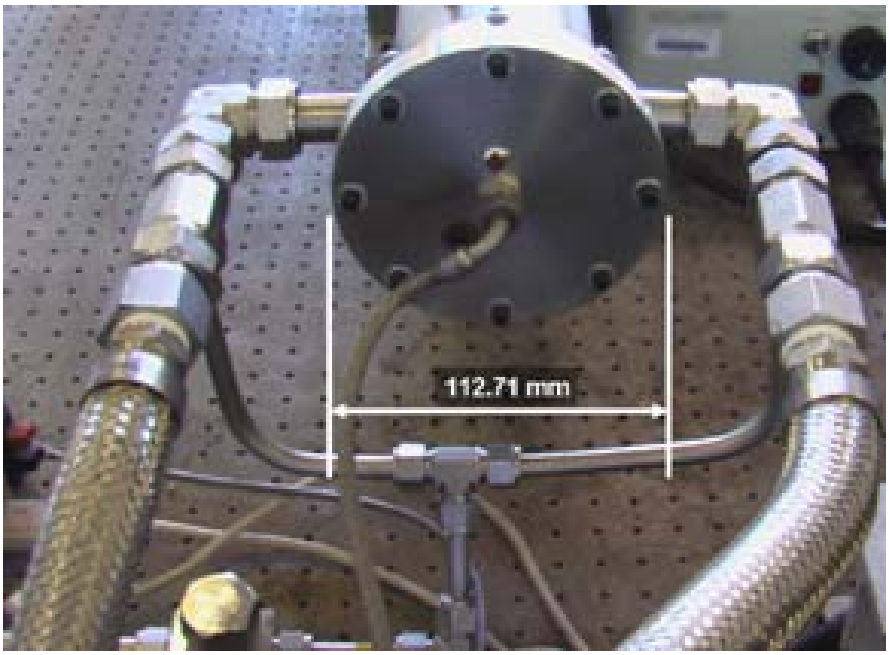

Figure 12. Combustor Section Forward View (From [7])

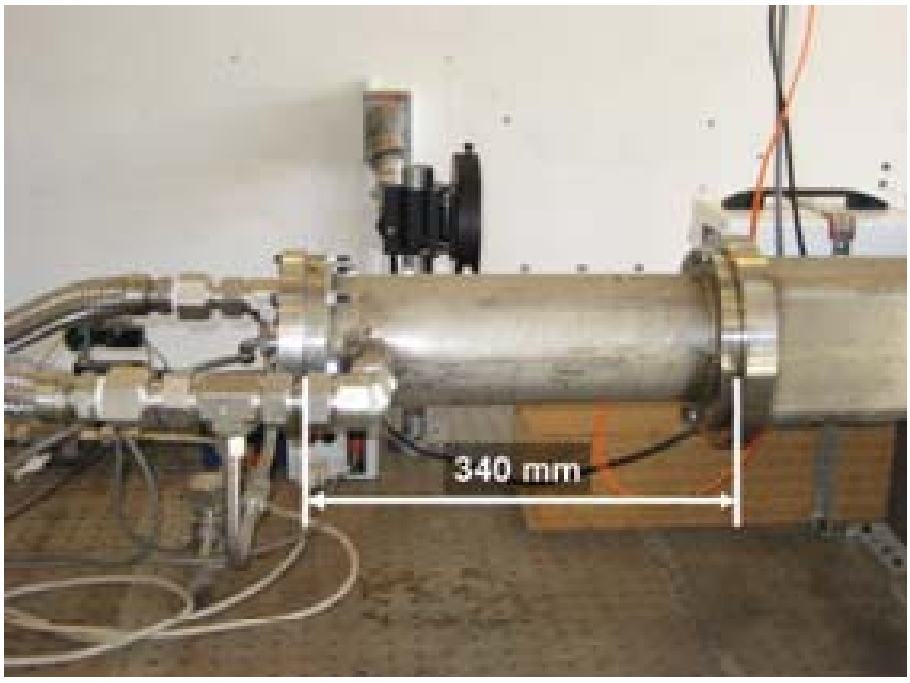

Figure 13. Combustor Section Side View (From [7])

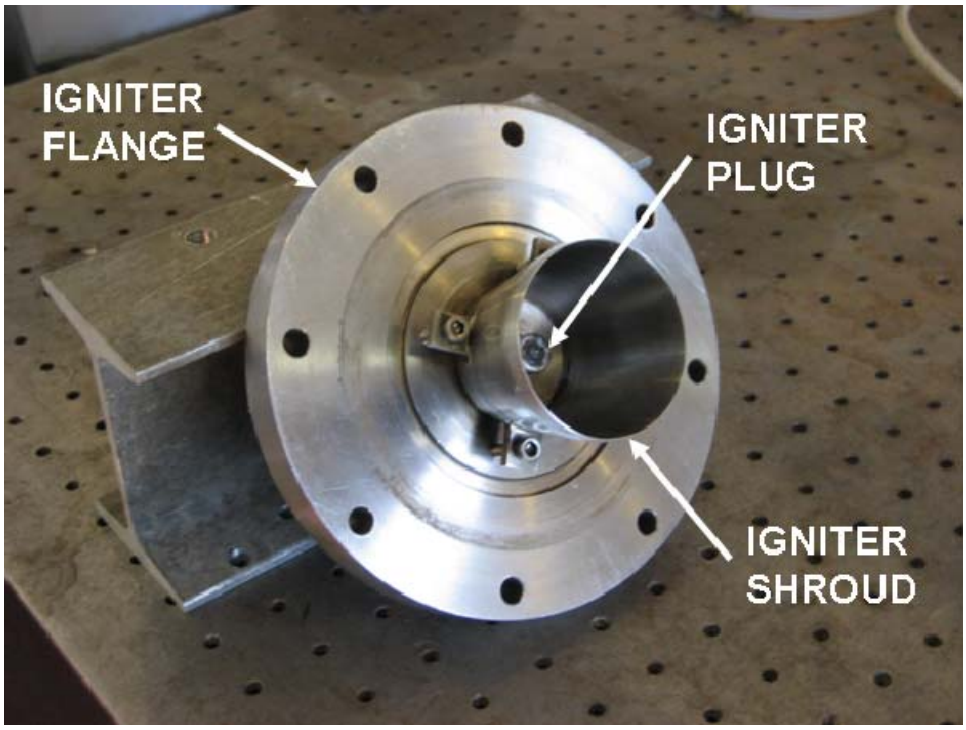

Figure 14. Igniter Flange with Shroud and Igniter Installed (From [7])

2. Shock Formation Tube

A shock formation tube of sufficient length was used to allow DDT to occur and could also be referred to as the detonation initiation section. The shock formation tube was constructed into a 13.0 cm square stainless steel tube 123.5 cm in length. This section was constructed by Michael A. Fludovich for use in previous thesis work. To prevent deformation during testing, eight ribs constructed of 2.54 cm thick aluminum plate were placed along the shock formation tube. The length of the shock formation tube was actually much longer than necessary for the experiments of this thesis and would have been reduced if not using a previously designed test assembly.

3. Test Section

The test section was then coupled to the aft end of the shock formation tube using fasteners and an o-ring seal. The test section was also designed by Fludovich to allow smooth transition from the larger 13.0 cm square shock formation tube to the 114 mm x 80 mm test section. Several types of connection ports were machined into the test section

to allow various types of instrumentation to be utilized. During this testing, two high-speed Kistler pressure transducers with approximately 10 cm of axial spacing between them were installed along the centerline as seen in Figure 15. The Kistler pressure transducers were utilized to determine the shock speed entering the test section. An optical sensor with the capability to detect the flame front passage was also installed in this section to provide a trigger signal to the high-speed camera as seen in Figure 16.

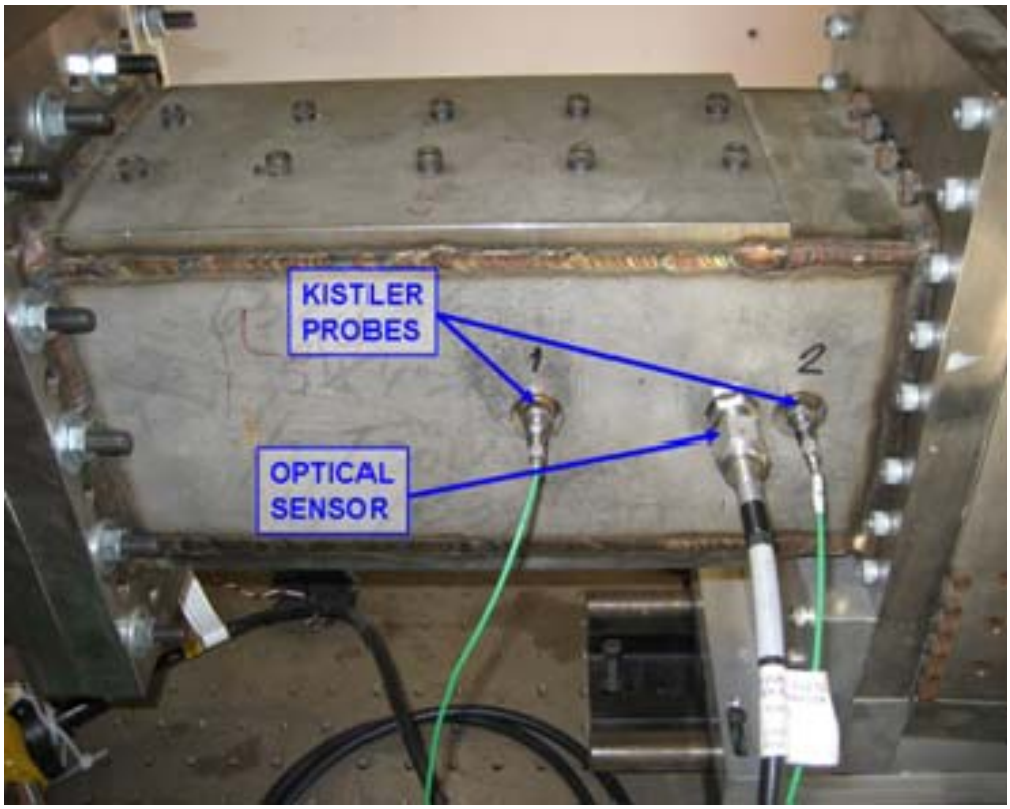

Figure 15. Test Section (From [7])

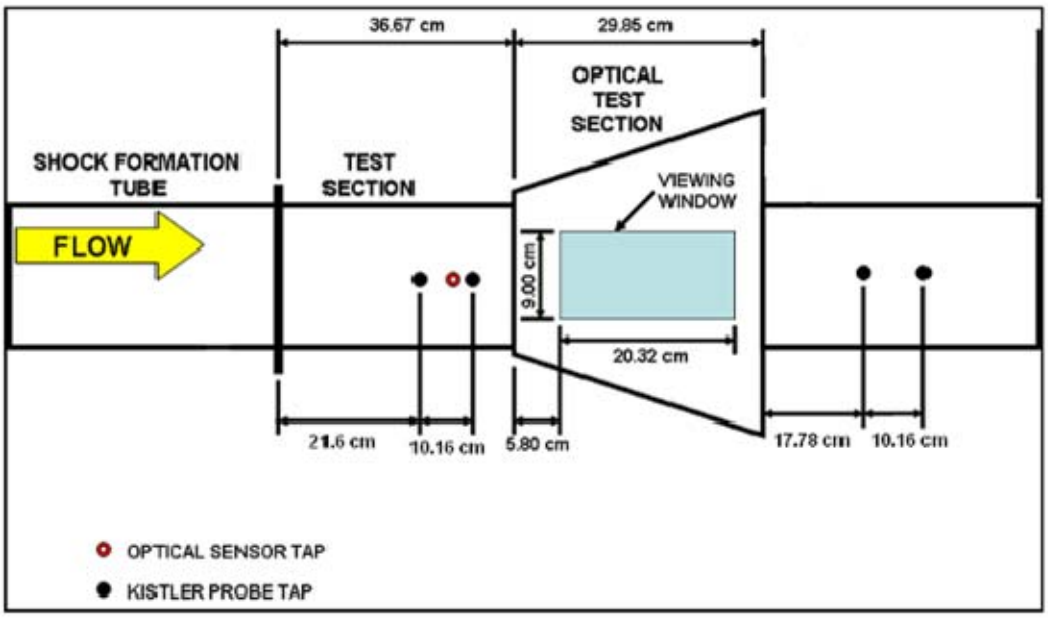

Figure 16. Test Section Drawing with Dimensions (From [7])

4. Optical Test Section

The optical test section was a previous nozzle inlet that was designed by Fludovich for thesis work and subsequently modified by Charles B. Myers IV for thesis work. The nozzle inlet had been modified since the nozzle components had been removed and replaced with plates extending from the test section and can be seen as the hollow piece in the bottom of the left figure in Figure 17. The two windows in the optical viewing section were 30.48 mm thick and were mounted flush with the section walls to form an imaging area 9 cm x 20.32 cm constructed from BK7 glass and polished to half wavelength as seen in Figure 11. Mounting brackets for attachment of the exhaust tube section were installed on the aft end of the optical test section.

a. Nozzle Mounting Structure

A nozzle mounting structure was designed and manufactured from 2024 Aluminum. The purpose of this piece was to provide a means of attaching the nozzle insert while simultaneously allowing flow of injection air to pass to the nozzle insert. The nozzle mounting structure was solid with the exception of 6 through holes to allow

the mounting of the nozzle insert and 9 tapped holes to allow injection air to pass through the structure to the nozzle insert. The nozzle mounting structure was 29.21 cm long x 11.43 cm wide. To allow mating with the current test rig, the structure was 10.16 cm tall at the tallest end and 7.62 cm tall at the shortest end. The nozzle mounting structure replaced one of the previously modified nozzle inlets described in the previous section and was attached via fasteners to the optical test section walls, top cap, and bottom cap previously designed by Fludovich. The top cap designed by Fludovich was also modified to allow sufficient space for injection air plumbing to be connected to the nozzle mounting structure while maintaining the original mounting orientation for structural support.

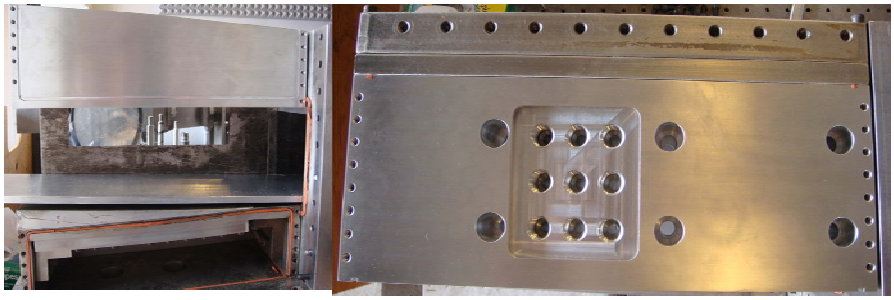

Figure 17. Nozzle Mounting Structure

Figure 17 shows an image of the nozzle mounting structure installed in the experimental test assembly on the left, and the image on the right shows a top-down view of the nozzle mounting structure. The image on the right also shows the six, through holes for mounting the nozzle insert and the nine holes allowing injection air to pass through to the nozzle insert.

b. Nozzle Insert

Three different nozzle inserts were designed and manufactured from 2024 Aluminum, and an example can be seen in Figure 18. The geometry of all three-nozzle inserts was identical with the exception of the angle at which the injection air passed through the individual nozzle insert. The three injection angles chosen to investigate were a relatively shallow 30-degree injection angle, a 45-degree injection angle, and a relatively steep 60-degree injection angle. Injection air was distributed on the backside of

the block by three 6.35 mm wide slots, each consisting of 21 holes of 3.175 mm diameter at the respective injection angle. The nozzle insert was 25.31 cm long x 11.43 cm wide. The nozzle insert was attached to the nozzle mounting structure via fasteners and allowed for a smooth transition from the top spacer in the forward test section. Once installed, the distance between the nozzle insert and the bottom spacer was 4.19 cm at the nozzle throat and 7.56 cm at the nozzle exit resulting in a nozzle expansion area ratio of 1.80.

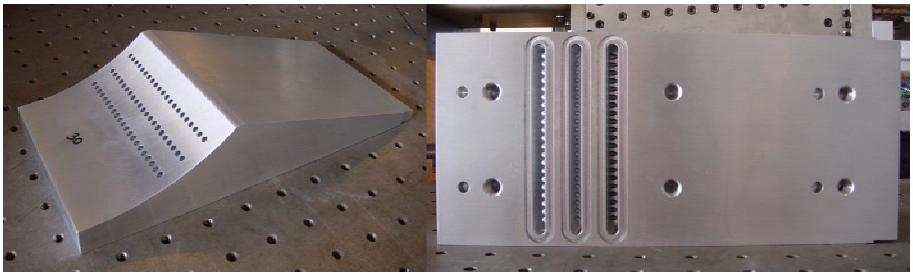

Figure 18. Nozzle Insert

c. Spacers

Top and bottom spacers were designed and manufactured to create a smooth transition between the ramp mounting plates and the optical test section. The bottom spacer was attached to the bottom ramp mounting plate, the test section, and the exhaust tube with fasteners, and the top spacer was attached to the top ramp mounting plate and the test section with fasteners. Both spacers are 11.30 cm wide and were manufactured from Aluminum. The spacers also served to fill the void remaining above and below the ramp mounting plates in the test section to minimize bending stresses experienced by the ramp mounting plates as the detonation and shock waves traveled down the test section, through the optical test section, and out of the assembly via the exhaust tube.

5. Ramp Mounting Plates

Two ramp mounting plates were designed by Myers to allow mounting of swept ramps both on the top and bottom of the test assembly; however, the swept ramps were only mounted on the top of the test assembly to continue the simulation of a symmetric half of a PDE assembly. The mounting plates were 137.8 cm x 8 cm and were tapered at

the front end as shown in Figure 19. The two ramp mounting plates were mounted to the top and bottom of the test assembly via fasteners. The ramp mounting plates were attached in the shock formation tube and the test section. Both of the plates were constructed with an array of tapped holes, which permitted multiple ramp configurations to be tested during Myers' research, but only a proven, six ramp configuration determined by Myers was utilized during this research. The remaining, unused fastening holes were plugged when not in use to prevent any of the combustion products from filtering through the plated during testing.

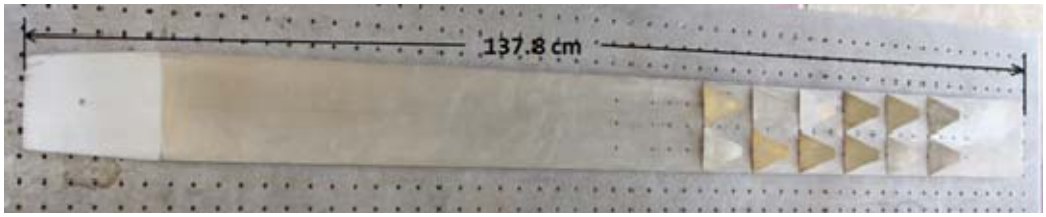

Figure 19. Mounting Plate with Swept Ramps installed (From [7])

6. Exhaust Tube

A removable exhaust tube was installed downstream of the optical test section to isolate the test section from ambient flow disturbances and to direct the shock and combustion products away from the instrumentation and test table as seen in Figure 20. The exhaust section was comprised of a square tube with two Kistler pressure transducers mounted 10.16 cm apart along the centerline of the right side of the exhaust tube. These sensors allowed precise measurements of the shock speed after the test section, which allowed for comparison to the upstream shock velocity measurements. The exhaust tube section was inserted into the test cell exhaust tube to minimize the pressure waves that could possibly be directed back toward the test instrumentation during testing.

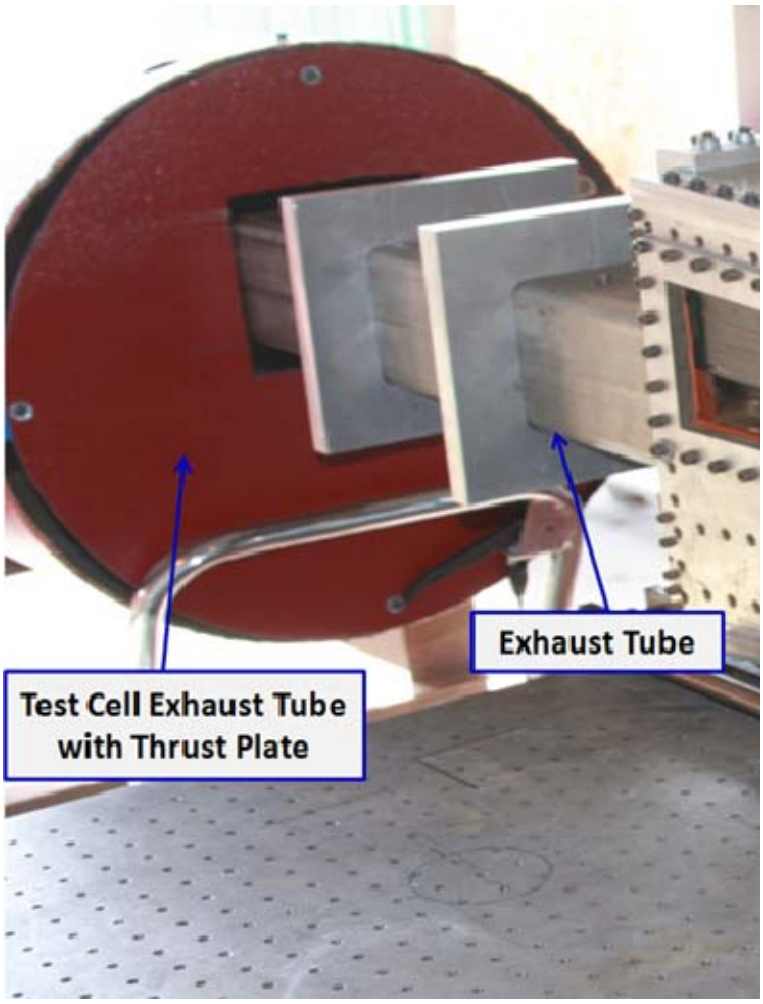

Figure 20. Exhaust Tube and Test Cell Exhaust Tube (From [7])

B. AIR AND FUEL DELIVERY

1. Combustion Chamber Air and Fuel

High-pressure air was provided to the test cell from the facility air system, and ethylene was provided from a single bottle. The main control room computer controlled the supply pressures for both the high-pressure air using the node 1 regulator and ethylene using the node 3 regulator with Tescom ER3000 Version 2.0 software, which allowed the pressures of the reactants to be set remotely and independently of each other as seen in Figure 21.

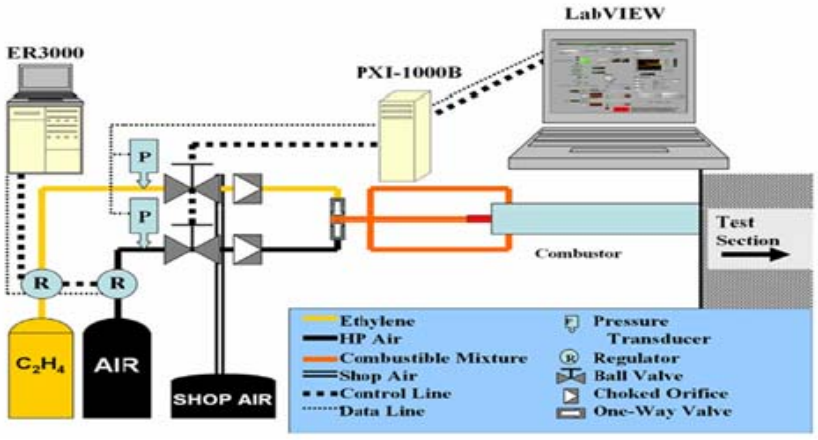

Figure 21. Schematic Diagram of Air and Fuel Delivery to Combustor Section (From [9])

High-pressure air was supplied via 1½ inch piping connected to a single inlet manifold and was then routed to the combustor section using flexible steel hoses. Gaseous ethylene was supplied via ½ inch tubing connected to each of the air inlets prior to entering the combustor section as seen in Figure 22.

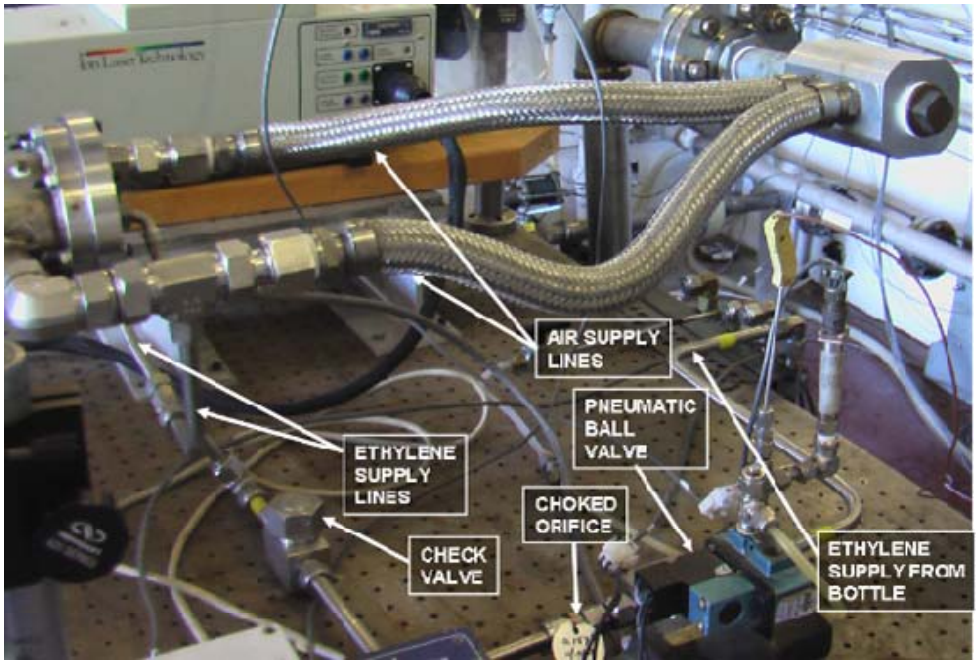

Figure 22. Fuel and Air Supply to Combustor Section (From [7])

Delivery of the high-pressure air was controlled using the ER3000 regulator controller, and gaseous ethylene was injected into the combustor section via a single Swagelock ball valve that was opened at user specified time for user specified duration. The ethylene ball valve was air actuated and controlled by the LabVIEW software via Crydom control solenoid switches located in an electronics cabinet in the test cell as seen in Figure 23.

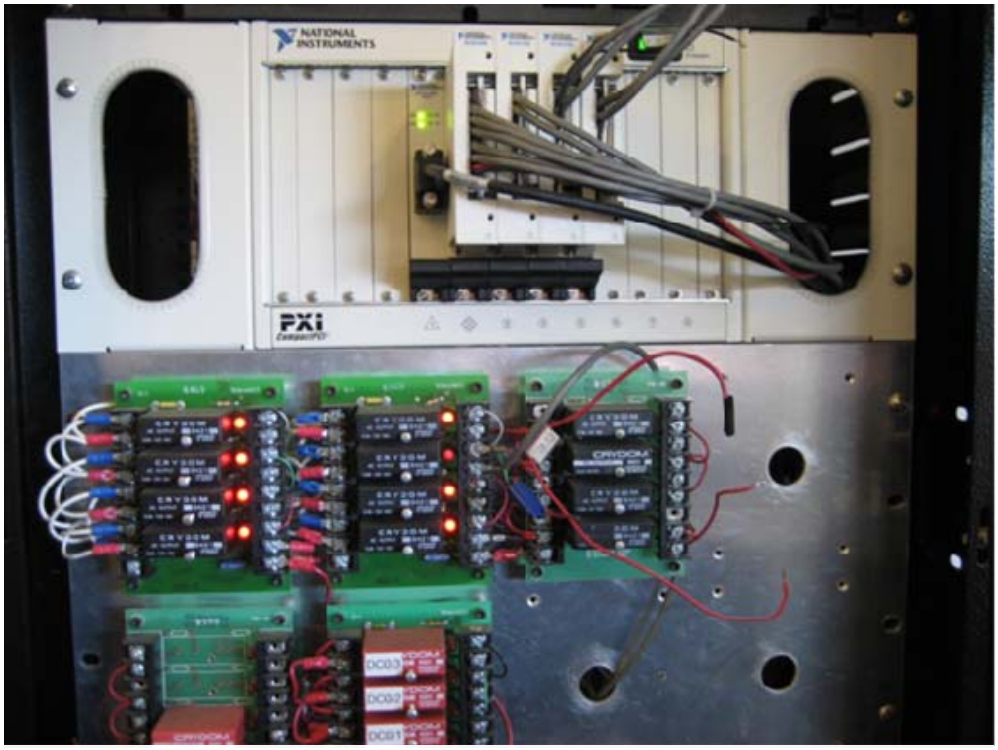

Figure 23. PXI-1000B Chassis (Upper Section) and Crydom Control Solenoid Switches (Lower Section) (From [7])

An orifice was located in each supply line to provide an accurate method of delivering the desired mass flow rates for each gas. The choke diameters used during this testing were 0.752 inches for the air supply and 0.157 inches for the ethylene supply. A check valve was installed between the combustor section and the ball valve, as seen in Figure 22, to prevent the possibility of backflow from the combustion event.

2. Optical Test Section Injection Air

High-pressure air was provided to the nozzle plenum from the facility air system. The main control room computer controlled the supply pressure for the injection air using a dome-loaded regulator and the Tescom ER3000 Version 2.0 software, which allowed the pressure to be set remotely and independently of the combustion chamber air.

The injection air was fed to the injection piping using ½ in tubing via a common feed line. A check valve was installed in the common feed line to prevent the possibility of backflow from the combustion event as was done in the combustion chamber air tubing. The common feed line was then split into three separate ½ tubes to allow independent control of each of the three rows of injection through the nozzle insert. The three ½ inch tubes were then stepped down to 3/8 inch tubing using Swagelock adapters, and a 0.0665 inch orifice was inserted into each of the adapters to provide an accurate method of delivering the desired mass flow rate for each injection row. The common feed line, injection tubing, and choke locations can be seen in Figure 24.

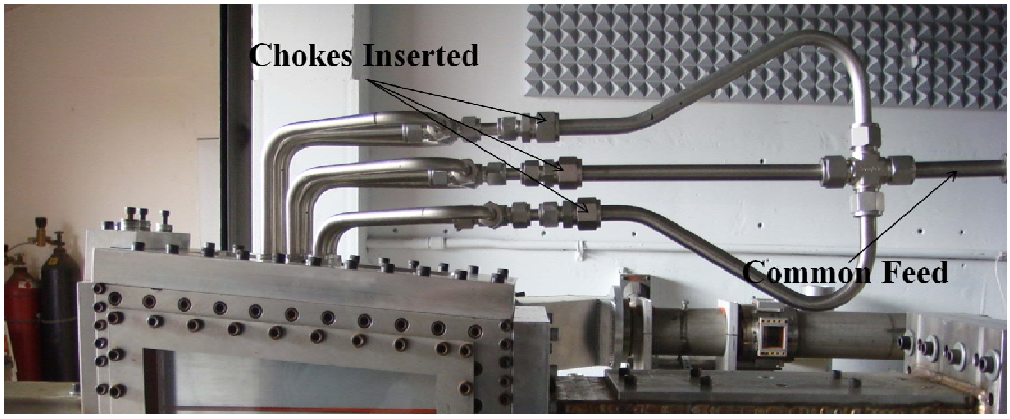

Figure 24. Injection Air Supply

C. IGNITION SYSTEM

The ignition system utilized in this test assembly was the Unison Vision-50 Variable Ignition System as seen in Figure 25. This ignition system is a capacitive discharge type system that uses an aviation grade spark plug mounted in the forward end of the combustor section. Prior to testing, the igniter was configured manually to provide a 2 Joule spark and was remotely triggered by LabVIEW software.

Figure 25. Unison Vision-50 Variable Ignition System (From [7])

D. INSTRUMENTATION AND SOFTWARE

The data acquisition instrumentation used during testing controlled the data collection during the experimental testing process. Each of the four pressure signals were routed through one of four National Instruments (NI) 14-bit PXI-6115 cards mounted in the NI PXI-1000B chassis as seen in the upper half of Figure 22. This chassis interfaced with the computers in the control room through the NI PXI-MXI-4 PXI Bridge and was capable of collecting either real time or high-speed buffered data. Optical data imaged from the DRS Hadland Lightning RDT 2000 high-speed digital camera was routed to a dedicated desktop computer in the control room using a fiber optic cable. A schematic of the data acquisition system utilized can be seen in Figure 26.

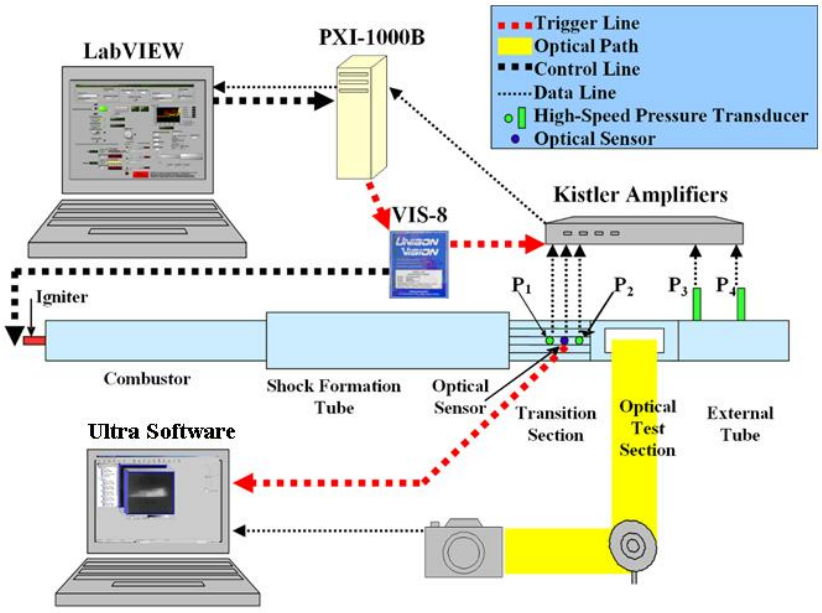

Figure 26. Schematic of Ignition and Instrumentation (From [10])

1. Dynamic Pressure Transducers

Before and after the test section were four high-frequency Kistler dynamic pressure transducers mounted in pairs in order to calculate the wave velocity based on the pressure transients. The pressure transducers were connected to Kistler Type 5010 Dual Mode amplifiers, which then routed the data to two NI PXI-6115 data cards in the PXI-1000B for high-speed data collection. Once the testing sequence was initiated, the cards were configured to begin collecting data with the triggering of the capacitive discharge igniter and collected data at a rate of 500 kHz. The data was stored in the card buffer and was later saved to the computer located in the control room. The pressure data supplied by the Kistler transducers provided high resolution of shock passage.

2. Thorlabs PDA36 Optical Sensor

An optical sensor was inserted in the test section 13.8 cm prior to the optical test section and was used to activate the imaging equipment once it detected the passage of

the flame front. When a flame front was detected, the optical sensor triggered the camera to begin collection of high-speed flame images during detonation experiments.

3. Lightning RDT 2000 Camera

A Lightning RDT 2000 camera from DRS Data & Imaging Systems, Inc., was used to image the optical test section during non-detonation experiments and can be seen in Figure 27. The RDT 2000 was able to image and store 1280 x 1084 of resolution at 500 full frames per second for up to 20 seconds without compression. Non-detonation images were captured at the full resolution available, but the frame rate was reduced to 200 frames per second allowing for more than 40 seconds of recording without compression.

Figure 27. Lightning RDT 2000 Camera (From [11])

Images were recorded using a standalone computer located in the test cell with MIDAS 2.0 software developed by Xcitex, Inc. The camera was controlled remotely from the control room using an Avocent LONGVIEW KVM extender. The extender allowed the video signal to be transmitted to a monitor located in the control room and inputs from the mouse and keyboard located in the control room to be transmitted to the computer in the test cell via an Ethernet connection.

4. Shimadzu Hyper-Vision 2 High-Speed Camera

A Shimadzu Hyper-Vision 2 high-speed camera was used to capture images during detonation testing. The camera was capable of imaging up to one million frames per second and store up to 99 frames. The camera frame rate was set to 125,000 frames per second allowing a four microsecond exposure time and was triggered remotely from the signal generated from the optical sensor located in the test section.

The camera settings were controlled using a laptop located in the control room, and the laptop and camera communicated via an Ethernet connection. The Shimadzu Hyper-Vision 2 can be seen in Figure 28.

Figure 28. Shimadzu Hyper-Vision 2 High-speed Camera (From [7])

5. Lexel Model 95 Ion Laser

A Lexel model 95 ion laser was used as the light source for shadowgraph imagery. The laser was set on its maximum output power for all image capturing during the experimental testing. The operation and settings of the laser were controlled via the power supply located in the test cell.

The emitted laser light was first passed through a four-micron spatial filter to approximate a point light source for the experiment. Mirrors were then used to direct the laser light through the optical test section and on to a white screen where a camera was then utilized to capture and record the images off the screen. The setup can be seen in Figures 29 and 30.

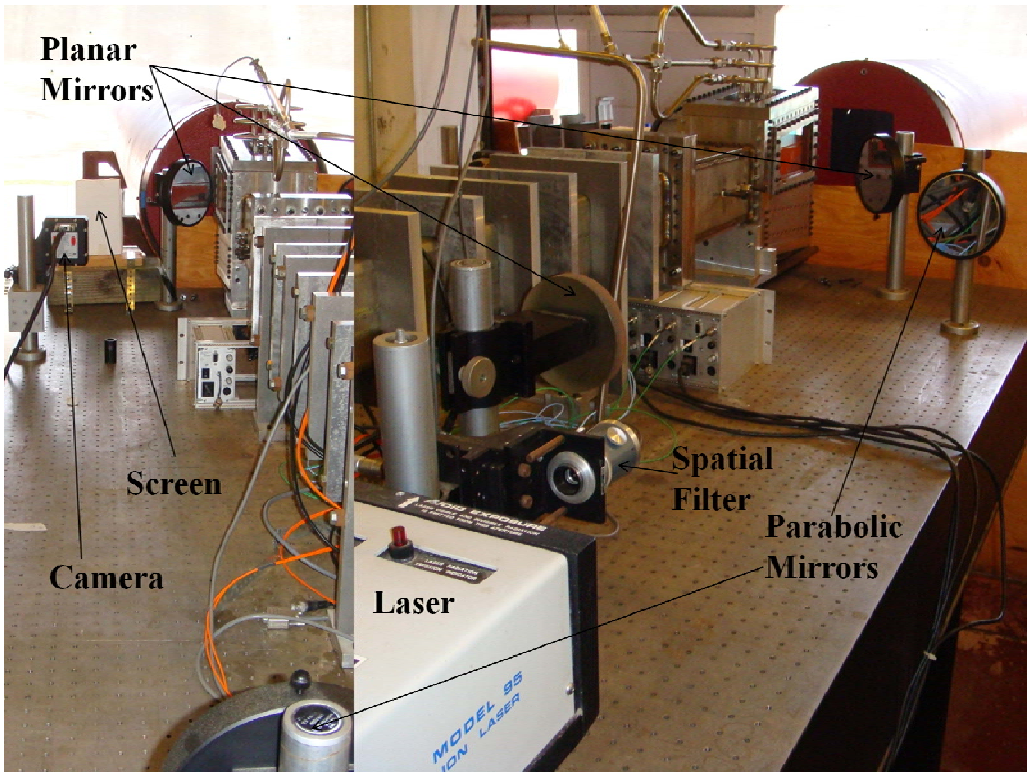

Figure 29. Laser and Imagery Setup

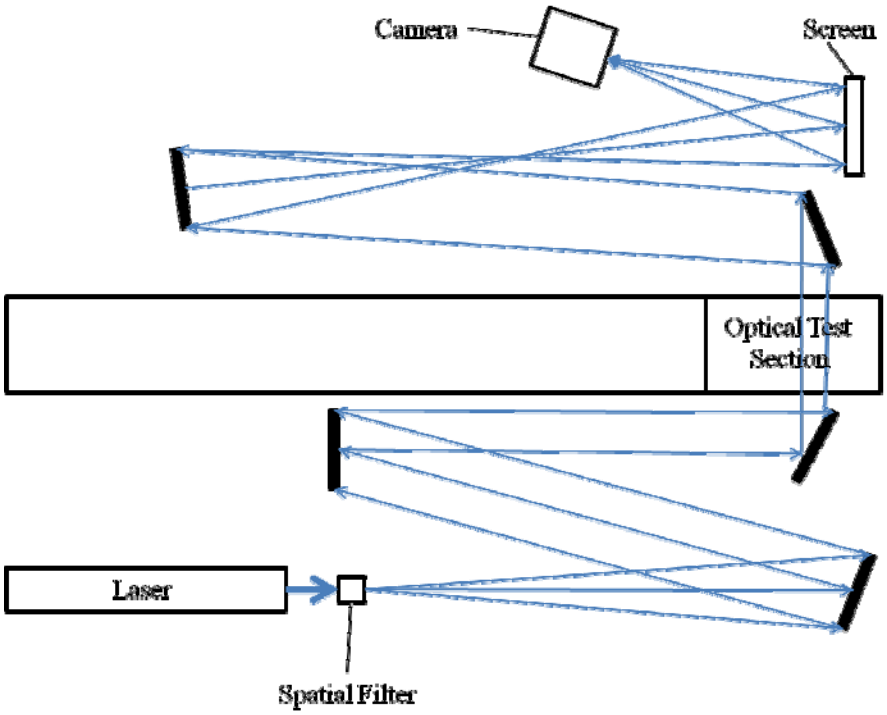

Figure 30. Basic Schematic of Laser and Imagery Setup

6. LabVIEW

Actual testing was controlled remotely form the control room with LabVIEW Professional Development System Version 8.5 and a graphical Virtual Interface developed specifically for the experiment installed on a desktop PC located in the control room. When the LabVIEW software and the Virtual Interface were placed in the run mode, the Virtual Interface controlled the injection of fuel, igniter ignition, and collection of the test results during testing. A screen capture of the LabVIEW GUI can be seen in Figure 31.

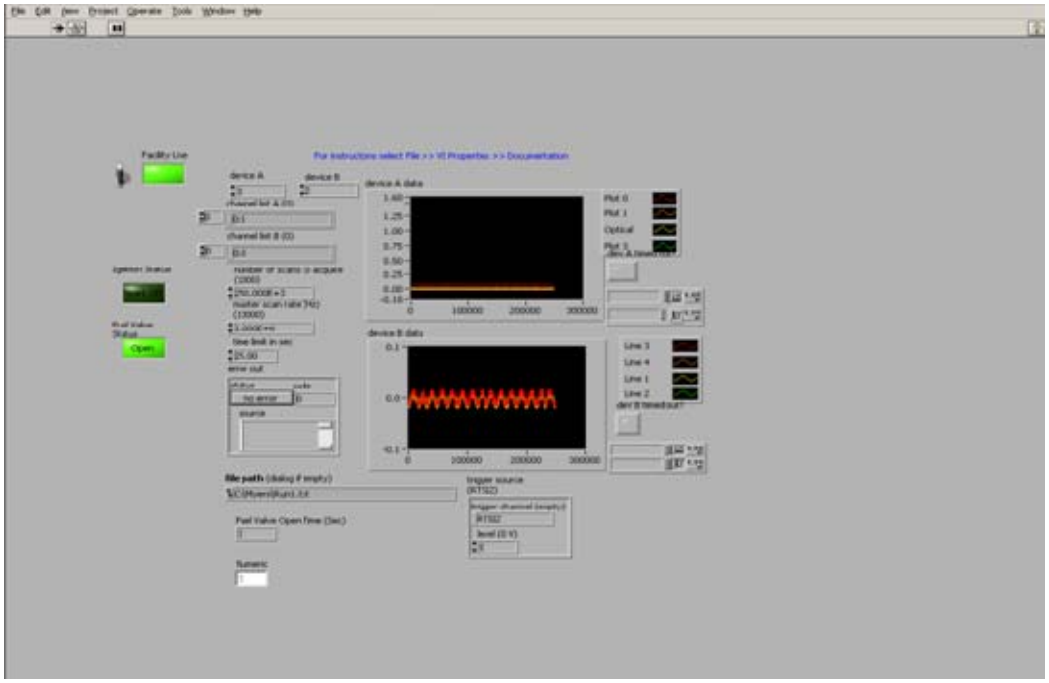

Figure 31. Screen Capture of LabVIEW VI

THIS PAGE INTENTIONALLY LEFT BLANK

IV. EXPERIMENTAL RESULTS

A. PURPOSE

The purpose of this testing was to observe the flow behave through the nozzle expansion region where the air injection was introduced using a shadowgraph method. The testing allowed images of the combustor fill event to be imaged.

It is important to understand how the different gases were introduced and controlled for the experimental setup. The main combustion chamber air was introduced and controlled using the Node 1 regulator controlled from the main control room computer. The gaseous ethylene was introduced and controlled using the Node 3 regulator controlled from the main control room computer. Finally, injection air was introduced and controlled using the Node 4 regulator controlled from the main control room computer. The ball valve initiating the injection air was controlled by the LabVIEW software. The controlling devices remained the same throughout the experimental testing unless stated otherwise.

All of the experimental testing was conducted using the 45 degree injection nozzle insert due to time constraints. The pressure, choke size, and calculated mass flow rates for each of the gases utilized can be found in table form in their respective sections.

B. FILL TESTING

1. Baseline Injection Mass Flow Rate Utilizing Air

The first experiment used the setup previously described but did not introduce gaseous ethylene in the main air sent to the combustion chamber. This experiment used a mass flow rate of 0.022 kg/s for the secondary injection air to be used as a baseline condition in this set of experimental tests. The settings for this experiment can be seen in Table 1.

Table 1. Settings for Baseline Mass Flow Rate Fill Testing (Air)

	Node 1	Node 3	Node 4
Gas Controlled	Air	Ethylene	Air
Pressure	5375842 Pa	Not Used	4272681 Pa
Choke Size	19.05 mm	3.99 mm	1.69 mm
Mass Flow Rate	3.61 kg/s	Not Used	0.022 kg/s

During this experiment, the secondary injection air was first introduced to the experimental test assembly, and then the main air was introduced at the pressures specified in Table 1. It was possible to see the secondary air injection zone form in the resulting images, but distinct lines of separation were difficult to see because both fluids introduced to the experimental test assembly were air at relatively the same temperature. All further experiments were conducted by injecting gaseous ethylene through the injection ports in an attempt to gain better optical results while maintaining nearly the same momentum ratios.

2. Baseline Mass Flow Rate Utilizing Ethylene

The second experiment was conducted at the baseline flow rate for this set of experimental tests and injected gaseous ethylene through the injection ports. The settings for this experiment can be seen in Table 2.

Table 2. Settings for Baseline Mass Flow Rate Fill Testing (Ethylene)

	Node 1	Node 3	Node 4
Gas Controlled	Air	Ethylene	Air
Pressure	5375842 Pa	4355418 Pa	Not Used
Choke Size	19.05 mm	3.99 mm	1.69 mm
Mass Flow Rate	3.61 kg/s	0.022 kg/s	Not Used

During this experiment, the main combustion chamber air was delivered first and allowed to reach the setpoint pressure for the experiment. It was possible to see the fluid encompass the full divergent section of the nozzle as the air pressure was gradually increased. With only the main chamber air flowing, the fluid encompassed the full divergent section of the nozzle until an extreme overexpansion condition resulted in flow separation within the nozzle. The secondary injection of ethylene was then initiated, and the secondary air injection zone became visible.

The following images were captured and show the description from the previous paragraph. Main combustion chamber air flow is from left to right, and injection flow is from bottom left to top right at a 45 degree angle from the horizontal axis.

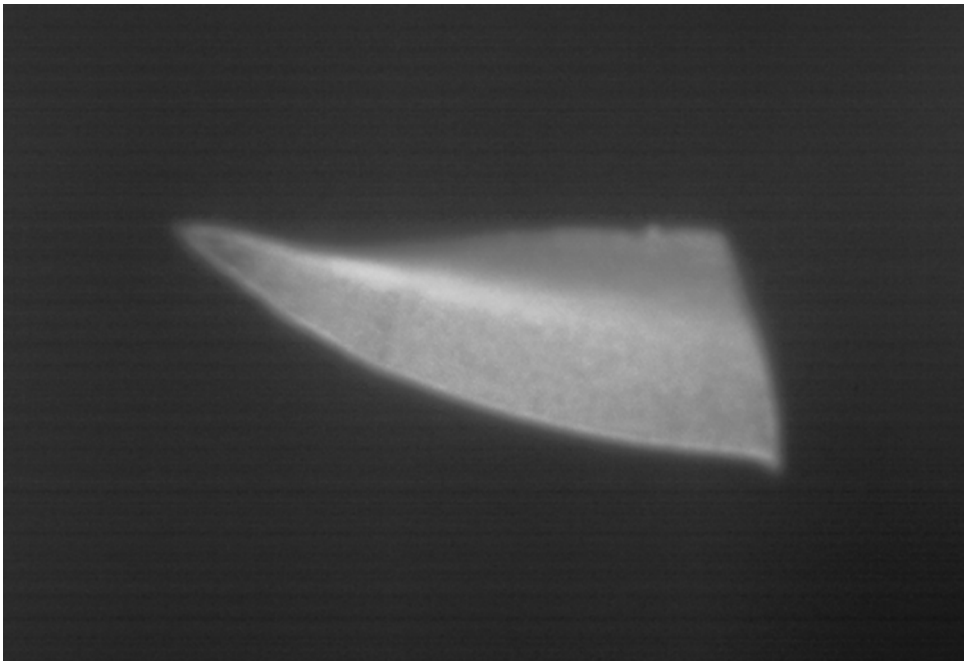

Figure 32. Start of Baseline Mass Flow Rate Experiment

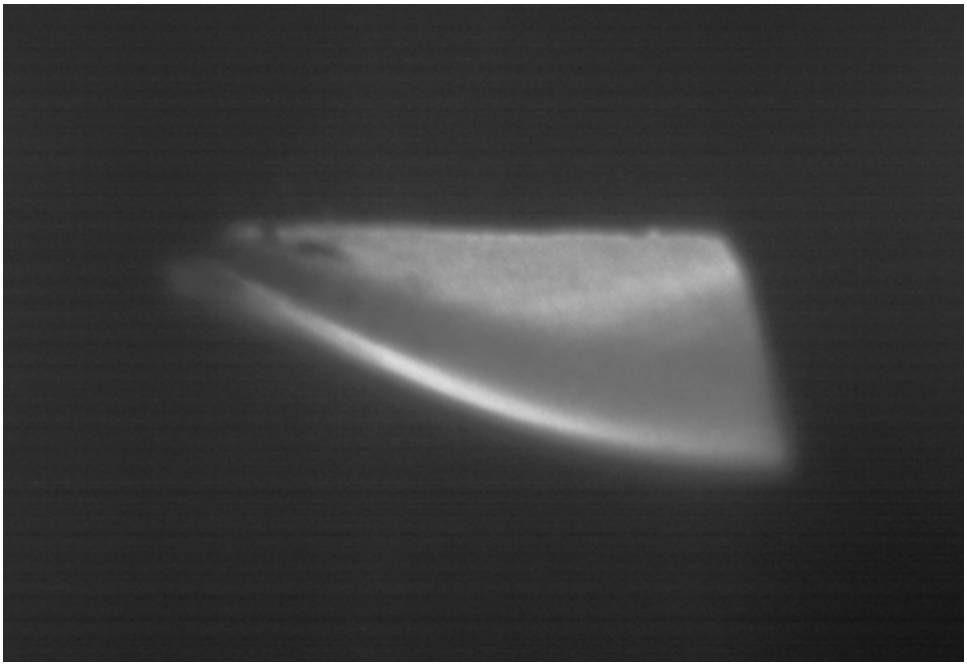

Figure 33. Baseline Mass Flow Rate Full Nozzle Expansion Area Use

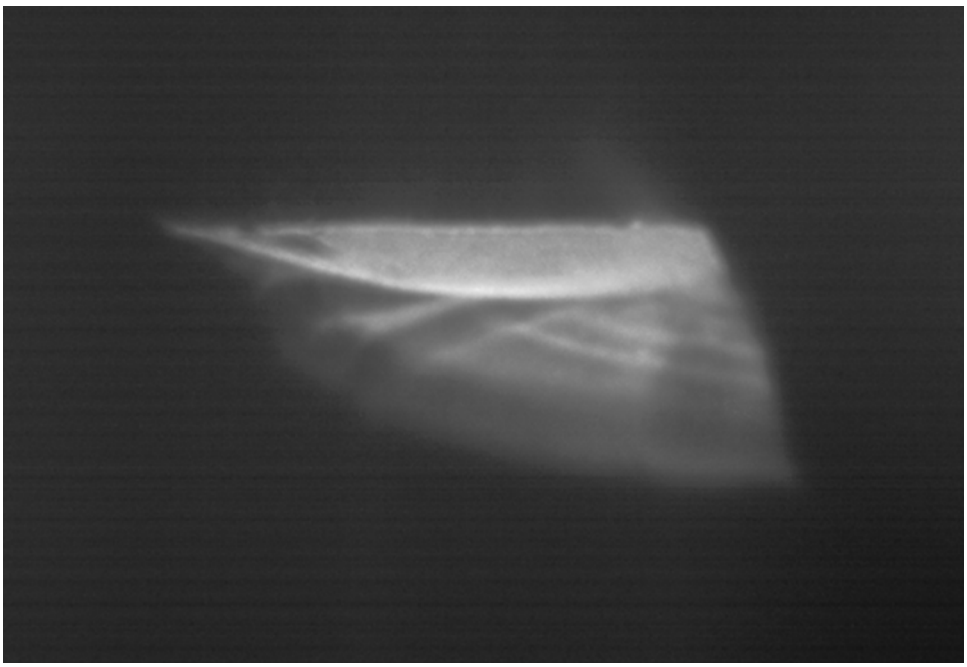

Figure 34. Baseline Mass Flow Rate Flow Separation

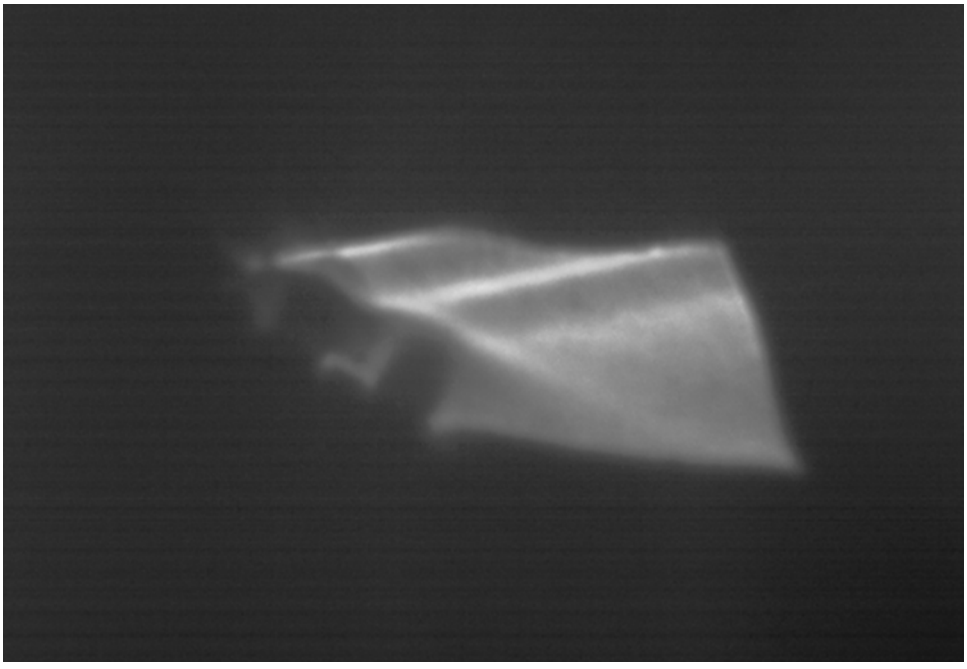

Figure 35. Baseline Mass Flow Rate Secondary Air Injection Zone

Figure 35 depicts the important shape of the secondary air injection zone that will be compared to the baseline mass flow rate fill computer simulations. It is difficult to

determine exactly where the secondary air injection zone resides after injection inlet 3. It is believed that the secondary air injection zone extends more horizontally toward the nozzle exit, which would agree more closely with the computer simulations.

3. 75 Percent of Baseline Mass Flow Rate Utilizing Ethylene

Experiment three used the same testing procedure as experiment two and very similar images were captured. Experiment three was performed at 75 percent of the secondary injection baseline mass flow rate for this set of experimental tests. The height of the secondary injection zone did decrease as expected when compared to the baseline mass flow rate injection case. Images for this experiment were not included as the difference in the secondary air injection height was much more pronounced in the 50 percent injection mass flow rate experiment conducted in experiment four. The settings for this experiment can be seen in Table 3.

Table 3. Settings for 75% of Baseline Mass Flow Rate Fill Testing (Ethylene)

	Node 1	Node 3	Node 4
Gas Controlled	Air	Ethylene	Air
Pressure	5375842 Pa	3293626 Pa	Not Used
Choke Size	19.05 mm	3.99 mm	1.69 mm
Mass Flow Rate	3.61 kg/s	0.01652 kg/s	Not Used

4. 50 Percent of Baseline Mass Flow Rate Utilizing Ethylene

Experiment four used the same testing procedure as experiments two and three with very similar images captured. Experiment three was performed at 50 percent of the baseline mass flow rate for this set of experimental tests. The height of the secondary injection zone decreased as expected when compared to the baseline and 75 percent of baseline mass flow rate of injection cases. The settings for this experiment can be seen in Table 4.

Table 4. Settings for 75% of Baseline Mass Flow Rate Fill Testing (Ethylene)

	Node 1	Node 3	Node 4
Gas Controlled	Air	Ethylene	Air
Pressure	5375842 Pa	2231833 Pa	Not Used
Choke Size	19.05 mm	3.99 mm	1.69 mm
Mass Flow Rate	3.61 kg/s	0.01101 kg/s	Not Used

The same images captured for the baseline mass flow rate experiment can be seen in the following images for the 50 percent of baseline mass flow rate case. These images show the same general shapes as seen in the baseline mass flow rate experiment, but the secondary air injection zone height is much lower than the baseline mass flow rate experiment image as expected.

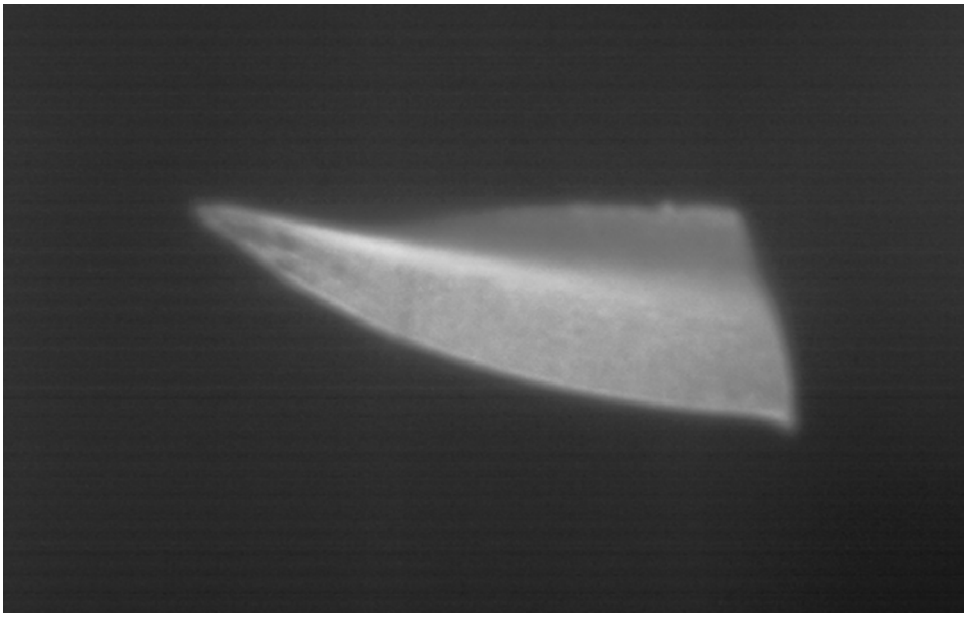

Figure 36. Start of 50 Percent of Baseline Mass Flow Rate Experiment

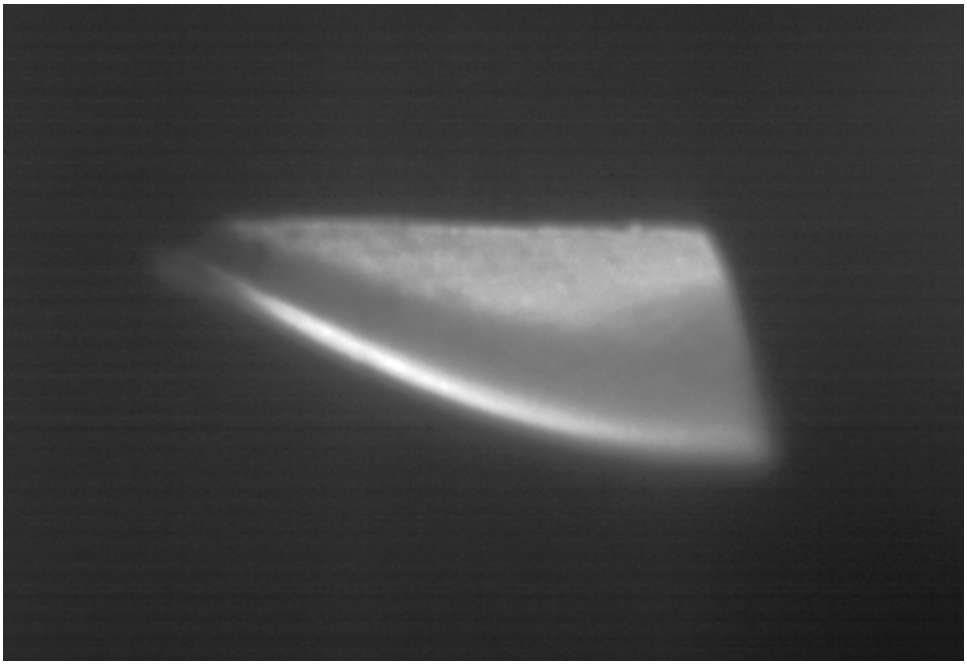

Figure 37. 50 Percent of Baseline Mass Flow Rate Full Nozzle Expansion Area Use

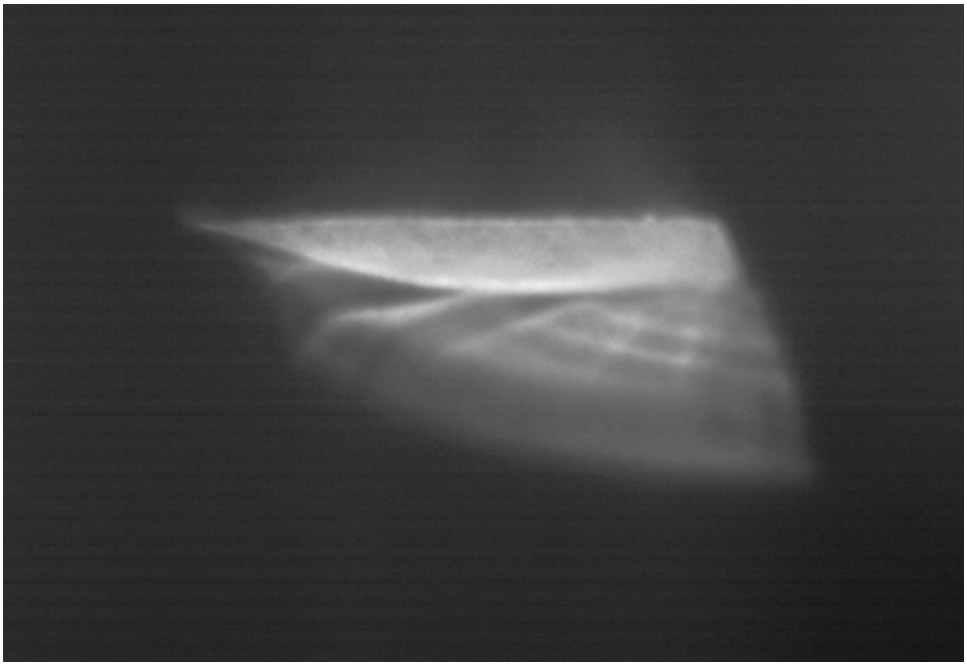

Figure 38. 50 Percent of Baseline Mass Flow Rate Flow Separation

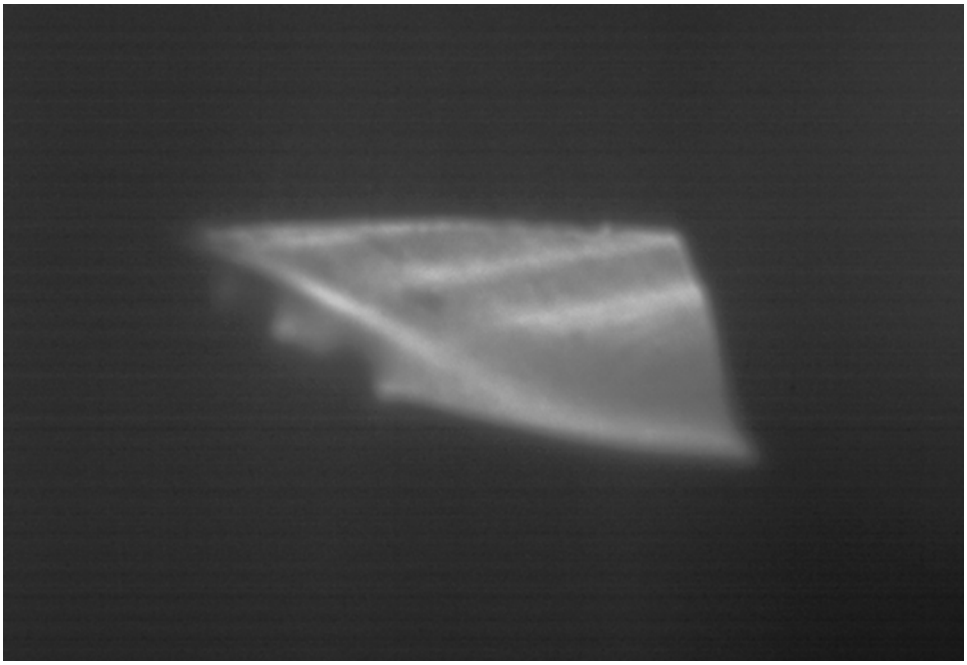

Figure 39. 50 Percent of Baseline Mass Flow Rate Secondary Air Injection Zone

Figure 39 depicts the important shape of the secondary air injection zone that will be compared to the baseline mass flow rate fill computer simulations. It is difficult to determine exactly where the secondary air injection zone resides after injection inlet 3. It is believed that the secondary air injection zone extends more horizontally toward the nozzle exit, which would agree more closely with the computer simulations. It is evident that the secondary air injection zone height is much lower than the height in the baseline mass flow rate experiment.

C. DETONATION TESTING

Due to time constraints and a mishap with one of the glass pieces for the viewing windows, detonation testing was not conducted. Although an extra piece of glass was available for use as a replacement, a proper seal could not be obtained between the glass and the metal of the optical test section. It was determined that the test assembly was unsafe for use at the much higher pressures experienced during the detonation event.

D. SUMMARY

A view of the secondary air injection zone images from the baseline and 50 percent of baseline mass flow rate experiments can be seen side by side in Figure 40 below for comparison.

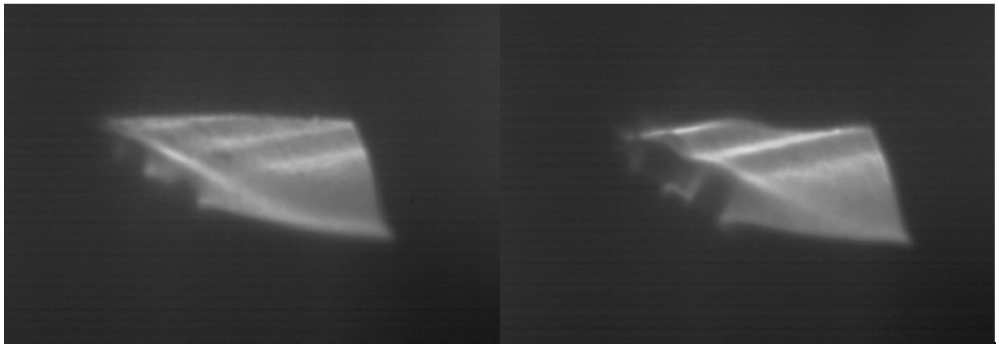

Figure 40. 50 Percent of Baseline (Left) and Baseline (Right)

It is evident that the secondary air injection zone height decreases as injection mass flow rate decreases as seen in the above images. After all of the experiments were completed, it was determined that the injection ports were only 70.9 percent of the targeted flow rate during the baseline injection mass flow rate case even though the flow controller was set to deliver the desired amount. This reduced pressure more closely resembles a 70.9 percent injection mass flow rate case rather than the desired 100 percent injection mass flow rate case. This means that the baseline injection mass flow rate experimental images should be compared to the 75 percent injection mass flow rate fill computer simulation. There was insufficient time to perform all of the experiments again while noting the actual pressure delivered to the injection ports to allow for better comparison to the fill computer simulations.

V. COMPUTER SIMULATION

Computational Fluid Dynamic (CFD) simulations were performed to examine the interaction of the secondary air injection zone during the refresh and detonation event for the various injection angles. Hydrogen (H_2) and air (O_2 + 3.76 N_2) were used as reactants for the computer simulations. The purpose of the simulations was to achieve results that were comparable to the experimental results. This would minimize manufacturing costs of future test specimens by eliminating poor designs from reaching the manufacturing process if computer simulations showed poor results.

Since the test section was approximately a two-dimensional expansion nozzle, two-dimensional simulations were conducted to minimize the computational resources required to solve the simulations while maintaining a high level of solution resolution. Simulations were conducted for each of the 30, 45, and 60-degree injection angle models for the fill phase of the PDE cycle. Another simulation was then conducted for each of the injection angles for the detonation and blow-down phases of the PDE cycle.

Each model consisted of approximately 1.1 million elements in a single plane and was far too large to run on a single processor, especially when chemistry was introduced for the detonation/blow-down phase. Each of the simulations was run on a cluster where 64 processors, each consisting of 2 gigabytes of memory, were utilized for the simulations. The fill phase simulations required approximately 1 day to achieve a solution, while the detonation/blow-down phase simulations required approximately 5 days to achieve a solution.

A. MODELING SOFTWARE

Four different software packages were used for the computer simulation process. SolidWorks 2008 developed by Dassault Systèmes SolidWorks Corporation was used for modeling each of the geometries. A Chemical Equilibrium with Applications (CEA) graphical user interface (GUI) developed by the National Aeronautics and Space Administration (NASA) was downloaded to determine hydrogen/air chemical reaction properties for the detonation event. CFD++ developed by Metacomp Technologies,

Incorporated was then used for creating the mesh and for solving the simulations. Post processing of the results was done utilizing Tecplot 360 developed by Tecplot, Incorporated.

1. SolidWorks 2008

SolidWorks 2008 was used to draw 3D parts for manufacture used during the experimental testing and to draw 2D models for use during the computer simulations. SolidWorks is a 3D mechanical CAD software package that is a parasolid based modeler and incorporates a parametric based approach used to create models. A single plane of the experimental test assembly was drawn using SolidWorks software to accurately simulate the actual conditions of the experimental test assembly with the nozzle insert attached.

There were two deviations from the experimental test assembly dimensions when constructing the simulation models. The ramp inserts were not modeled because they were used to achieve detonation in the experimental test assembly, and detonation was controlled using settings within the CFD++ software discussed in the next section. The other difference was that the shock formation tube and test section length were reduced to 24 inches to reduce computational resources required for the simulations.

Three different models were created for simulating the 30-, 45-, and 60-degree injection angles. The models were saved as parasolid files to allow their incorporation into the CFD++ meshing and simulation software. The 45-degree injection angle model can be seen in Figure 41. The only difference between each of the models is the angle at which the injection air enters the expansion portion of the nozzle.

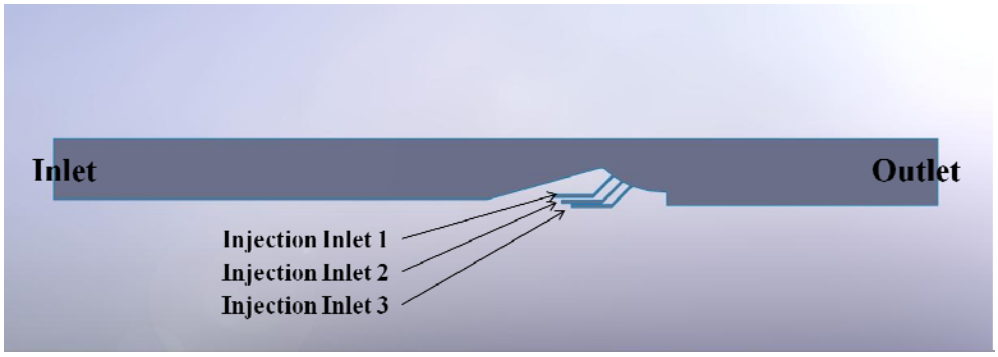

Figure 41. 45 Degree Injection Planar Model

2. NASA CEA GUI

The NASA CEA GUI is a program, which calculates chemical equilibrium product concentrations from any set of reactants and determines thermodynamic and transport properties for the product mixture [12]. The NASA CEA GUI was utilized to determine the CJ pressure, chemical reactants, velocity, and temperature associated with a hydrogen/air detonation reaction at three atmospheres of pressure and a stoichiometric fuel mixture ratio. The results can be seen in Appendix B, and these results were used as input parameters for the CFD++ simulations discussed in the next section.

3. CFD++

All of the CFD simulations were performed using CFD++ developed by Metacomp Technologies, Inc., on a Linux operating system. Prior to performing the CFD simulations, each of the SolidWorks parasolid models was meshed using MIME provided in the CFD++ software package.

The boundary conditions were setup as illustrated in Figure 41 from the SolidWorks section above. The opening on the left of the model was the Inlet, and the opening on the right of the model was the Outlet. The top injection port was Injinlet1, the middle was Injinlet2, and the bottom was Injinlet3. The top wall was called Symmetry from early models where the wall was treated as a symmetry condition. All other edges were the Walls boundary condition, and a q-L turbulence model was utilized.

The CFD++ software allowed for initial conditions for the model to be specified. It was possible to create different regions of the model defined by boxes and apply separate initial conditions to each of the boxes independently. Figure 42 shows how the boxes were setup for the 45-degree injection model by utilizing 6 separate boxes. Box 1 is the thin box outlined in red at the inlet of the model. The next box that covered the combustion chamber and test section to the beginning of the nozzle was Box 2 outlined in green. Box 4 outlined in yellow then covered the first half of the nozzle convergence section. Box 6 outlined in purple then covered the second half of the nozzle convergence section and ended almost at the throat of the nozzle. Box 6 outlined in light blue covered the divergence section of the nozzle and the exhaust tube. Box 3 was constructed to cover all three of the injection inlets.

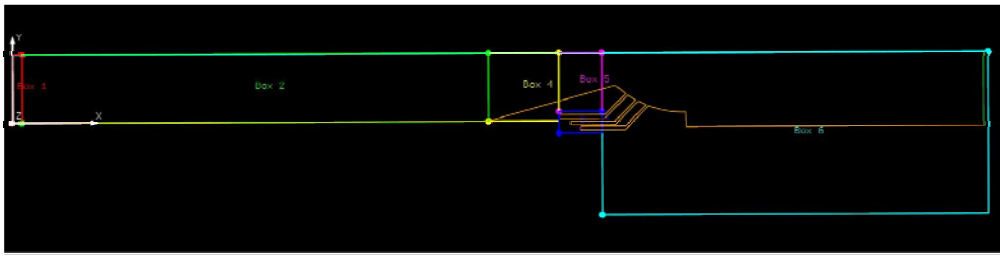

Figure 42. CFD++ Initial Condition Boxes

Two separate simulations were performed for each of the models. The first simulation, referred to as the fill simulation, allowed the reactants to be distributed throughout the model as they were in the experimental tests. Once the reactants filled to the exit of the nozzle, this output file was used as the starting point for the second simulation, referred to as the detonation simulation. In addition to the two standard simulations for the 45 degree injection angle, fill simulations were also performed at 0, 25, 50, 75, and 125 percent of the original injection mass flow rate by reducing or increasing the injection velocity to 25, 50, 75, and 125 percent of the baseline value respectively to determine the effects of mass flow rate on the secondary air injection zone formation. The injection inlet boundary conditions were change to a wall for the 0

percent injection mass flow rate condition. Detonation simulations were also performed for the 45-degree injection angle for 50 and 75 percent of the baseline injection mass flow rate.

A brief description of the boundary conditions for each of the two types of simulations can be found in the tables of the respective sections. A more detailed description of the boundary conditions, initial conditions of the specific boxes, chemistry conditions, and solver settings can be found in Appendices C and D.

a. Fill Simulations

For the fill simulations, the inlet was assigned a boundary condition of a multi-species pressure volume based inflow/outflow condition. This allowed the reactants to travel down the chamber and through the nozzle as was performed for the experimental testing. A general description of the boundary conditions assigned can be seen in Tables 5 and 6.

Table 5. Boundary Conditions for Fill Simulations of 25, 50, 75, 100, and 125 Percent of Original Injection Mass Flow Rate

Name	Boundary Condition
Inlet	Multi-species Pressure/Velocity Based Inflow/Outflow
Outlet	Simple Back Pressure
Injinlet1, Injinlet2, and Injinlet3	Pressure, Temperature, and Normal Velocity Inflow
Symmetry and Walls	Multi-species Adiabatic Wall

Table 6. Boundary Conditions for Fill Simulation of 0 Percent of Original Injection Mass Flow Rate

Name	Boundary Condition
Inlet	Multi-species Pressure/Velocity Based Inflow/Outflow
Outlet	Simple Back Pressure
Injinlet1, Injinlet2, and Injinlet3	Multi-species Adiabatic Wall
Symmetry and Walls	Multi-species Adiabatic Wall

For the initial fill simulations, Box 1 was filled with reactants and allowed to flow down the model as the simulation progressed. All of the other boxes were filled with air by specifying the oxygen mass fraction. This allowed the reactants to be introduced into the model up to the nozzle exit and was used as the starting point for the detonation simulations. All of the fill simulations for the various injection angles were performed in this same manner.

b. Detonation Simulations

For the detonation simulations, Box 1 was filled with combustion products at four times the Chapman-Jouget pressure to cause a detonation. This was done by using the desired output file from the fill simulation and overwriting the conditions of Box 1. The inlet boundary condition was also changed to a multi-species adiabatic wall condition to simulate the closing of the fill valve in a PDE and to better simulate the conditions of the experimental testing. The simulation was then run to see a detonation travel down the combustion chamber through the nozzle followed by blow-down back to the original three atmosphere starting pressure of the fill simulation. A brief description of the boundary conditions assigned can be seen in Table 7.

Table 7. Boundary Conditions for Detonation Simulations

Name	Boundary Condition
Inlet	Multi-species Adiabatic Wall
Outlet	Simple Back Pressure
Injinlet1, Injinlet2, and Injinlet3	Pressure, Temperature, and Normal Velocity Inflow
Symmetry and Walls	Multi-species Adiabatic Wall

4. Tecplot 360

Tecplot 360 developed by Tecplot, Inc., was used for all simulation post processing. The CFD++ software had post processing capability, but this had to be done on a Linux operating system. The image resolution also seemed to be much better with the Tecplot 360 software and allowed schlieren images to be seen from the CFD++ simulations. This was very helpful when comparing experimental results to computer simulation results because all of the experimental result images were obtained using a shadowgraph method very similar to the schlieren method.

B. SIMULATION RESULTS

1. Fill Simulations

The fill simulations were analyzed at the 7.0 millisecond time step of the simulation. This time step was chosen because it was the point at which the reactants had sufficient time to travel to the nozzle exit plane, and this time step was used as the starting condition for the detonation simulations. The height of the secondary air injection zone was then obtained using the probing tool of Tecplot 360 at the nozzle exit plane for comparison between each of the different injection mass flow rates simulated.

A separate analysis of the case with zero secondary mass injection was performed at the 8.3 millisecond time step of the simulation. This time step was chosen because the secondary air injection zone had fully developed with minimal oscillations in height. The secondary air injection zone height was again obtained using the probing tool of Tecplot 360 at the nozzle exit plane. This time step was used as the baseline secondary air injection zone height.

The following figures generated by Tecplot 360 were used for obtaining the secondary air injection zone heights. The images show the Mach number profile as this was the best representation of the secondary air injection zone formation. The secondary air injection zone height was considered the vertical distance at the nozzle exit plane from the lip of the nozzle exit to the forward most velocity stream line exiting injection inlet 1. If no velocity stream line was present from injection inlet 1, the upper limit for the secondary injection zone height was considered the color transition from light blue to green as this was the subsonic to supersonic transition.

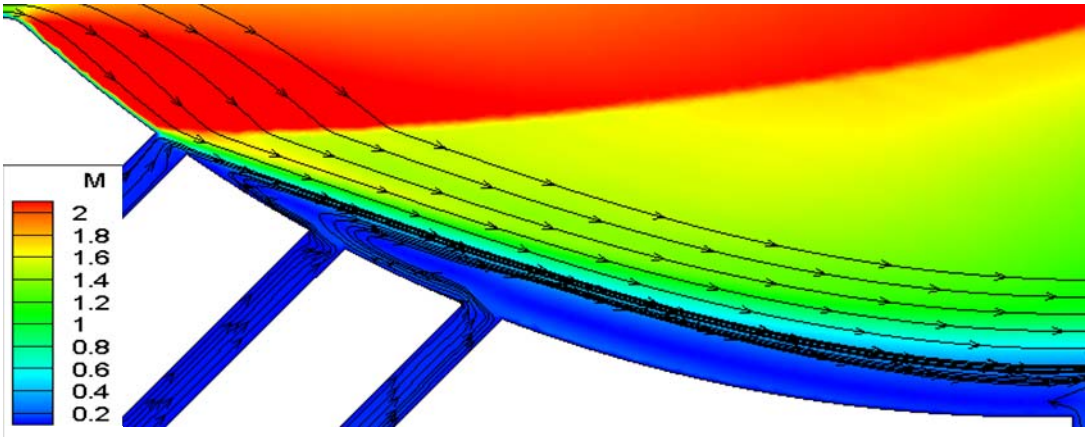

Figure 43. Fill Simulation 0 Percent of Baseline Mass Flow Rate at 7 milliseconds

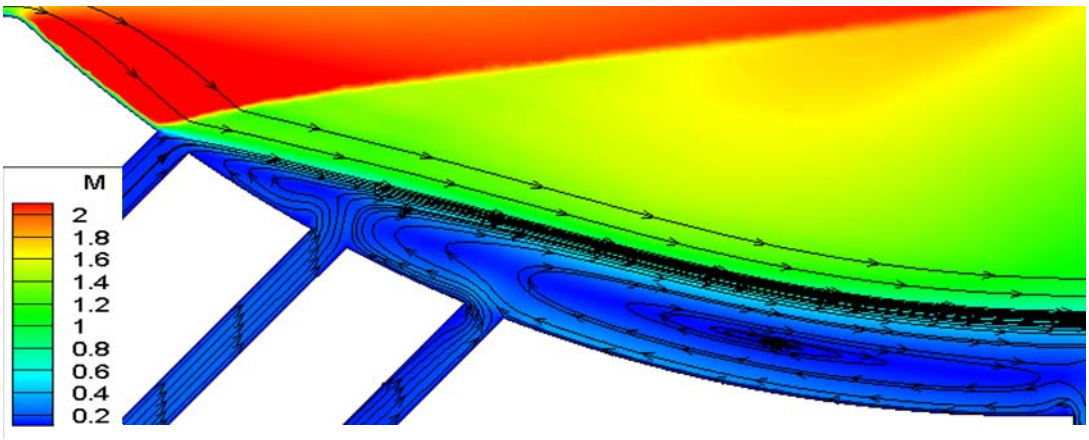

Figure 44. Fill Simulation 25 Percent of Baseline Mass Flow Rate at 7 milliseconds

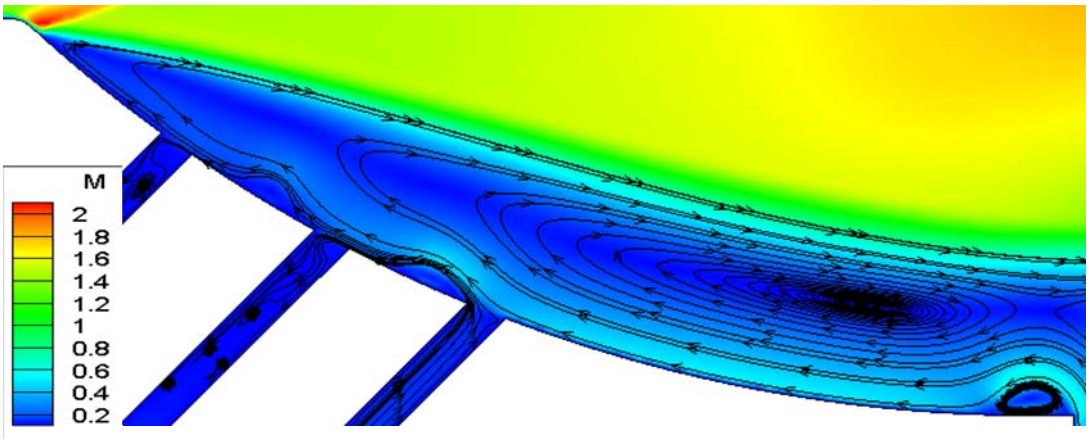

Figure 45. Fill Simulation 50 Percent of Baseline Mass Flow Rate at 7 milliseconds

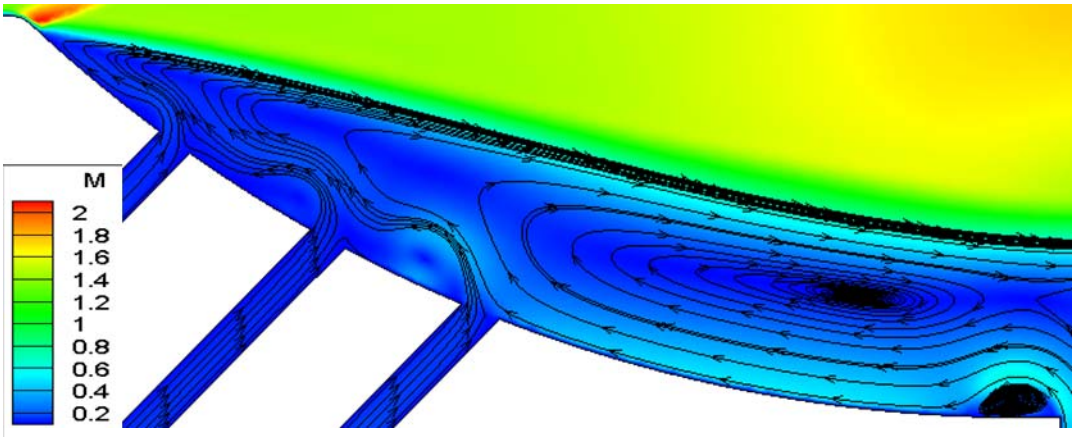

Figure 46. Fill Simulation 75 Percent of Baseline Mass Flow Rate at 7 milliseconds

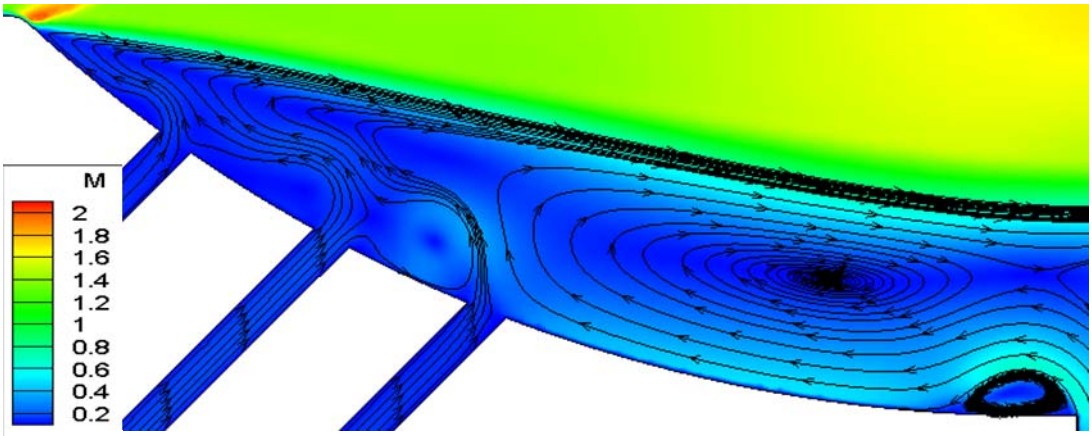

Figure 47. Fill Simulation 100 Percent of Baseline Mass Flow Rate at 7 milliseconds

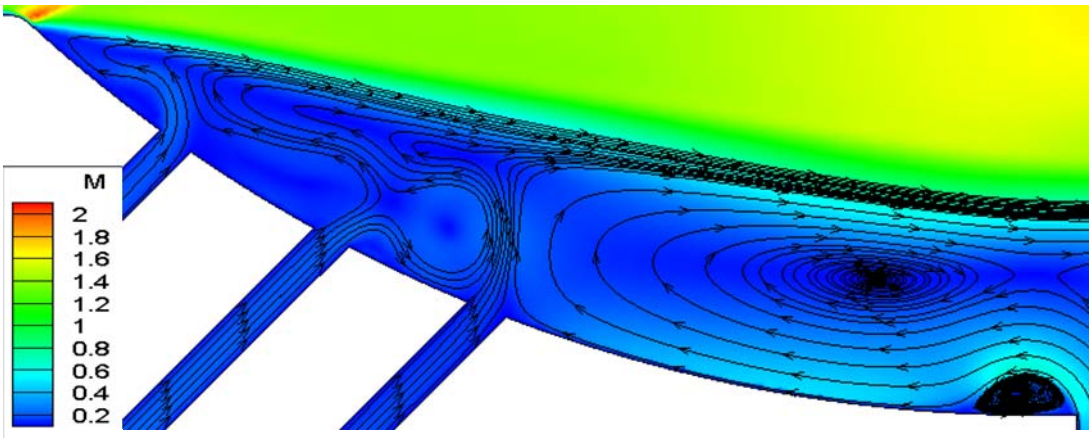

Figure 48. Fill Simulation 125 Percent of Baseline Mass Flow Rate at 7 milliseconds

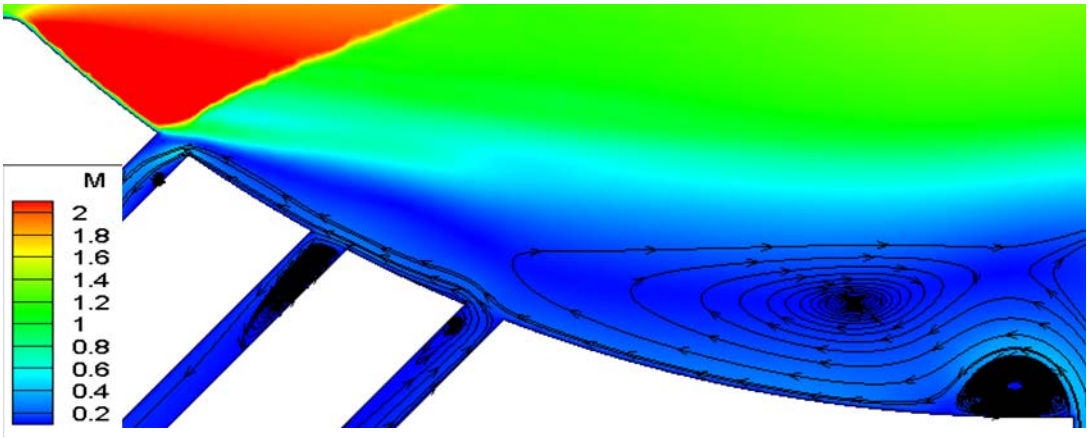

Figure 49. Fill Simulation 0 Percent of Baseline Mass Flow Rate at 8.3 milliseconds

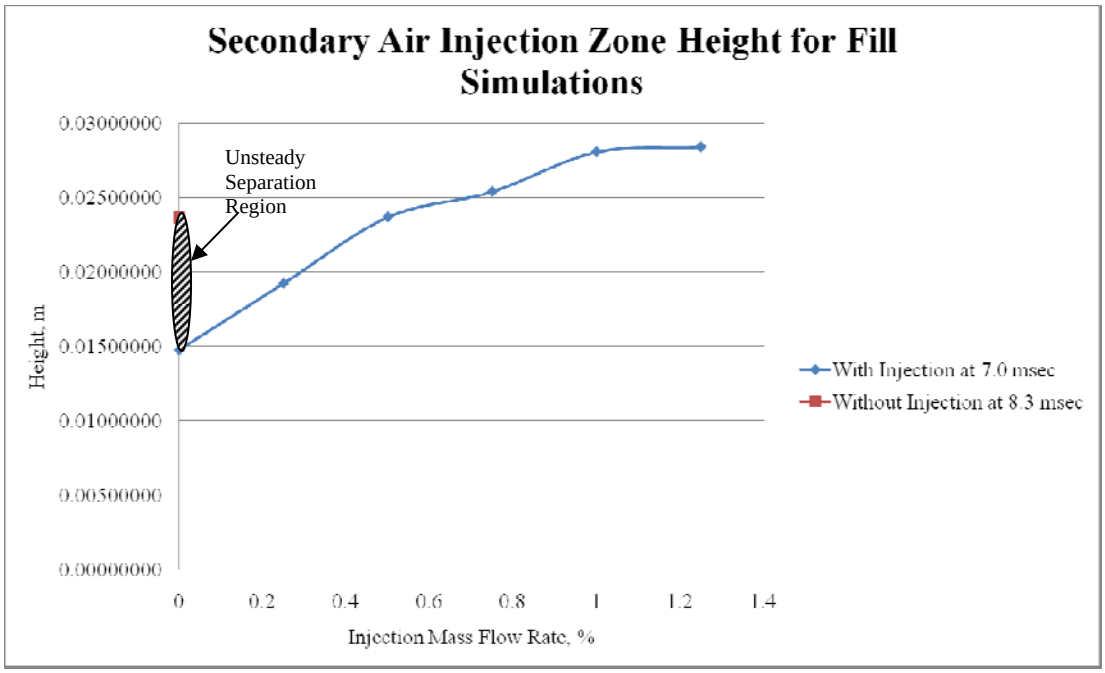

Figure 50. Plot of Secondary Air Injection Zone Height for Fill Simulations versus Percent Injection Mass Flow Rate

Figure 50 shows how the secondary air injection zone height changed for different injection mass flow rates at a 45-degree injection angle. By treating the 0 percent of baseline mass flow rate as the control case, it was possible to determine when the injection mass flow rate began affecting the secondary air injection zone height rather than being due to flow separation alone. The upper point of the unsteady separation region depicted in Figure 50 was determined by selecting the largest secondary injection zone height seen during the 0 percent of baseline mass flow rate simulation, which occurred at 8.3 msec. The conclusion was that the height of the secondary air injection zone was not affected by injection mass flow rate until the injection mass flow rate was greater than 50 percent of baseline mass flow rate. It was also noted that the secondary air injection zone height changed very little when the injection mass flow rate was increased from baseline to 125 percent of baseline mass flow rate. Further analysis with injection air mass flow rate greater than 125 percent of baseline is recommended but was not possible due to time constraints.

2. Detonation Simulations

Detonation simulations for the 30-, 45-, and 60-degree injection angles with baseline injection mass flow rate were conducted and analyzed in a similar manner as the fill simulations. Two additional detonation simulations for the 45-degree injection angle with 50 and 75 percent of baseline mass flow rate were also performed, but these results were not analyzed due to a lack of sufficient time.

The following figures illustrate how the secondary air injection zone changes as the detonation passes through the nozzle for the 45-degree injection angle with baseline injection mass flow rate cases. Figures for the 30 and 60-degree injection angle are not included but behaved in a very similar manner. The figures illustrate the events that occur as the detonation travels through the diverging section of the nozzle, and it is clear that the detonation removes the secondary air injection zone allowing for a maximum nozzle area expansion ratio of the fixed nozzle to be utilized. Subsequent reformation of the secondary air injection zone is also evident.

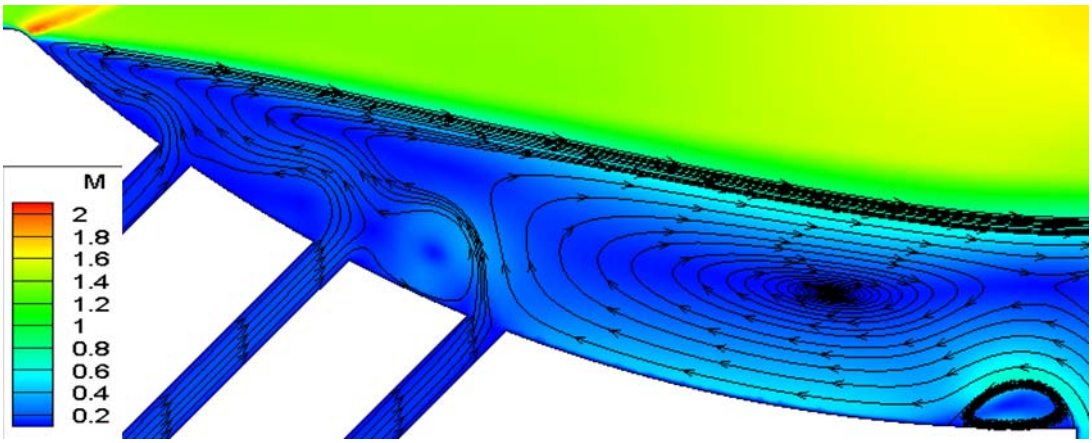

Figure 51. Detonation Simulation at 10 microseconds

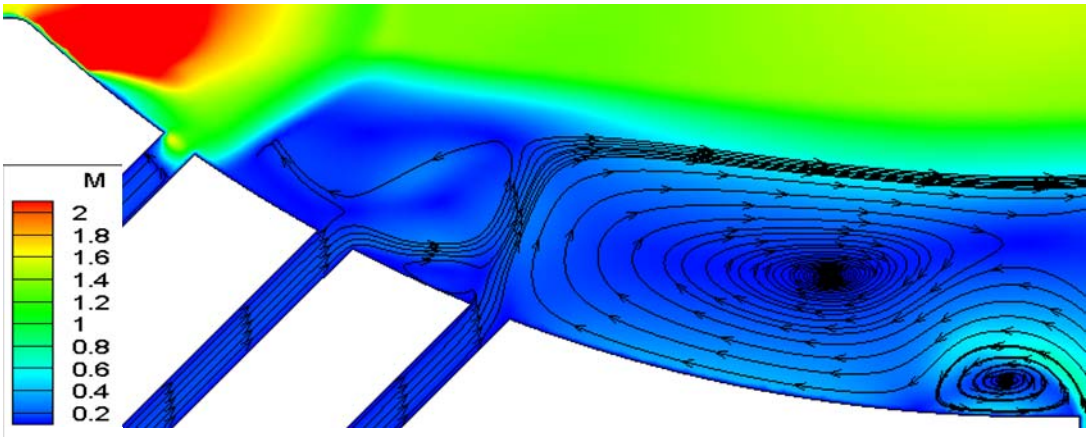

Figure 52. Detonation Simulation at 300 microseconds

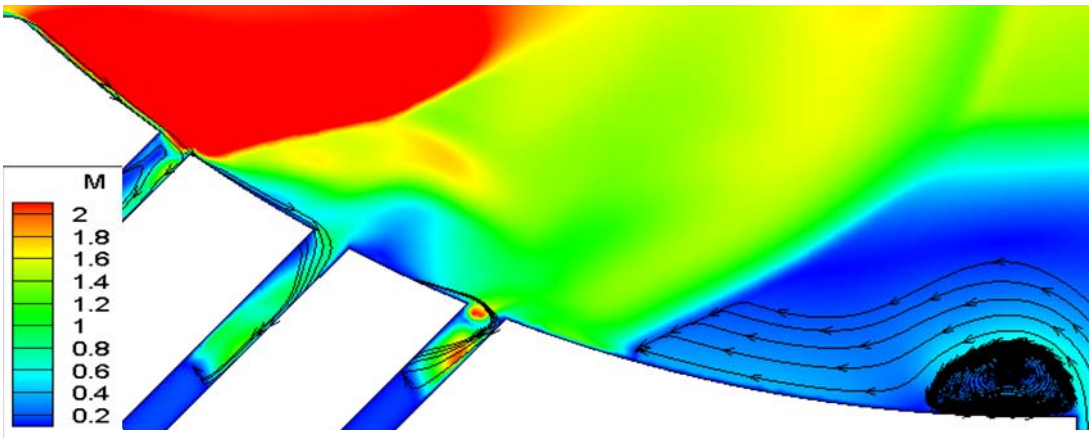

Figure 53. Detonation Simulation 320 microseconds

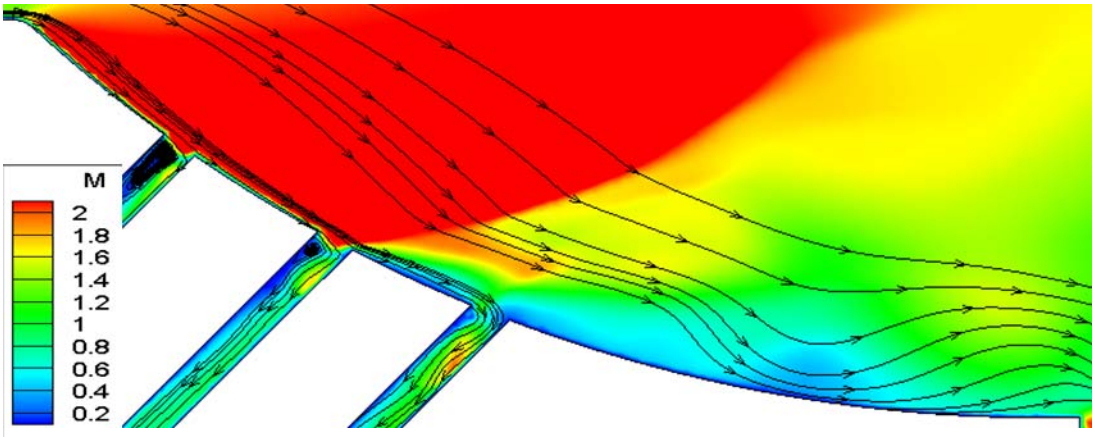

Figure 54. Detonation Simulation at 340 microseconds

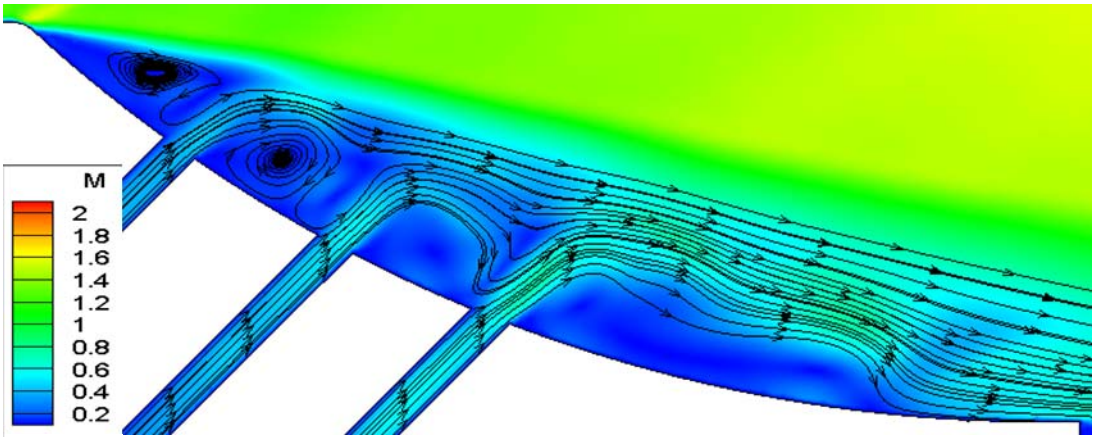

Figure 55. Detonation Simulation at 3.4 milliseconds

The detonation simulations were analyzed in a slightly different manner than the fill simulations. In the same way as with the fill simulations, the secondary air injection zone height was found using Tecplot 360. The secondary air injection zone height was then converted to a nozzle area expansion ratio that was compared to the nozzle area expansion ratio of the fixed nozzle with no injection. In addition, the pressures at the centerline of the nozzle inlet and exit plane were also determined and then plotted. The centerline was considered the vertical distance half way between the nozzle throat and the top wall (symmetry) for the simulations. All of these data points were plotted versus time to show how the secondary air injection zone reacted to the conditions at specific instances in time. The following figures show the resulting plots for the 45-degree injection angle with baseline injection mass flow rate. The resulting plots for the 30-, 45-, and 60-degree injection angle cases can be found with increased resolution in Appendix E, and each data point plotted can be found in Appendix F.

For each of the plots, data was taken every 100 microseconds with an exception between 200 and 450 microseconds where data was taken every 10 microseconds. Data was also collected at 10 and 500 microseconds of the event. This was done to better capture the highly dynamic pressure transients as the detonation traveled from the nozzle inlet plane to the nozzle exit plane. The data for each of the following plots was taken as close as possible to the points found in Table 8.

Table 8. Coordinates for Data Collection

	X Value (m)	Y Value (m)
Pressure at Nozzle Inlet Centerline	0.609088	0.0652304
Pressure at Nozzle Exit Centerline	0.862743	0.0652304
Secondary Air Injection Zone Height	0.862743	N/A

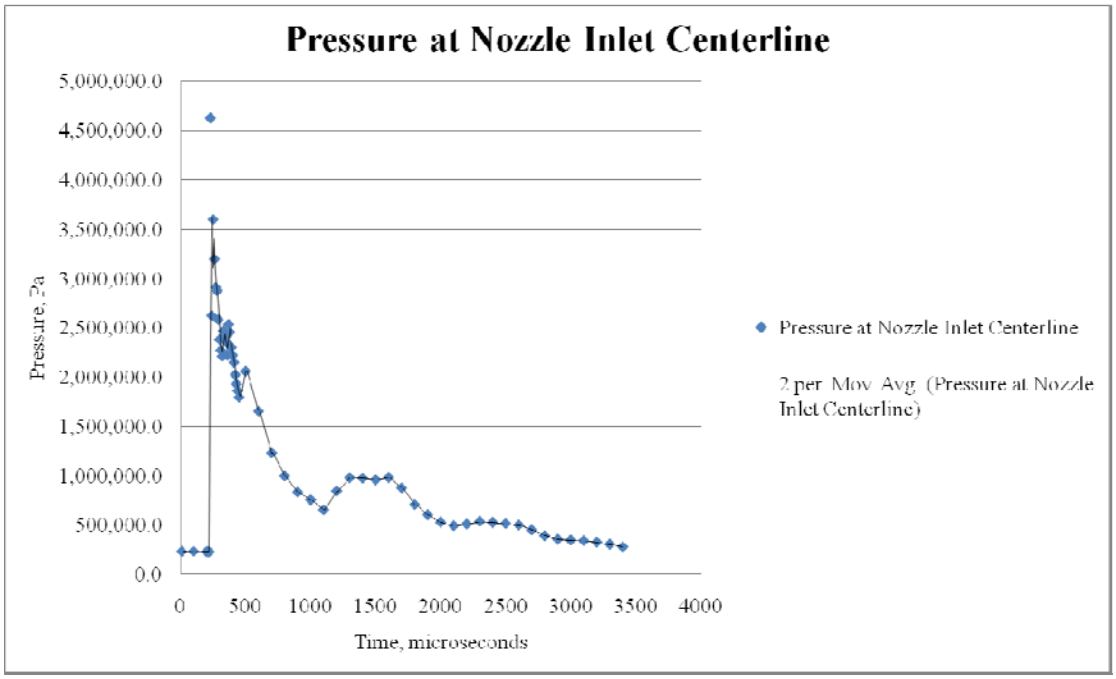

Figure 56. Pressure at Nozzle Inlet Centerline versus Time

Figure 56 shows the typical pressure trend of a PDE at the nozzle inlet and closely resembles expected trends. The sawtooth-like decay of the pressure is visible in the 200 to 500 microsecond region where data was plotted more frequently. A two period moving average trend line was fit to the data in an attempt to allow a better visualization of the phenomenon occurring.

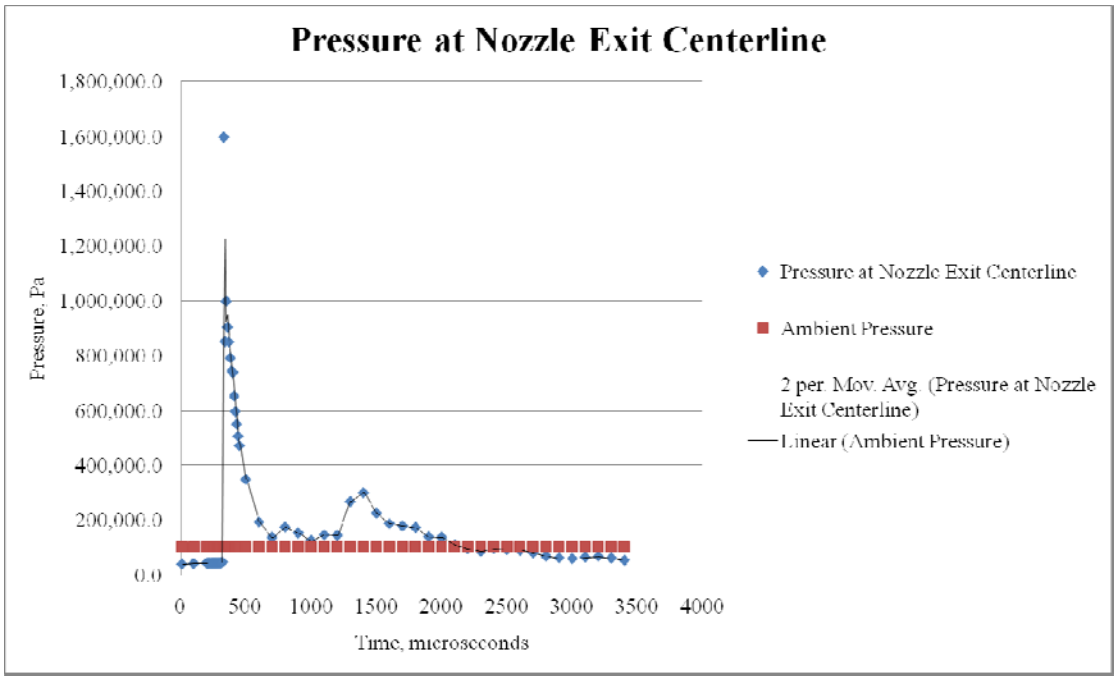

Figure 57. Pressure at Nozzle Exit Centerline versus Time

Figure 57 shows an extreme pressure spike as the detonation traveled through the nozzle exit as expected. The second pressure spike at the 1400 microsecond time point is due to the ring down of the original pressure wave traveling forward, being reflected off the forward wall of the combustion chamber, and subsequently travelling back through the nozzle exit.

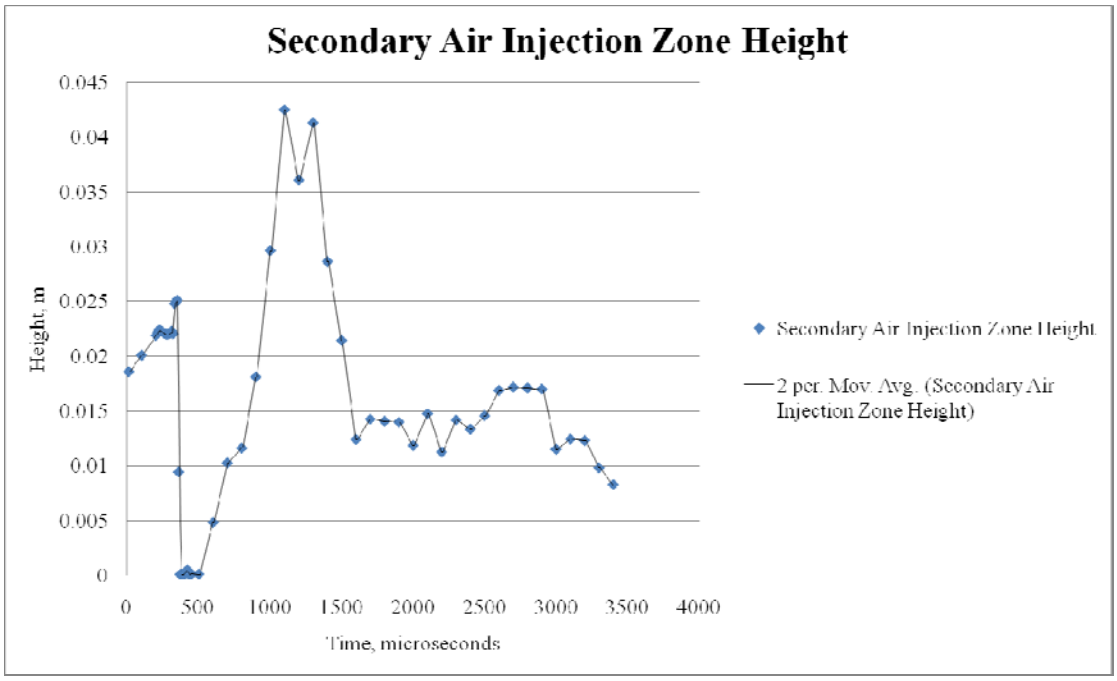

Figure 58. Secondary Air Injection Zone Height versus Time

Figure 58 depicts the secondary air injection zone height during the event. When higher pressures were experienced at the nozzle exit, the secondary air injection zone height decreased rapidly as expected. The opposite was also true where the secondary air injection zone height rapidly increased as the pressure at the nozzle exit decreased. The secondary air injection zone height did not reach a steady state condition after the detonation passed due to the transient blow-down dynamics.

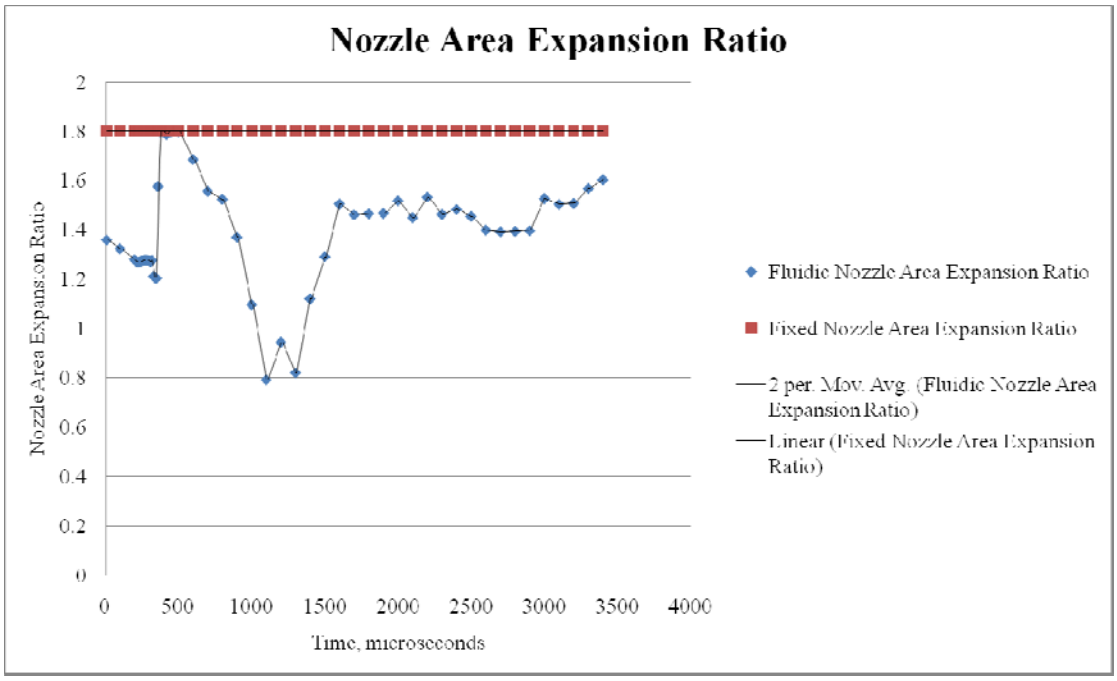

Figure 59. Nozzle Area Expansion Ratio versus Time

Figure 59 offers a comparison between the actual nozzle area expansion ratio achieved when injection was utilized and the fixed nozzle with no injection utilized. It is clear from this figure how the larger fixed nozzle area expansion ratio is only required for a very small portion of time. It is also clear that the fluidic nozzle's area expansion ratio was able to change very quickly as the conditions changed.

An additional piece of information that could be helpful when designing the injection angle and the amount of injection mass flow rate to use is a means of determining how the nozzle is performing. This could be done by utilizing a dimensionless nozzle deviation factor (NDF), which determines the deviation from optimal conditions where the nozzle exit pressure is equal to the ambient pressure. Equation 13, which is similar to the trapezoidal rule, depicts the method utilized in this thesis, and the results for the 30, 45, and 60-degree injection angle cases can be found in Table 9.

$$NDF = \left(\frac{1}{p_3 t_{total}}\right)\sum_{n=1}^{\infty}\frac{\left|p_{2,n}-p_3\right|+\left|p_{2,n+1}-p_3\right|}{2}\left(t_{n+1}-t_n\right) \qquad (13)$$

Table 9. Detonation Simulation Nozzle Factors

Injection Angle	Percent Injection Mass Flow Rate	Nozzle Deviation Factor
30	100	0.768971
45	100	0.822494
60	100	0.981825

The calculation of the nozzle deviation factor does not give an exact deviation but does attempt to provide a quantitative metric for making appropriate design decisions. A lower nozzle performance loss factor is better with an ideal nozzle having a nozzle deviation factor of zero. From the results in Table 9, the 30-degree injection angle nozzle would be the preferred nozzle based on the data collected during the detonation simulations. This same concept of nozzle deviation factor could be applied to the different injection mass flow rate cases to determine the correct injection mass flow rate to utilize. The nozzle deviation factor could also be used on different geometries and for different time durations than those used in the detonation computer simulations of this thesis because the nozzle deviation factor is dimensionless.

THIS PAGE INTENTIONALLY LEFT BLANK

VI. CONCLUSIONS AND FUTURE WORK

A. CONCLUSIONS

This thesis explored the use of a fluidic nozzle configuration in an attempt to maintain optimal nozzle performance during all phases of a PDE cycle. Experimental tests without detonation were conducted at various injection mass flow rates for a 45-degree injection angle fluidic nozzle, and images were captured using a shadowgraph technique. A complete matrix analyzing injection angle and mass flow rate simultaneously was not completed due to insufficient time, however promising results were seen as the secondary air injection zone height increased as injection mass flow rate was increased and decreased as the injection air mass flow rate was decreased. Optimization of the secondary air injection parameters would require further analysis due to the inherent dependence of nozzle operation at a particular flight condition and engine operating parameters.

Computer simulations were performed for various injection mass flow rates with various injection angles for fill and detonation phases of the PDE cycle. The images from the computer simulations for the fill conditions were in good agreement with the images from the fill experiments and validated the computer simulation technique utilized. The computer simulations allowed for investigation of flow field characteristics at specific points for further analysis during the detonation testing and allowed for visualization of how the fluidic nozzle designs demonstrated the ability to effectively change over time to maintain optimum performance.

A metric for determining the deviation from optimal performance for a PDE nozzle was determined with the Nozzle Deviation Factor (NDF) that can be used for nozzle performance comparisons. Because the Nozzle Deviation Factor is dimensionless, it can be applied to any nozzle geometry and for any time duration.

B. FUTURE WORK

The computer simulation results and plots of this thesis show that further analysis on different injection mass flow rates and injection angles could improve the performance

of the fluidic nozzle. Data is available for analyzing both 50 and 75 percent of baseline mass flow rates and compared to the baseline injection mass flow rate results utilizing the nozzle performance loss factor that were not analyzed in this thesis due to time constraints. Another item to consider is varying the longitudinal location of the injection sites and analyzing the results for comparison.

Experimental detonation testing should be performed, and a three-dimensional computer simulation should be conducted for a more exact comparison of resultant data once the design parameters concerning the injection angle, injection mass flow rate, and longitudinal injection location have been refined. This would allow for an exact comparison of experimental to computer simulation results.

APPENDIX A: DRAWINGS FOR MANUFACTURE

A. NOZZLE MOUNTING STRUCTURE DRAWINGS

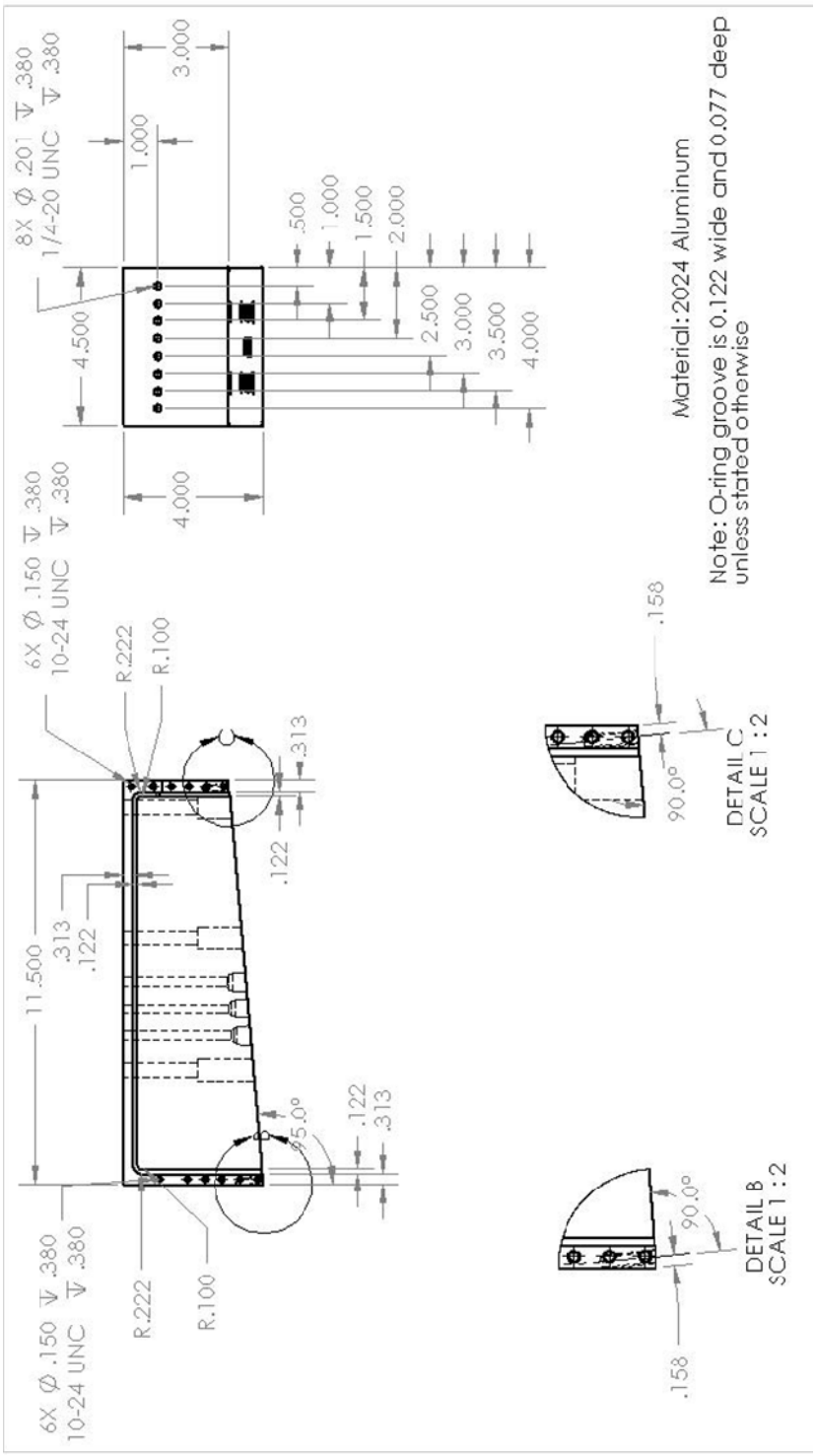

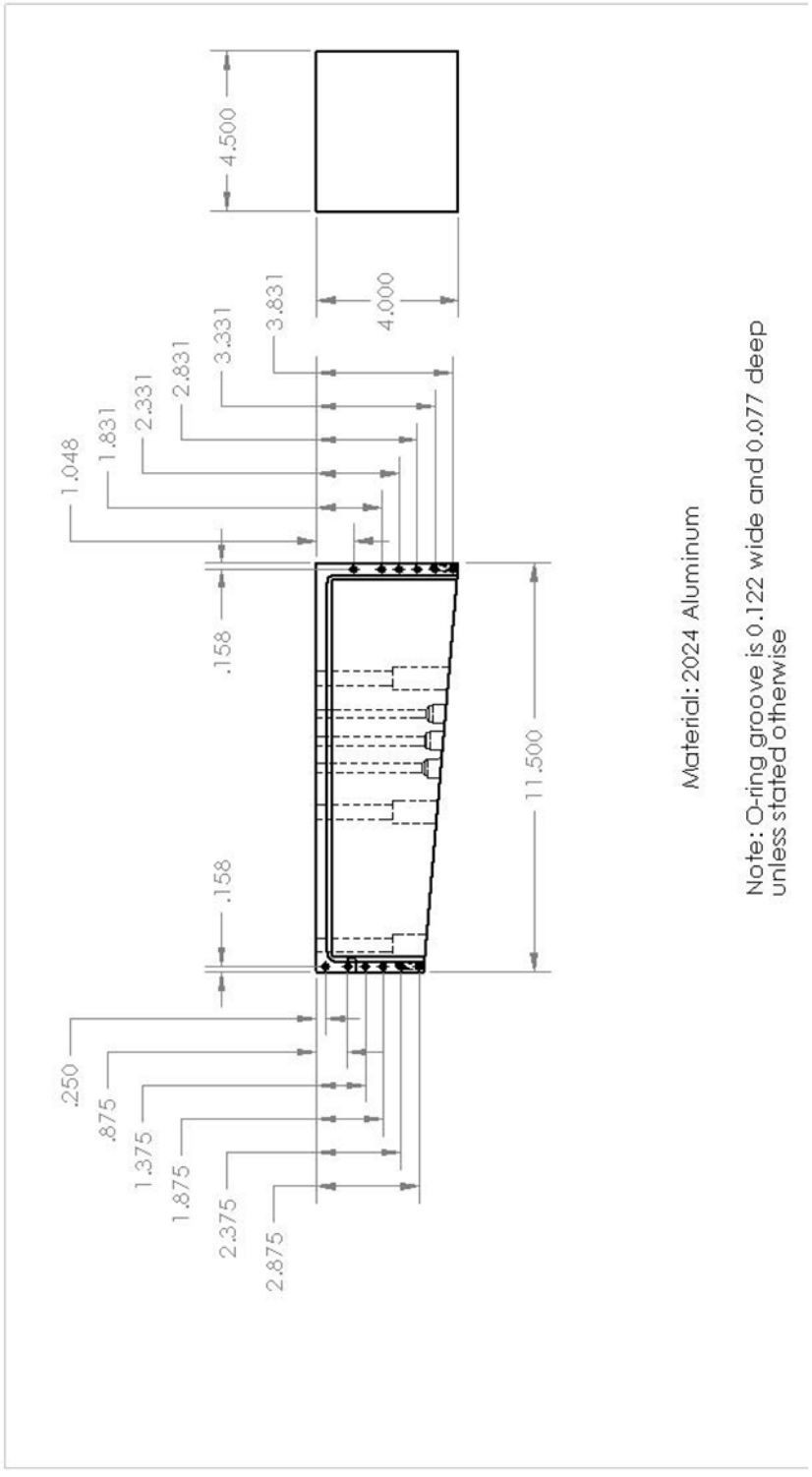
4.500
4.000
3.831
3.331
2.831
2.331
1.831
1.048
.158
11.500
.158
.250
.875
1.375
1.875
2.375
2.875
Material: 2024 Aluminum
Note: O-ring groove is 0.122 wide and 0.077 deep
unless stated otherwise

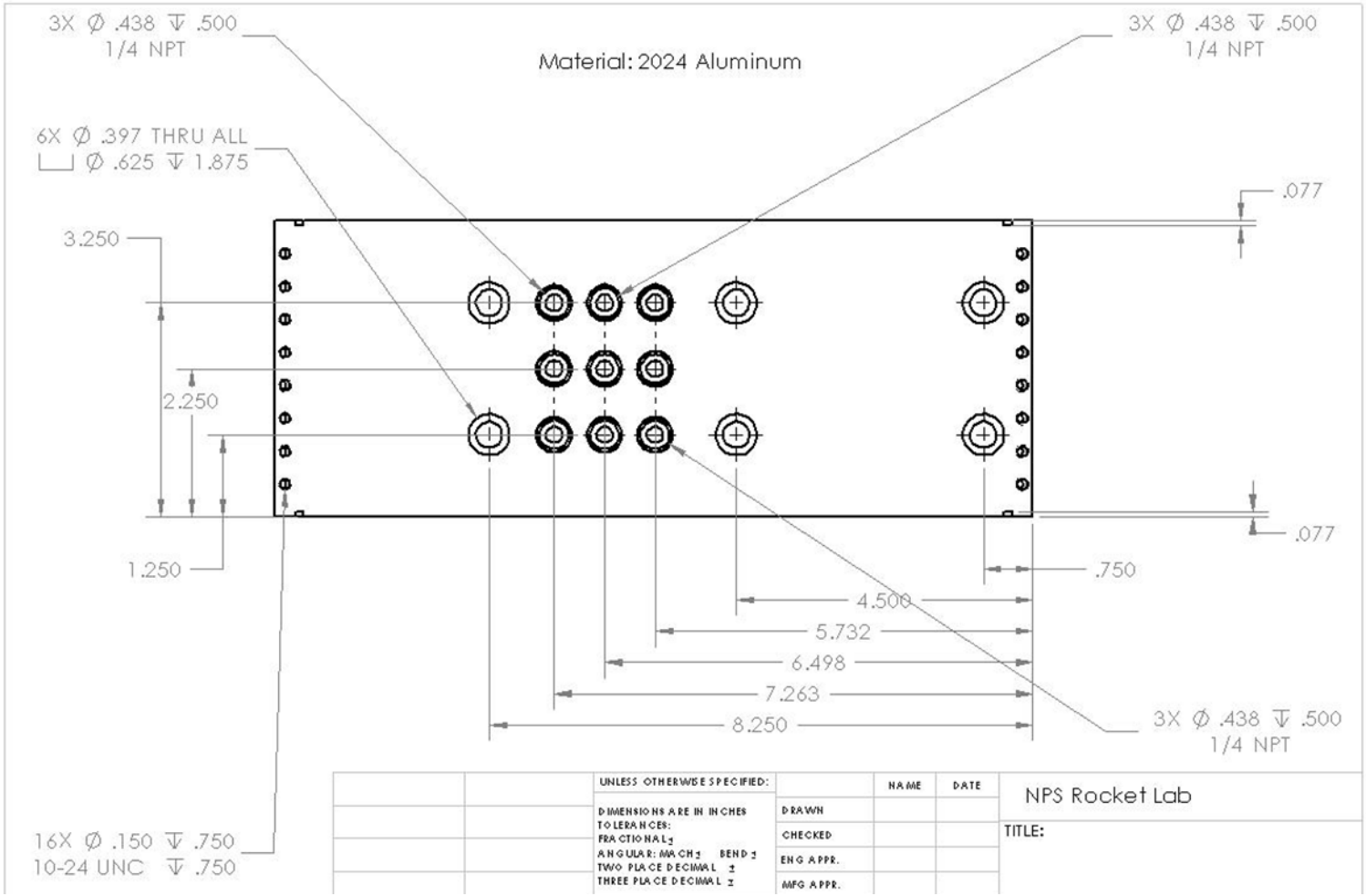
3X Ø .438 ↧ .500
1/4 NPT
Material: 2024 Aluminum
3X Ø .438 ↧ .500
1/4 NPT
6X Ø .397 THRU ALL
⌴ Ø .625 ↧ 1.875
.077
3.250
2.250
1.250
.077
.750
4.500
5.732
6.498
7.263
8.250
3X Ø .438 ↧ .500
1/4 NPT
16X Ø .150 ↧ .750
10-24 UNC ↧ .750
UNLESS OTHERWISE SPECIFIED:
DIMENSIONS ARE IN INCHES
TOLERANCES:
FRACTIONAL ±
ANGULAR: MACH ± BEND ±
TWO PLACE DECIMAL ±
THREE PLACE DECIMAL ±
NAME
DATE
DRAWN
CHECKED
ENG APPR.
MFG APPR.
NPS Rocket Lab
TITLE:

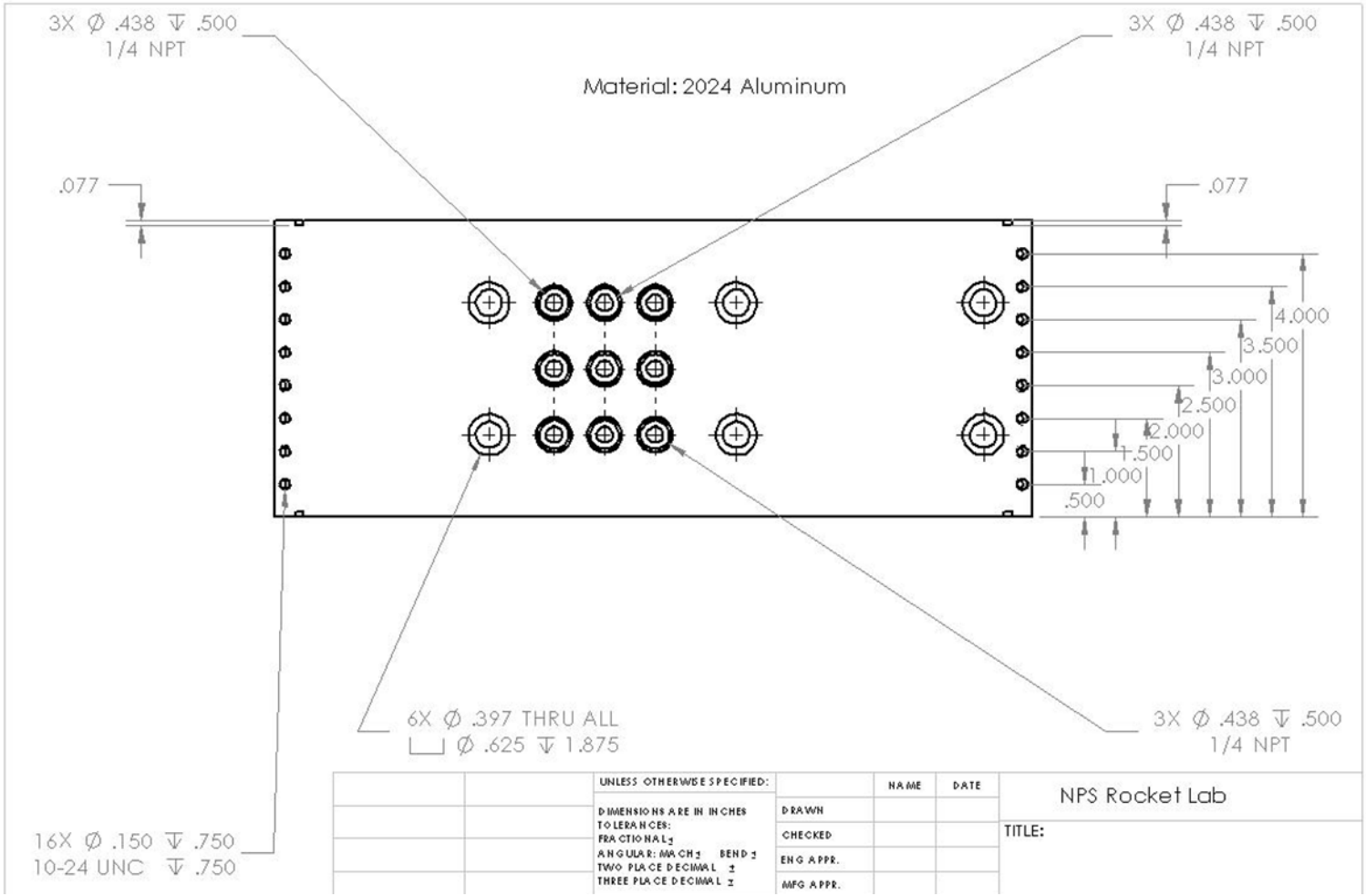
3X Ø .438 ↧ .500
1/4 NPT
Material: 2024 Aluminum
3X Ø .438 ↧ .500
1/4 NPT
.077
.077
4.000
3.500
3.000
2.500
2.000
1.500
1.000
.500
6X Ø .397 THRU ALL
⌴ Ø .625 ↧ 1.875
3X Ø .438 ↧ .500
1/4 NPT
16X Ø .150 ↧ .750
10-24 UNC ↧ .750
UNLESS OTHERWISE SPECIFIED:
DIMENSIONS ARE IN INCHES
TOLERANCES:
FRACTIONAL ±
ANGULAR: MACH ± BEND ±
TWO PLACE DECIMAL ±
THREE PLACE DECIMAL ±
DRAWN
CHECKED
ENG APPR.
MFG APPR.
NAME
DATE
NPS Rocket Lab
TITLE:

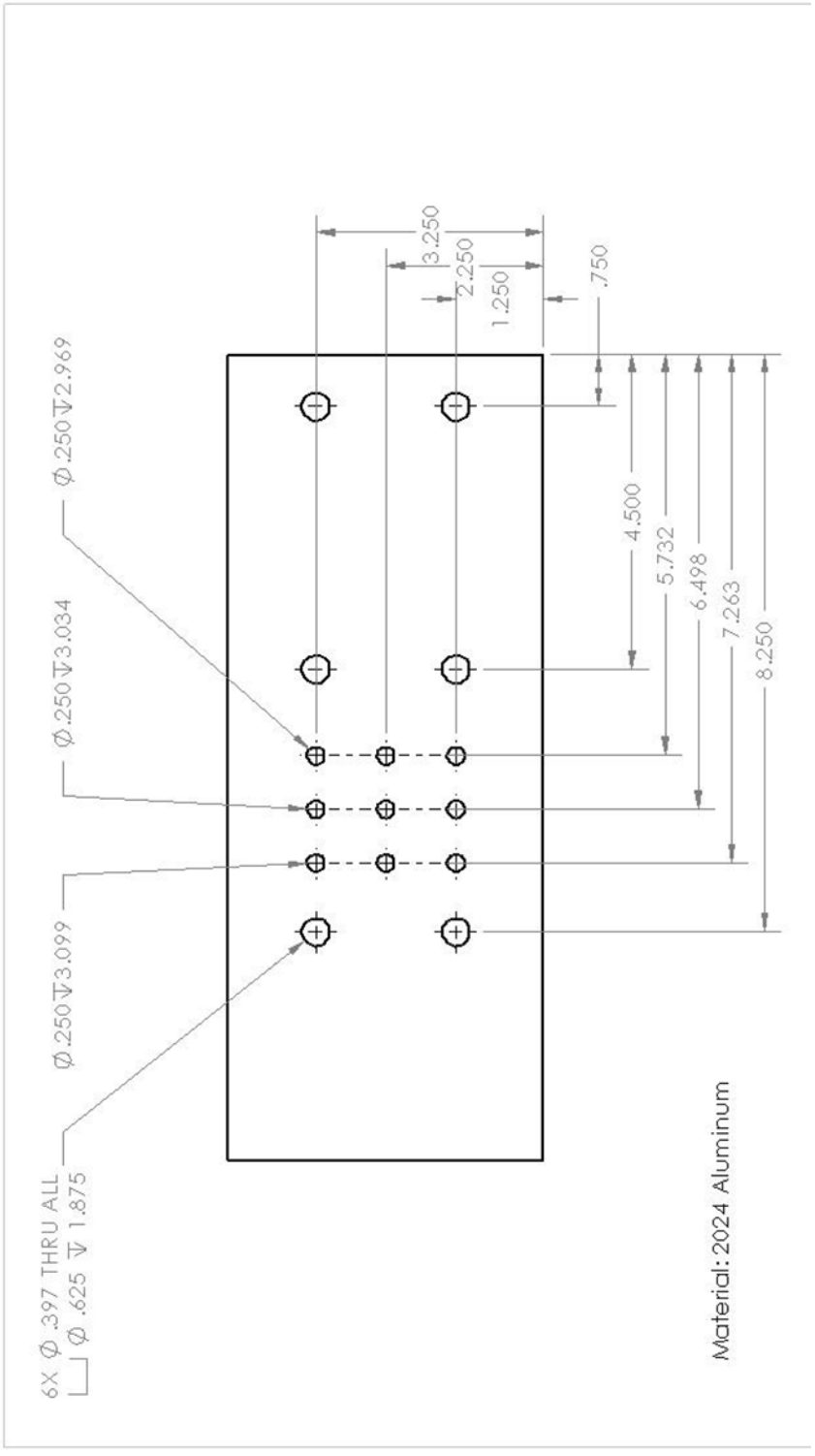
3.250
2.250
1.250
.750
4.500
5.732
6.498
7.263
8.250
Ø.250⩛2.969
Ø.250⩛3.034
Ø.250⩛3.099
6X Ø .397 THRU ALL
⌴ Ø .625 ⩛ 1.875
Material: 2024 Aluminum

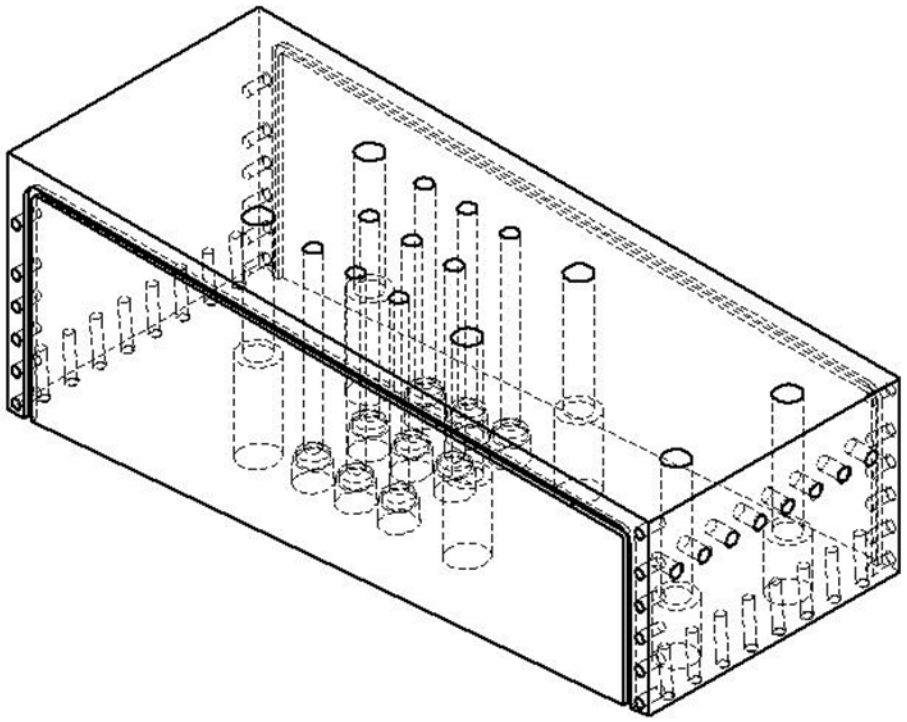

Material: 2024 Aluminum

Note: O-ring groove is 0.122 wide and 0.077 deep unless stated otherwise

B. 45 DEG NOZZLE INSERT DRAWINGS

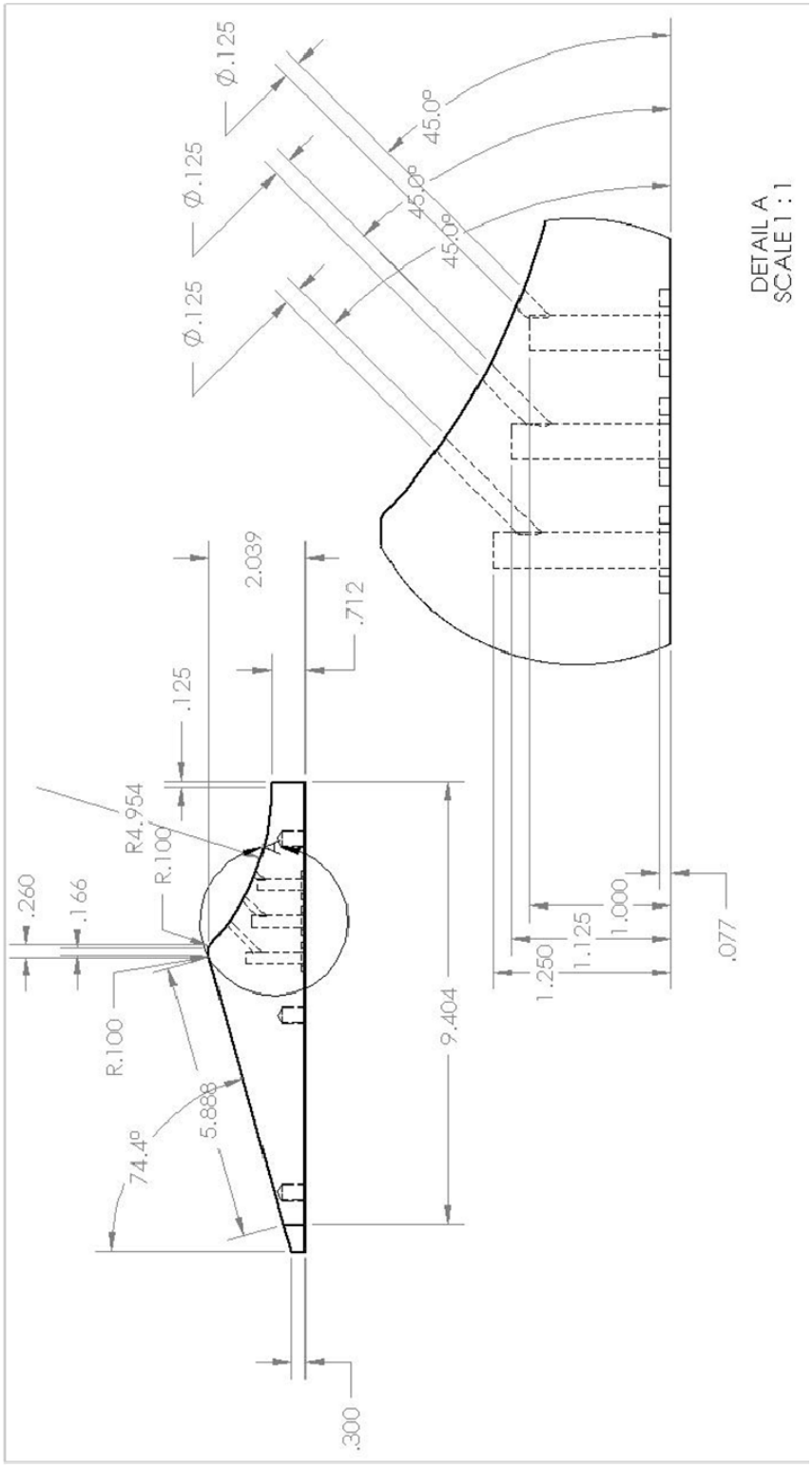

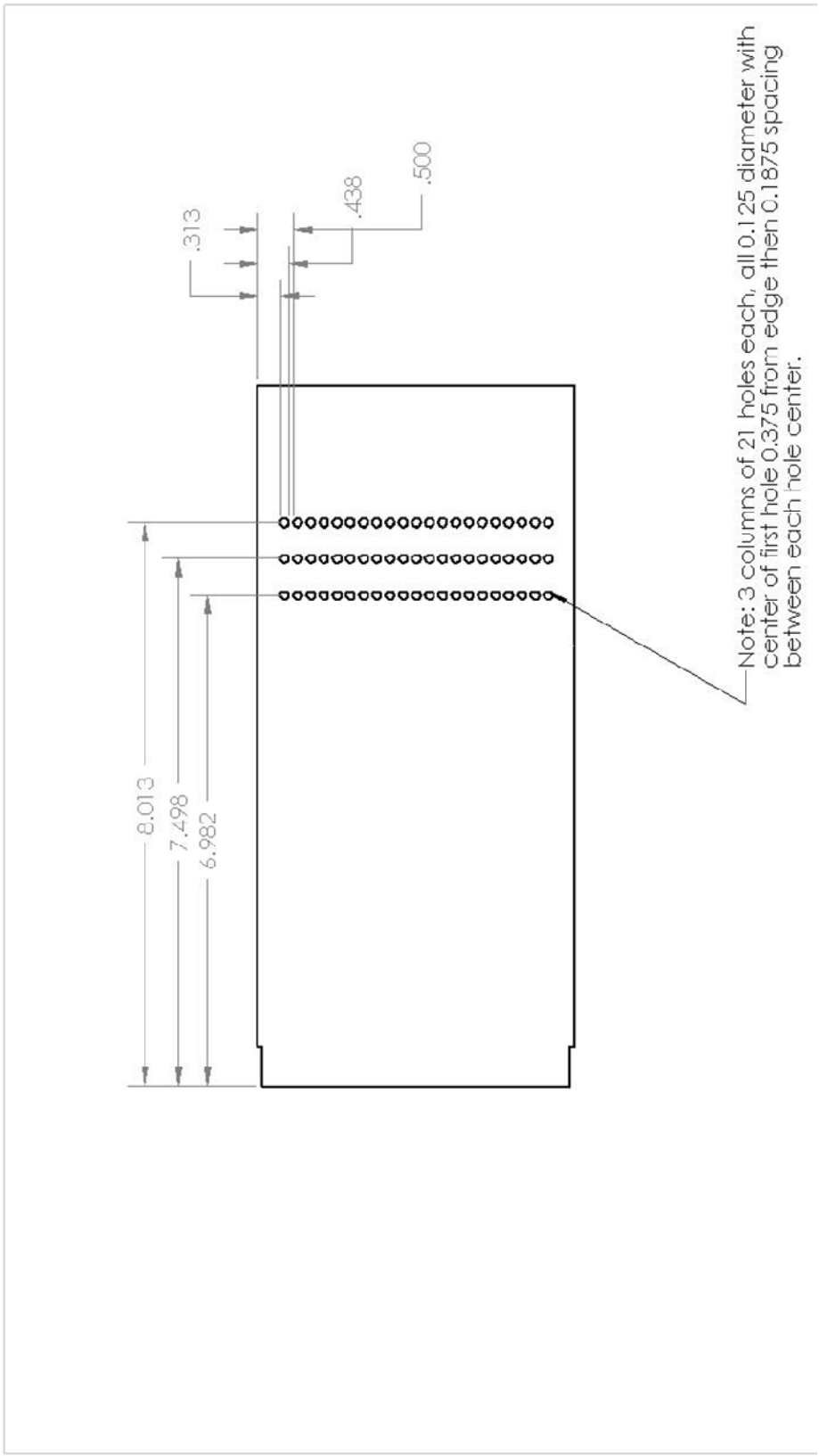
.313
.438
.500
8.013
7.498
6.982
Note: 3 columns of 21 holes each, all 0.125 diameter with center of first hole 0.375 from edge then 0.1875 spacing between each hole center.

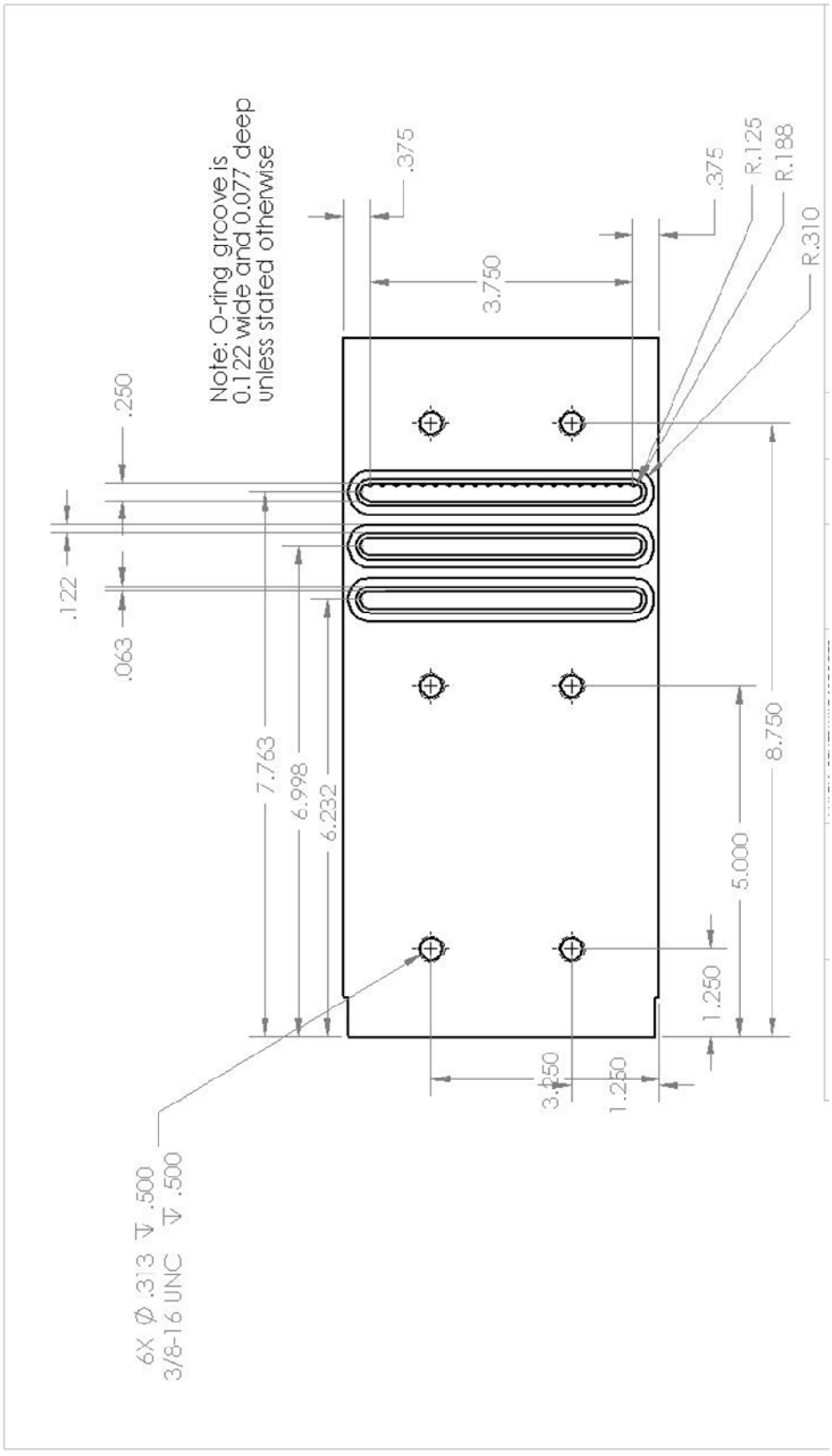
Note: O-ring groove is
0.122 wide and 0.077 deep
unless stated otherwise
.375
.375
R.125
R.188
R.310
3.750
.250
.122
.063
7.763
6.998
6.232
8.750
5.000
1.250
3.750
1.250
6X Ø .313 ↧ .500
3/8-16 UNC ↧ .500

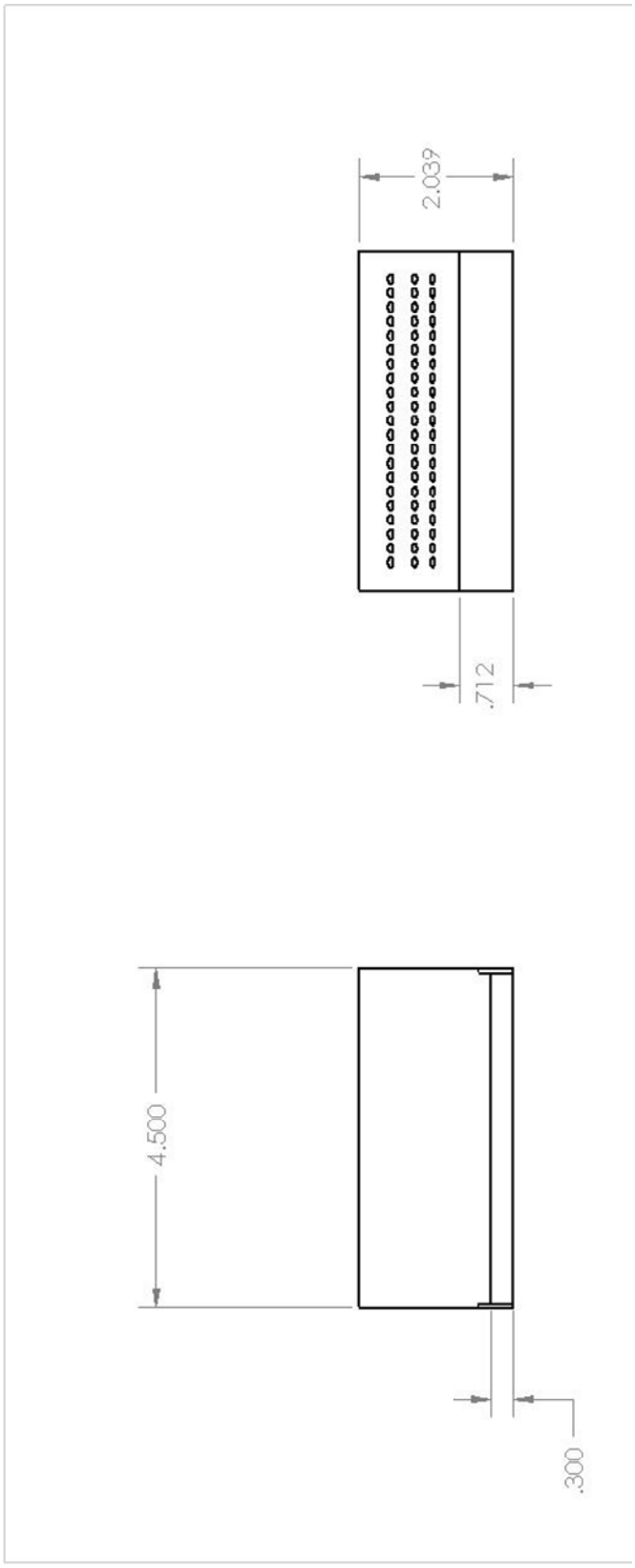
2.039
.712
4.500
.300

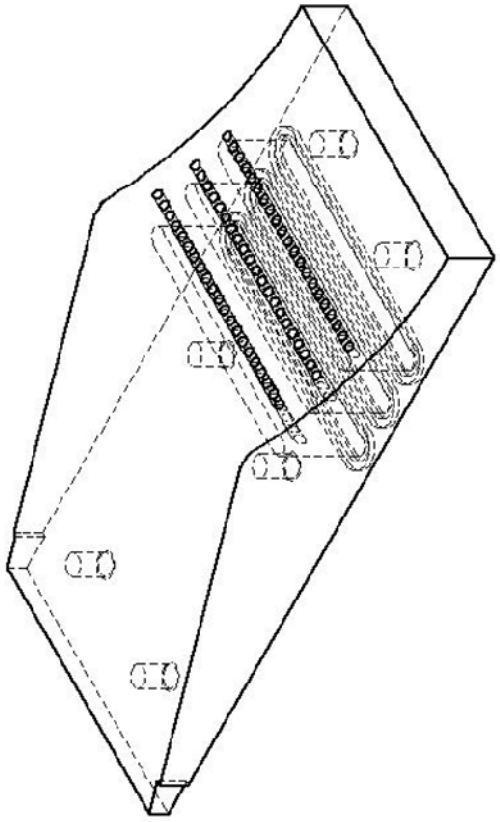

C. TOP SPACER DRAWING

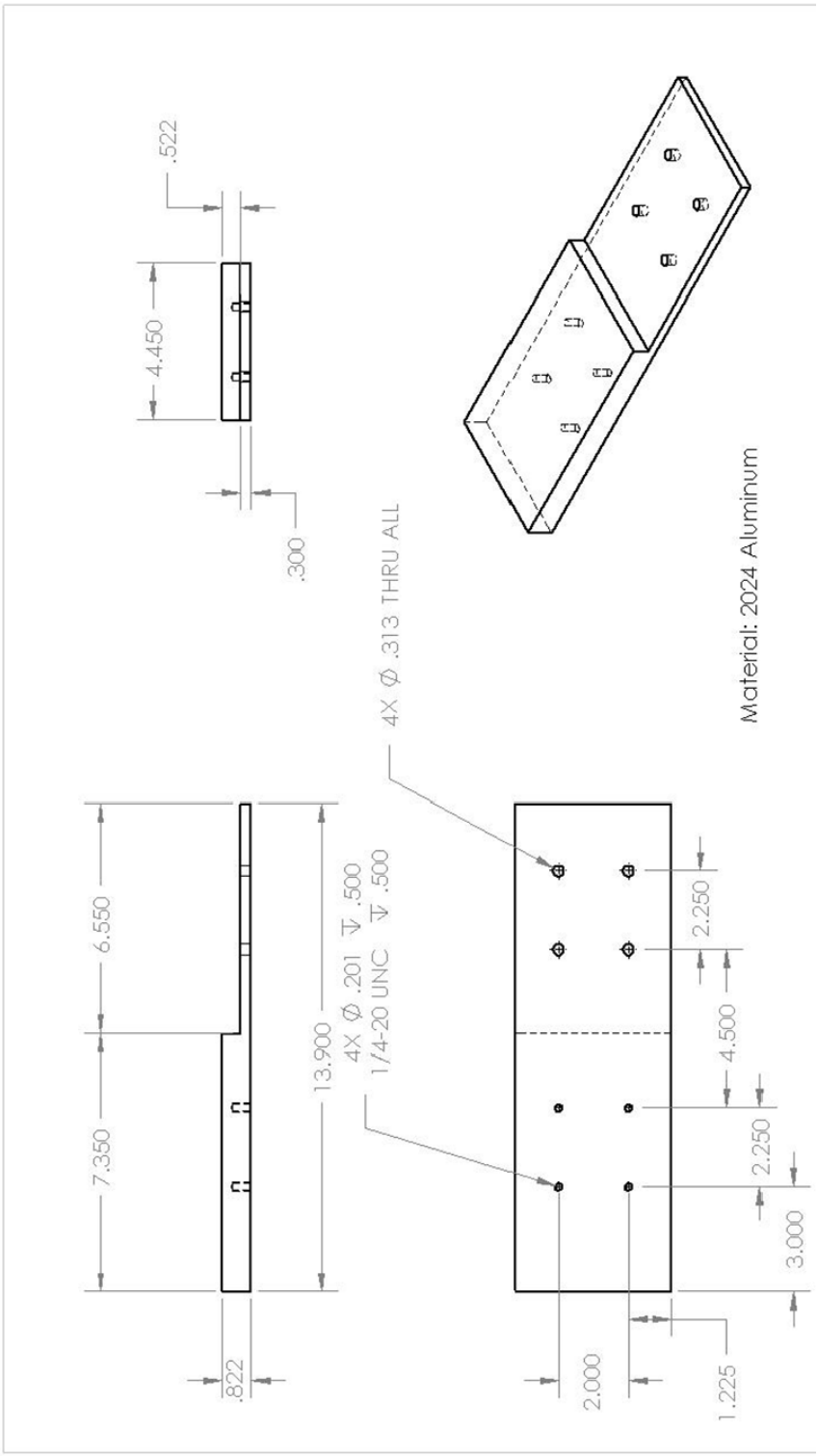

D. BOTTOM SPACER DRAWING

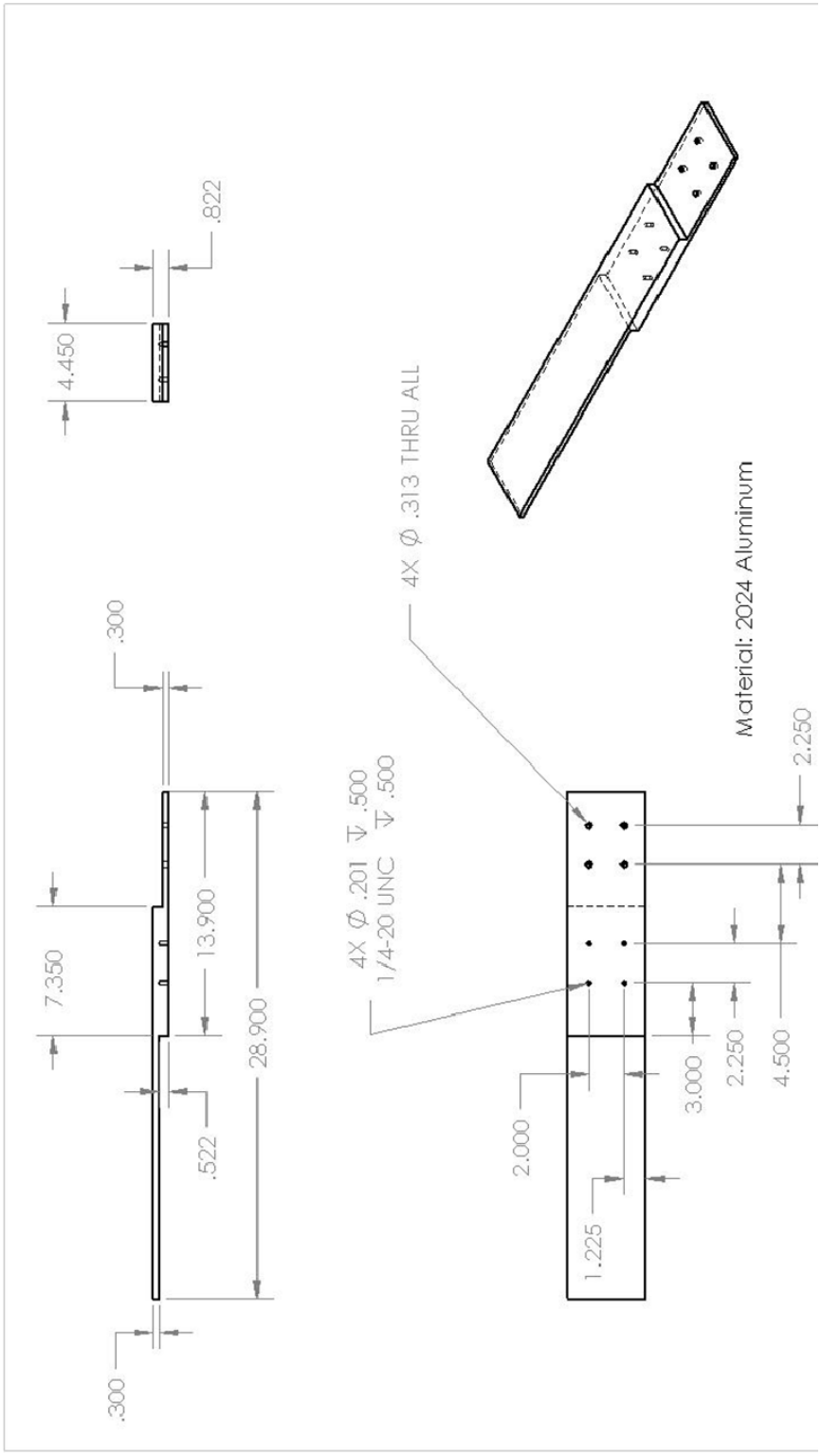

THIS PAGE INTENTIONALLY LEFT BLANK

APPENDIX B: NASA CEA GUI

```
NASA-GLENN CHEMICAL EQUILIBRIUM PROGRAM CEA2, FEBRUARY 5, 2004
                  BY  BONNIE MCBRIDE AND SANFORD GORDON
      REFS: NASA RP-1311, PART I, 1994 AND NASA RP-1311, PART II, 1996


*************************************************************************
********

 output massf
 prob case=12341524 det
 phi=1

 p(atm)=1,2,3,10
 output trace=1e-10

 reac
 oxid  Air  t,k= 298 wt%=  100.
 fuel  H2  t,k= 298 wt%=  100.
 end

 OPTIONS: TP=F  HP=F  SP=F  TV=F  UV=F  SV=F  DETN=T  SHOCK=F  REFL=F
INCD=F
 RKT=F  FROZ=F  EQL=F  IONS=F  SIUNIT=T  DEBUGF=F  SHKDBG=F  DETDBG=F
TRNSPT=F

 TRACE= 1.00E-10  S/R= 0.000000E+00  H/R= 0.000000E+00  U/R=
0.000000E+00

 P,BAR =     1.013250     2.026500     3.039750    10.132500

    REACTANT          WT.FRAC   (ENERGY/R),K   TEMP,K  DENSITY
        EXPLODED FORMULA
 O: Air               1.000000  -0.156227E+02   298.00  0.0000
          N  1.56168  O  0.41959  AR 0.00937  C  0.00032
 F: H2                1.000000  -0.520220E+00   298.00  0.0000
          H  2.00000

  SPECIES BEING CONSIDERED IN THIS SYSTEM
 (CONDENSED PHASE MAY HAVE NAME LISTED SEVERAL TIMES)
  LAST thermo.inp UPDATE:    9/09/04

  g 3/98  *Ar              g 7/97  *C               tpis79  *CH
  g 4/02  CH2              g 4/02  CH3              g11/00  CH2OH
  g 7/00  CH3O             g 8/99  CH4              g 7/00  CH3OH
  srd 01  CH3OOH           g 8/99  *CN              g12/99  CNN
  tpis79  *CO              g 9/99  *CO2             tpis91  COOH
  tpis91  *C2              g 6/01  C2H              g 1/91
C2H2,acetylene
  g 5/01  C2H2,vinylidene  g 4/02  CH2CO,ketene     g 3/02  O(CH)2O
  srd 01  HO(CO)2OH        g 7/01  C2H3,vinyl       g 9/00  CH3CN
```

```
  g 6/96  CH3CO,acetyl     g 1/00  C2H4             g 8/88
C2H4O,ethylen-o
  g 8/88  CH3CHO,ethanal   g 6/00  CH3COOH          srd 01  OHCH2COOH
  g 7/00  C2H5             g 7/00  C2H6             g 8/88  CH3N2CH3
  g 8/88  C2H5OH           g 7/00  CH3OCH3          srd 01  CH3O2CH3
  g 7/00  CCN              tpis91  CNC              srd 01  OCCN
  tpis79  C2N2             g 8/00  C2O              tpis79  *C3
  n 4/98  C3H3,1-propynl   n 4/98  C3H3,2-propynl   g 2/00  C3H4,allene
  g 1/00  C3H4,propyne     g 5/90  C3H4,cyclo-      g 3/01  C3H5,allyl
  g 2/00  C3H6,propylene   g 1/00  C3H6,cyclo-      g 6/01
C3H6O,propylox
  g 6/97  C3H6O,acetone    g 1/02  C3H6O,propanal   g 7/01  C3H7,n-
propyl
  g 9/85  C3H7,i-propyl    g 2/00  C3H8             g 2/00
C3H8O,1propanol
  g 2/00  C3H8O,2propanol  srd 01  CNCOCN           g 7/88  C3O2
  g tpis  *C4              g 7/01  C4H2,butadiyne   g 8/00  C4H4,1,3-
cyclo-
  n10/92  C4H6,butadiene   n10/93  C4H6,1butyne     n10/93
C4H6,2butyne
  g 8/00  C4H6,cyclo-      n 4/88  C4H8,1-butene    n 4/88  C4H8,cis2-
buten
  n 4/88  C4H8,tr2-butene  n 4/88  C4H8,isobutene   g 8/00  C4H8,cyclo-
  g10/00  (CH3COOH)2       n10/84  C4H9,n-butyl     n10/84  C4H9,i-
butyl
  g 1/93  C4H9,s-butyl     g 1/93  C4H9,t-butyl     g12/00  C4H10,n-
butane
  g 8/00  C4H10,isobutane  g 6/01  C4N2             g 8/00  *C5
  g 5/90  C5H6,1,3cyclo-   g 1/93  C5H8,cyclo-      n 4/87  C5H10,1-
pentene
  g 2/01  C5H10,cyclo-     n10/84  C5H11,pentyl     g 1/93  C5H11,t-
pentyl
  n10/85  C5H12,n-pentane  n10/85  C5H12,i-pentane  n10/85
CH3C(CH3)2CH3
  g 2/93  C6H2             g11/00  C6H5,phenyl      g 8/00
C6H5O,phenoxy
  g 8/00  C6H6             g 8/00  C6H5OH,phenol    g 1/93
C6H10,cyclo-
  n 4/87  C6H12,1-hexene   g 6/90  C6H12,cyclo-     n10/83  C6H13,n-
hexyl
  g 6/01  C6H14,n-hexane   g 7/01  C7H7,benzyl      g 1/93  C7H8
  g12/00  C7H8O,cresol-mx  n 4/87  C7H14,1-heptene  n10/83  C7H15,n-
heptyl
  n10/85  C7H16,n-heptane  n10/85  C7H16,2-methylh  n 4/89
C8H8,styrene
  n10/86  C8H10,ethylbenz  n 4/87  C8H16,1-octene   n10/83  C8H17,n-
octyl
  n 4/85  C8H18,n-octane   n 4/85  C8H18,isooctane  n10/83  C9H19,n-
nonyl
  g 3/01  C10H8,naphthale  n10/83  C10H21,n-decyl   g 8/00  C12H9,o-
bipheny
  g 8/00  C12H10,biphenyl  g 6/97  *H               g 6/01  HCN
  g 1/01  HCO              tpis89  HCCN             g 6/01  HCCO
  g 6/01  HNC              g 7/00  HNCO             g10/01  HNO
  tpis89  HNO2             g 5/99  HNO3             g 4/02  HO2
```

```
 tpis78  *H2             g 5/01  HCHO,formaldehy  g 6/01  HCOOH
 g 8/89  H2O             g 6/99  H2O2             g 6/01  (HCOOH)2
 g 5/97  *N              g 6/01  NCO              g 4/99  *NH
 g 3/01  NH2             tpis89  NH3              tpis89  NH2OH
 tpis89  *NO             g 4/99  NO2              j12/64  NO3
 tpis78  *N2             g 6/01  NCN              g 5/99  N2H2
 tpis89  NH2NO2          g 4/99  N2H4             g 4/99  N2O
 g 4/99  N2O3            tpis89  N2O4             g 4/99  N2O5
 tpis89  N3              g 4/99  N3H              g 5/97  *O
 g 4/02  *OH             tpis89  *O2             g 8/01  O3
 g 12/0  THDCPD,endo     g 12/0  THDCPD,exo       n 4/83  C(gr)
 n 4/83  C(gr)           n 4/83  C(gr)           g11/99  H2O(cr)
 g 8/01  H2O(L)          g 8/01  H2O(L)

 O/F =  34.296226

                      EFFECTIVE FUEL     EFFECTIVE OXIDANT
MIXTURE
 ENTHALPY                  h(2)/R             h(1)/R
h0/R
 (KG-MOL)(K)/KG       -0.25806109E+00     -0.53936211E+00     -
0.53139239E+00

 KG-FORM.WT./KG            bi(2)              bi(1)               b0i
  *N                   0.00000000E+00      0.53915890E-01
0.52388364E-01
  *O                   0.00000000E+00      0.14486046E-01
0.14075632E-01
  *Ar                  0.00000000E+00      0.32331996E-03
0.31415977E-03
  *C                   0.00000000E+00      0.11013248E-04
0.10701224E-04
  *H                   0.99212255E+00      0.00000000E+00
0.28108460E-01

 POINT ITN      T            N           O           AR          C
                   H
   1   28    2937.961     -13.027     -16.181     -24.263     -23.800
               -10.758

 POINT ITN      T            N           O           AR          C
                   H
   1    3    2940.769     -13.010     -16.167     -24.227     -23.778
               -10.743

 POINT ITN      T            N           O           AR          C
                   H
   1    2    2943.610     -13.011     -16.166     -24.229     -23.773
               -10.741

 POINT ITN      T            N           O           AR          C
                   H
   1    2    2943.630     -13.011     -16.166     -24.228     -23.773
               -10.741
   2    7    2979.757     -12.705     -15.939     -23.598     -23.401
```

		-10.489				
2	3	2987.901	-12.686	-15.921	-23.556	-23.365
		-10.468				
2	2	2991.520	-12.687	-15.919	-23.558	-23.359
		-10.465				
2	2	2991.545	-12.687	-15.919	-23.557	-23.359
		-10.465				
3	7	3002.686	-12.515	-15.799	-23.208	-23.170
		-10.333				
3	3	3014.115	-12.495	-15.778	-23.163	-23.127
		-10.308				
3	2	3018.090	-12.497	-15.776	-23.164	-23.120
		-10.306				
3	2	3018.117	-12.497	-15.776	-23.164	-23.120
		-10.306				
4	7	3063.724	-11.948	-15.391	-22.045	-22.502
		-9.875				
4	4	3085.325	-11.927	-15.363	-21.992	-22.437
		-9.841				
4	2	3089.932	-11.929	-15.361	-21.993	-22.429
		-9.838				
4	2	3089.965	-11.929	-15.361	-21.993	-22.428
		-9.838				

DETONATION PROPERTIES OF AN IDEAL REACTING GAS

CASE = 12341524

	REACTANT	WT FRACTION (SEE NOTE)	ENERGY KJ/KG-MOL	TEMP K
OXIDANT	Air	1.0000000	-129.895	298.000
FUEL	H2	1.0000000	-4.325	298.000

O/F= 34.29623 %FUEL= 2.833164 R,EQ.RATIO= 1.000000 PHI,EQ.RATIO= 1.000000

UNBURNED GAS

P1, BAR	1.0132	2.0265	3.0397	10.1325
T1, K	298.00	298.00	298.00	298.00
H1, KJ/KG	-4.36	-4.36	-4.36	-4.36
M1, (1/n)	21.008	21.008	21.008	21.008
GAMMA1	1.4015	1.4015	1.4015	1.4015
SON VEL1,M/SEC	406.6	406.6	406.6	406.6

BURNED GAS

P, BAR	15.801	31.953	48.216	163.23
T, K	2943.63	2991.54	3018.12	3089.96
RHO, KG/CU M	1.5500 0	3.0940 0	4.6358 0	1.5402 1
H, KJ/KG	1333.33	1350.13	1359.31	1383.66
U, KJ/KG	313.90	317.38	319.22	323.84

G, KJ/KG	-29833.7	-29612.8	-29459.5	-28898.1
S, KJ/(KG)(K)	10.5880	10.3501	10.2113	9.8000
M, (1/n)	24.008	24.085	24.127	24.241
(dLV/dLP)t	-1.00954	-1.00825	-1.00755	-1.00571
(dLV/dLT)p	1.2062	1.1769	1.1611	1.1207
Cp, KJ/(KG)(K)	3.3542	3.1183	2.9946	2.6835
GAMMAs	1.1637	1.1697	1.1732	1.1832
SON VEL,M/SEC	1089.2	1099.1	1104.6	1119.8

DETONATION PARAMETERS

P/P1	15.595	15.768	15.862	16.109
T/T1	9.878	10.039	10.128	10.369
M/M1	1.1428	1.1464	1.1484	1.1539
RHO/RHO1	1.8042	1.8007	1.7987	1.7927
DET MACH NUMBER	4.8335	4.8680	4.8869	4.9377
DET VEL,M/SEC	1965.1	1979.1	1986.8	2007.5

MASS FRACTIONS

*Ar	1.2550-2	1.2550-2	1.2550-2	1.2550-2
*CO	1.3093-4	1.2358-4	1.1899-4	1.0435-4
*CO2	2.6525-4	2.7679-4	2.8400-4	3.0700-4
COOH	2.6149-9	4.1568-9	5.4139-9	1.1495-8
*H	2.4760-4	1.9230-4	1.6446-4	9.9637-5
HCN	5.658-11	9.213-11	1.212-10	2.606-10
HCO	1.0225-9	1.4459-9	1.7513-9	2.9468-9
HNCO	2.395-10	4.369-10	6.167-10	1.664 -9
HNO	3.1235-6	4.2263-6	5.0018-6	7.9515-6
HNO2	8.9839-7	1.4261-6	1.8570-6	3.9540-6
HNO3	1.028-10	2.092-10	3.144-10	1.017 -9
HO2	1.5250-5	1.7914-5	1.9518-5	2.4267-5
*H2	2.6254-3	2.3784-3	2.2348-3	1.8221-3
HCHO,formaldehy	2.849-11	4.951-11	6.777-11	1.653-10
HCOOH	3.735-10	7.274-10	1.069 -9	3.278 -9
H2O	2.2035-1	2.2374-1	2.2568-1	2.3115-1
H2O2	2.3080-6	3.3346-6	4.1082-6	7.4114-6
*N	1.1146-6	1.0731-6	1.0355-6	8.7825-7
NCO	3.420-11	5.439-11	7.052-11	1.448-10
*NH	4.5040-7	5.4186-7	5.9623-7	7.5029-7
NH2	2.7000-7	3.9356-7	4.8569-7	8.6828-7
NH3	3.4969-7	5.9130-7	7.9940-7	1.9090-6
NH2OH	4.217-10	9.511-10	1.517 -9	5.823 -9
*NO	9.4235-3	9.2818-3	9.1502-3	8.5645-3
NO2	6.6339-6	8.3429-6	9.4740-6	1.3400-5
NO3	2.383-11	4.088-11	5.541-11	1.300-10
*N2	7.2938-1	7.2945-1	7.2951-1	7.2977-1
N2H2	7.855-11	1.676-10	2.582-10	8.858-10
N2O	2.7711-6	3.8979-6	4.7318-6	8.2048-6
N3	3.527-11	6.737-11	9.710-11	2.715-10
N3H	1.400-11	3.300-11	5.387-11	2.197-10
*O	1.3571-3	1.0460-3	8.8936-4	5.2626-4
*OH	1.3522-2	1.2211-2	1.1434-2	9.1623-3
*O2	1.0117-2	8.7129-3	7.9392-3	5.8756-3

```
 O3              6.2078-9 7.8935-9 8.9657-9 1.2344-8

  * THERMODYNAMIC PROPERTIES FITTED TO 20000.K

    PRODUCTS WHICH WERE CONSIDERED BUT WHOSE MASS FRACTIONS
    WERE LESS THAN 1.000000E-10 FOR ALL ASSIGNED CONDITIONS

 *C              *CH             CH2             CH3             CH2OH
 CH3O            CH4             CH3OH           CH3OOH          *CN
 CNN             *C2             C2H             C2H2,acetylene
C2H2,vinylidene
 CH2CO,ketene    O(CH)2O         HO(CO)2OH       C2H3,vinyl      CH3CN
 CH3CO,acetyl    C2H4            C2H4O,ethylen-o CH3CHO,ethanal
CH3COOH
 OHCH2COOH       C2H5            C2H6            CH3N2CH3        C2H5OH
 CH3OCH3         CH3O2CH3        CCN             CNC             OCCN
 C2N2            C2O             *C3             C3H3,1-propynl
C3H3,2-propynl
 C3H4,allene     C3H4,propyne    C3H4,cyclo-     C3H5,allyl
C3H6,propylene
 C3H6,cyclo-     C3H6O,propylox  C3H6O,acetone   C3H6O,propanal
C3H7,n-propyl
 C3H7,i-propyl   C3H8            C3H8O,1propanol C3H8O,2propanol CNCOCN
 C3O2            *C4             C4H2,butadiyne  C4H4,1,3-cyclo-
C4H6,butadiene
 C4H6,1butyne    C4H6,2butyne    C4H6,cyclo-     C4H8,1-butene
C4H8,cis2-buten
 C4H8,tr2-butene C4H8,isobutene  C4H8,cyclo-     (CH3COOH)2
C4H9,n-butyl
 C4H9,i-butyl    C4H9,s-butyl    C4H9,t-butyl    C4H10,n-butane
C4H10,isobutane
 C4N2            *C5             C5H6,1,3cyclo-  C5H8,cyclo-
C5H10,1-pentene
 C5H10,cyclo-    C5H11,pentyl    C5H11,t-pentyl  C5H12,n-pentane
C5H12,i-pentane
 CH3C(CH3)2CH3   C6H2            C6H5,phenyl     C6H5O,phenoxy   C6H6
 C6H5OH,phenol   C6H10,cyclo-    C6H12,1-hexene  C6H12,cyclo-
C6H13,n-hexyl
 C6H14,n-hexane  C7H7,benzyl     C7H8            C7H8O,cresol-mx
C7H14,1-heptene
 C7H15,n-heptyl  C7H16,n-heptane C7H16,2-methylh C8H8,styrene
C8H10,ethylbenz
 C8H16,1-octene  C8H17,n-octyl   C8H18,n-octane  C8H18,isooctane
C9H19,n-nonyl
 C10H8,naphthale C10H21,n-decyl  C12H9,o-bipheny C12H10,biphenyl HCCN
 HCCO            HNC             (HCOOH)2        NCN             NH2NO2
 N2H4            N2O3            N2O4            N2O5
THDCPD,endo
 THDCPD,exo      C(gr)           H2O(cr)         H2O(L)

 NOTE. WEIGHT FRACTION OF FUEL IN TOTAL FUELS AND OF OXIDANT IN TOTAL
OXIDANTS
```

APPENDIX C: CFD++ FILL SIMULATION SETTINGS

A. FILL SIMULATION SETTINGS FOR 45 DEGREE INJECTION ANGLE

45 Degree Injection Angle			
Mesh Size	1104504		
Boundary Conditions			
Inlet	Multi-species PV Based Inflow/Outflow		
	Pressure	303975	Pa
	Temperature	450	K
	x-velocity	100	m/s
	y-velocity	0.0	m/s
	z-velocity	0.0	m/s
	q	1.224745	m/s
	L	.0006482519	m
	H_2	0.02833164	Mass Fraction
	H	0.0	
	O	0.0	
	O_2	0.2265	
	H_2O	0.0	
	H_2O_2	0.0	
	HO_2	0.0	
	OH	0.0	
Outlet	Simple Back Pressure		

	Pressure	101325	Pa
Injinlet1, Injinlet2, and Injinlet3	Pressure Temperature and Normal Velocity Inflow		
	Pressure	167558	Pa
	Temperature	450	K
	Normal Velocity	50	m/s
	q	0.6123724	m/s
	L	0.01736194	M
	H_2	0.0	Mass Fraction
	H	0.0	
	O	0.0	
	O_2	0.2265	
	H_2O	0.0	
	H_2O_2	0.0	
	HO_2	0.0	
	OH	0.0	
Symmetry	Multi-species Adiabatic Wall		
Walls	Multi-species Adiabatic Wall		
Initial Conditions			
Box 1	xmin	-0.00005	m
	xmax	0.0125	m
	ymin	-0.00005	m
	ymax	0.0875	m
	zmin	0.0	m

	zmax	0.0	m
	Pressure	303975	Pa
	Temperature	450	K
	x-velocity	100	m/s
	y-velocity	0.0	m/s
	z-velocity	0.0	m/s
	q	1.224745	m/s
	L	0.006482519	m
	H_2	0.02833164	Mass Fraction
	H	0.0	
	O	0.0	
	O_2	0.2265	
	H_2O	0.0	
	H_2O_2	0.0	
	HO_2	0.0	
	OH	0.0	
Box 2	xmin	0.0125	m
	xmax	0.61	m
	ymin	-0.00005	m
	ymax	0.0875	m
	zmin	0.0	m
	zmax	0.0	m
	Pressure	303975	Pa

	Temperature	450	K
	x-velocity	100	m/s
	y-velocity	0.0	m/s
	z-velocity	0.0	m/s
	q	1.224745	m/s
	L	0.004785153	m
	H_2	0.0	Mass Fraction
	H	0.0	
	O	0.0	
	O_2	0.2265	
	H_2O	0.0	
	H_2O_2	0.0	
	HO_2	0.0	
	OH	0.0	
Box 3	xmin	0.7	m
	xmax	0.755	m
	ymin	-0.015	m
	ymax	0.012	m
	zmin	0.0	m
	zmax	0.0	m
	Pressure	167558	Pa
	Temperature	450	K
	x-velocity	50	m/s

	y-velocity	0.0	m/s
	z-velocity	0.0	m/s
	q	0.6123724	m/s
	L	0.01736194	m
	H_2	0.0	Mass Fraction
	H	0.0	
	O	0.0	
	O_2	0.2265	
	H_2O	0.0	
	H_2O_2	0.0	
	HO_2	0.0	
	OH	0.0	
Box 4	xmin	0.61	m
	xmax	0.7	m
	ymin	-0.00005	m
	ymax	0.0875	m
	zmin	0.0	m
	zmax	0.0	m
	Pressure	303975	Pa
	Temperature	450	K
	x-velocity	100	m/s
	y-velocity	0.0	m/s
	z-velocity	0.0	m/s

	q	1.224745	m/s
	L	0.004785153	m
	H_2	0.0	Mass Fraction
	H	0.0	
	O	0.0	
	O_2	0.2265	
	H_2O	0.0	
	H_2O_2	0.0	
	HO_2	0.0	
	OH	0.0	
Box 5	xmin	0.7	m
	xmax	0.755	m
	ymin	0.012	m
	ymax	0.0875	m
	zmin	0.0	m
	zmax	0.0	m
	Pressure	200000	Pa
	Temperature	450	K
	x-velocity	100	m/s
	y-velocity	0.0	m/s
	z-velocity	0.0	m/s
	q	1.224745	m/s
	L	0.005950135	m

	H_2	0.0	Mass Fraction
	H	0.0	
	O	0.0	
	O_2	0.2265	
	H_2O	0.0	
	H_2O_2	0.0	
	HO_2	0.0	
	OH	0.0	
Box 6	xmin	0.755	m
	xmax	1.25	m
	ymin	-0.12	m
	ymax	0.0875	m
	zmin	0.0	m
	zmax	0.0	m
	Pressure	101325	Pa
	Temperature	298	K
	x-velocity	0.0	m/s
	y-velocity	0.0	m/s
	z-velocity	0.0	m/s
	q	0.001224745	m/s
	L	7.036989	m
	H_2	0.0	Mass Fraction
	H	0.0	

	O	0.0	
	O_2	0.2265	
	H_2O	0.0	
	H_2O_2	0.0	
	HO_2	0.0	
	OH	0.0	

Time Integration	
Is this a restart:	No
Simulation Strategy:	Transient
Integration Type:	Implicit
Number of global time steps for this run:	1000
Max. cumulative # of global time steps:	0
Turn on dual time-stepping:	Yes
Stop run at a given global time value:	No
Implicit scheme type:	Point-Implicit
Global time step based on Courant #:	No
Spatially varying local time step:	Yes
At restart, use Courant # for local time step from:	Values Below
Courant # for local time step ramped from:	1 to 100
Local Courant # ramped from global step number:	1 to 100
Local Max. Courant # adjustment factor:	0.95

Terminate run if adjusted local Courant # is <:	1.00E-04
Global time step size:	1.00E-05 s
Max. # of internal (local) iter. per global step:	50
Global step internal iter. Termination criterion:	0.1
Order of global time stepping:	2nd
Extrapolate using old dq/dt (1st iteration):	No
Local iteration convergence acceler.:	Multigrid (old)
Turn on temporal-smoothing:	Yes
Smoothing factor:	0.75
Turn on time-step spatial-smoothing:	Yes
Number of smoothing passes:	4
Maximum time-step growth factor:	1.5

B. FILL SIMULATION SETTINGS FOR 30 DEGREE INJECTION ANGLE

30 Degree Injection Angle			
Mesh Size	1142195		
Boundary Conditions			
Inlet	Multi-species PV Based Inflow/Outflow		
	Pressure	303975	Pa
	Temperature	450	K

	x-velocity	100	m/s
	y-velocity	0.0	m/s
	z-velocity	0.0	m/s
	q	1.224745	m/s
	L	.0006482519	m
	H_2	0.02833164	Mass Fraction
	H	0.0	
	O	0.0	
	O_2	0.2265	
	H_2O	0.0	
	H_2O_2	0.0	
	HO_2	0.0	
	OH	0.0	
Outlet	Simple Back Pressure		
	Pressure	101325	Pa
Injinlet1, Injinlet2, and Injinlet3	Pressure Temperature and Normal Velocity Inflow		
	Pressure	167558	Pa
	Temperature	450	K
	Normal Velocity	50	m/s
	q	0.6123724	m/s
	L	0.01736194	M
	H_2	0.0	Mass Fraction
	H	0.0	

	O	0.0	
	O_2	0.2265	
	H_2O	0.0	
	H_2O_2	0.0	
	HO_2	0.0	
	OH	0.0	
Symmetry	Multi-species Adiabatic Wall		
Walls	Multi-species Adiabatic Wall		
Initial Conditions			
Box 1	xmin	-0.00005	m
	xmax	0.0125	m
	ymin	-0.00005	m
	ymax	0.0875	m
	zmin	0.0	m
	zmax	0.0	m
	Pressure	303975	Pa
	Temperature	450	K
	x-velocity	100	m/s
	y-velocity	0.0	m/s
	z-velocity	0.0	m/s
	q	1.224745	m/s
	L	0.006482519	m
	H_2	0.02833164	Mass Fraction

	H	0.0	
	O	0.0	
	O_2	0.2265	
	H_2O	0.0	
	H_2O_2	0.0	
	HO_2	0.0	
	OH	0.0	
Box 2	xmin	0.0125	m
	xmax	0.61	m
	ymin	-0.00005	m
	ymax	0.0875	m
	zmin	0.0	m
	zmax	0.0	m
	Pressure	303975	Pa
	Temperature	450	K
	x-velocity	100	m/s
	y-velocity	0.0	m/s
	z-velocity	0.0	m/s
	q	1.224745	m/s
	L	0.004785153	m
	H_2	0.0	Mass Fraction
	H	0.0	
	O	0.0	

	O_2	0.2265	
	H_2O	0.0	
	H_2O_2	0.0	
	HO_2	0.0	
	OH	0.0	
Box 3	xmin	0.695	m
	xmax	0.755	m
	ymin	-0.015	m
	ymax	0.02	m
	zmin	0.0	m
	zmax	0.0	m
	Pressure	167558	Pa
	Temperature	450	K
	x-velocity	50	m/s
	y-velocity	0.0	m/s
	z-velocity	0.0	m/s
	q	0.6123724	m/s
	L	0.01736194	m
	H_2	0.0	Mass Fraction
	H	0.0	
	O	0.0	
	O_2	0.2265	
	H_2O	0.0	

	H_2O_2	0.0	
	HO_2	0.0	
	OH	0.0	
Box 4	xmin	0.61	m
	xmax	0.695	m
	ymin	-0.00005	m
	ymax	0.0875	m
	zmin	0.0	m
	zmax	0.0	m
	Pressure	303975	Pa
	Temperature	450	K
	x-velocity	100	m/s
	y-velocity	0.0	m/s
	z-velocity	0.0	m/s
	q	1.224745	m/s
	L	0.004785153	m
	H_2	0.0	Mass Fraction
	H	0.0	
	O	0.0	
	O_2	0.2265	
	H_2O	0.0	
	H_2O_2	0.0	
	HO_2	0.0	

	OH	0.0	
Box 5	xmin	0.695	m
	xmax	0.755	m
	ymin	0.02	m
	ymax	0.0875	m
	zmin	0.0	m
	zmax	0.0	m
	Pressure	200000	Pa
	Temperature	450	K
	x-velocity	100	m/s
	y-velocity	0.0	m/s
	z-velocity	0.0	m/s
	q	1.224745	m/s
	L	0.005950135	m
	H_2	0.0	Mass Fraction
	H	0.0	
	O	0.0	
	O_2	0.2265	
	H_2O	0.0	
	H_2O_2	0.0	
	HO_2	0.0	
	OH	0.0	
Box 6	xmin	0.755	m

	xmax	1.25	m
	ymin	-0.12	m
	ymax	0.0875	m
	zmin	0.0	m
	zmax	0.0	m
	Pressure	101325	Pa
	Temperature	298	K
	x-velocity	0.0	m/s
	y-velocity	0.0	m/s
	z-velocity	0.0	m/s
	q	0.001224745	m/s
	L	7.036989	m
	H_2	0.0	Mass Fraction
	H	0.0	
	O	0.0	
	O_2	0.2265	
	H_2O	0.0	
	H_2O_2	0.0	
	HO_2	0.0	
	OH	0.0	
Time Integration			
Is this a restart:		No	
Simulation Strategy:		Transient	

Integration Type:	Implicit
Number of global time steps for this run:	1000
Max. cumulative # of global time steps:	0
Turn on dual time-stepping:	Yes
Stop run at a given global time value:	No
Implicit scheme type:	Point-Implicit
Global time step based on Courant #:	No
Spatially varying local time step:	Yes
At restart, use Courant # for local time step from:	Values Below
Courant # for local time step ramped from:	1 to 100
Local Courant # ramped from global step number:	1 to 100
Local Max. Courant # adjustment factor:	0.95
Terminate run if adjusted local Courant # is <:	1.00E-04
Global time step size:	1.00E-05 s
Max. # of internal (local) iter. per global step:	50
Global step internal iter. Termination criterion:	0.1
Order of global time stepping:	2nd
Extrapolate using old dq/dt (1st iteration):	No
Local iteration convergence acceler.:	Multigrid (old)

Turn on temporal-smoothing:	Yes
Smoothing factor:	0.75
Turn on time-step spatial-smoothing:	Yes
Number of smoothing passes:	4
Maximum time-step growth factor:	1.5

C. FILL SIMULATION SETTINGS FOR 60 DEGREE INJECTION ANGLE

60 Degree Injection Angle			
Mesh Size	1096640		
Boundary Conditions			
Inlet	Multi-species PV Based Inflow/Outflow		
	Pressure	303975	Pa
	Temperature	450	K
	x-velocity	100	m/s
	y-velocity	0.0	m/s
	z-velocity	0.0	m/s
	q	1.224745	m/s
	L	.0006482519	m
	H_2	0.02833164	Mass Fraction
	H	0.0	
	O	0.0	
	O_2	0.2265	

	H_2O	0.0	
	H_2O_2	0.0	
	HO_2	0.0	
	OH	0.0	
Outlet	Simple Back Pressure		
	Pressure	101325	Pa
Injinlet1, Injinlet2, and Injinlet3	Pressure Temperature and Normal Velocity Inflow		
	Pressure	167558	Pa
	Temperature	450	K
	Normal Velocity	50	m/s
	q	0.6123724	m/s
	L	0.01736194	M
	H_2	0.0	Mass Fraction
	H	0.0	
	O	0.0	
	O_2	0.2265	
	H_2O	0.0	
	H_2O_2	0.0	
	HO_2	0.0	
	OH	0.0	
Symmetry	Multi-species Adiabatic Wall		
Walls	Multi-species Adiabatic Wall		
Initial Conditions			

Box 1	xmin	-0.00005	m
	xmax	0.0125	m
	ymin	-0.00005	m
	ymax	0.0875	m
	zmin	0.0	m
	zmax	0.0	m
	Pressure	303975	Pa
	Temperature	450	K
	x-velocity	100	m/s
	y-velocity	0.0	m/s
	z-velocity	0.0	m/s
	q	1.224745	m/s
	L	0.006482519	m
	H_2	0.02833164	Mass Fraction
	H	0.0	
	O	0.0	
	O_2	0.2265	
	H_2O	0.0	
	H_2O_2	0.0	
	HO_2	0.0	
	OH	0.0	
Box 2	xmin	0.0125	m
	xmax	0.61	m

	ymin	-0.00005	m
	ymax	0.0875	m
	zmin	0.0	m
	zmax	0.0	m
	Pressure	303975	Pa
	Temperature	450	K
	x-velocity	100	m/s
	y-velocity	0.0	m/s
	z-velocity	0.0	m/s
	q	1.224745	m/s
	L	0.004785153	m
	H_2	0.0	Mass Fraction
	H	0.0	
	O	0.0	
	O_2	0.2265	
	H_2O	0.0	
	H_2O_2	0.0	
	HO_2	0.0	
	OH	0.0	
Box 3	xmin	0.7	m
	xmax	0.755	m
	ymin	-0.02	m
	ymax	0.012	m

	zmin	0.0	m
	zmax	0.0	m
	Pressure	167558	Pa
	Temperature	450	K
	x-velocity	50	m/s
	y-velocity	0.0	m/s
	z-velocity	0.0	m/s
	q	0.6123724	m/s
	L	0.01736194	m
	H_2	0.0	Mass Fraction
	H	0.0	
	O	0.0	
	O_2	0.2265	
	H_2O	0.0	
	H_2O_2	0.0	
	HO_2	0.0	
	OH	0.0	
Box 4	xmin	0.61	m
	xmax	0.7	m
	ymin	-0.00005	m
	ymax	0.0875	m
	zmin	0.0	m
	zmax	0.0	m

	Pressure	303975	Pa
	Temperature	450	K
	x-velocity	100	m/s
	y-velocity	0.0	m/s
	z-velocity	0.0	m/s
	q	1.224745	m/s
	L	0.004785153	m
	H_2	0.0	Mass Fraction
	H	0.0	
	O	0.0	
	O_2	0.2265	
	H_2O	0.0	
	H_2O_2	0.0	
	HO_2	0.0	
	OH	0.0	
Box 5	xmin	0.7	m
	xmax	0.755	m
	ymin	0.012	m
	ymax	0.0875	m
	zmin	0.0	m
	zmax	0.0	m
	Pressure	200000	Pa
	Temperature	450	K

	x-velocity	100	m/s
	y-velocity	0.0	m/s
	z-velocity	0.0	m/s
	q	1.224745	m/s
	L	0.005950135	m
	H_2	0.0	Mass Fraction
	H	0.0	
	O	0.0	
	O_2	0.2265	
	H_2O	0.0	
	H_2O_2	0.0	
	HO_2	0.0	
	OH	0.0	
Box 6	xmin	0.755	m
	xmax	1.25	m
	ymin	-0.12	m
	ymax	0.0875	m
	zmin	0.0	m
	zmax	0.0	m
	Pressure	101325	Pa
	Temperature	298	K
	x-velocity	0.0	m/s
	y-velocity	0.0	m/s

	z-velocity	0.0	m/s
	q	0.001224745	m/s
	L	7.036989	m
	H_2	0.0	Mass Fraction
	H	0.0	
	O	0.0	
	O_2	0.2265	
	H_2O	0.0	
	H_2O_2	0.0	
	HO_2	0.0	
	OH	0.0	

Time Integration	
Is this a restart:	No
Simulation Strategy:	Transient
Integration Type:	Implicit
Number of global time steps for this run:	1000
Max. cumulative # of global time steps:	0
Turn on dual time-stepping:	Yes
Stop run at a given global time value:	No
Implicit scheme type:	Point-Implicit
Global time step based on Courant #:	No
Spatially varying local time step:	Yes
At restart, use Courant # for local time step	Values Below

from:	
Courant # for local time step ramped from:	1 to 100
Local Courant # ramped from global step number:	1 to 100
Local Max. Courant # adjustment factor:	0.95
Terminate run if adjusted local Courant # is <:	1.00E-04
Global time step size:	1.00E-05 s
Max. # of internal (local) iter. per global step:	50
Global step internal iter. Termination criterion:	0.1
Order of global time stepping:	2nd
Extrapolate using old dq/dt (1st iteration):	No
Local iteration convergence acceler.:	Multigrid (old)
Turn on temporal-smoothing:	Yes
Smoothing factor:	0.75
Turn on time-step spatial-smoothing:	Yes
Number of smoothing passes:	4
Maximum time-step growth factor:	1.5

APPENDIX D: CFD++ DETONATION SIMULATION SETTINGS

A. DETONATION SIMULATION SETTINGS FOR 45 DEGREE INJECTION ANGLE

45 Degree Injection Angle			
Mesh Size	1104504		
Boundary Conditions			
Inlet	Multi-species Adiabatic Wall		
Outlet	Simple Back Pressure		
	Pressure	101325	Pa
Injinlet1, Injinlet2, and Injinlet3	Pressure Temperature and Normal Velocity Inlfow		
	Pressure	167558	Pa
	Temperature	450	K
	Normal Velocity	50	m/s
	q	0.6123724	m/s
	L	0.01736194	M
	H_2	0.0	Mass Fraction
	H	0.0	
	O	0.0	
	O_2	0.2265	
	H_2O	0.0	
	H_2O_2	0.0	
	HO_2	0.0	
	OH	0.0	

Symmetry	Multi-species Adiabatic Wall		
Walls	Multi-species Adiabatic Wall		
Initial Conditions			
Box 1	xmin	-0.00005	m
	xmax	0.0125	m
	ymin	-0.00005	m
	ymax	0.0875	m
	zmin	0.0	m
	zmax	0.0	m
	Pressure	303975	Pa
	Temperature	450	K
	x-velocity	100	m/s
	y-velocity	0.0	m/s
	z-velocity	0.0	m/s
	q	1.224745	m/s
	L	0.006482519	m
	H_2	0.02833164	Mass Fraction
	H	0.0	
	O	0.0	
	O_2	0.2265	
	H_2O	0.0	
	H_2O_2	0.0	
	HO_2	0.0	

	OH	0.0	
Box 2	xmin	0.0125	m
	xmax	0.61	m
	ymin	-0.00005	m
	ymax	0.0875	m
	zmin	0.0	m
	zmax	0.0	m
	Pressure	303975	Pa
	Temperature	450	K
	x-velocity	100	m/s
	y-velocity	0.0	m/s
	z-velocity	0.0	m/s
	q	1.224745	m/s
	L	0.004785153	m
	H_2	0.0	Mass Fraction
	H	0.0	
	O	0.0	
	O_2	0.2265	
	H_2O	0.0	
	H_2O_2	0.0	
	HO_2	0.0	
	OH	0.0	
Box 3	xmin	0.7	m

	xmax	0.755	m
	ymin	-0.015	m
	ymax	0.012	m
	zmin	0.0	m
	zmax	0.0	m
	Pressure	167558	Pa
	Temperature	450	K
	x-velocity	50	m/s
	y-velocity	0.0	m/s
	z-velocity	0.0	m/s
	q	0.6123724	m/s
	L	0.01736194	m
	H_2	0.0	Mass Fraction
	H	0.0	
	O	0.0	
	O_2	0.2265	
	H_2O	0.0	
	H_2O_2	0.0	
	HO_2	0.0	
	OH	0.0	
Box 4	xmin	0.61	m
	xmax	0.7	m
	ymin	-0.00005	m

	ymax	0.0875	m
	zmin	0.0	m
	zmax	0.0	m
	Pressure	303975	Pa
	Temperature	450	K
	x-velocity	100	m/s
	y-velocity	0.0	m/s
	z-velocity	0.0	m/s
	q	1.224745	m/s
	L	0.004785153	m
	H_2	0.0	Mass Fraction
	H	0.0	
	O	0.0	
	O_2	0.2265	
	H_2O	0.0	
	H_2O_2	0.0	
	HO_2	0.0	
	OH	0.0	
Box 5	xmin	0.7	m
	xmax	0.755	m
	ymin	0.012	m
	ymax	0.0875	m
	zmin	0.0	m

	zmax	0.0	m
	Pressure	200000	Pa
	Temperature	450	K
	x-velocity	100	m/s
	y-velocity	0.0	m/s
	z-velocity	0.0	m/s
	q	1.224745	m/s
	L	0.005950135	m
	H_2	0.0	Mass Fraction
	H	0.0	
	O	0.0	
	O_2	0.2265	
	H_2O	0.0	
	H_2O_2	0.0	
	HO_2	0.0	
	OH	0.0	
Box 6	xmin	0.755	m
	xmax	1.25	m
	ymin	-0.12	m
	ymax	0.0875	m
	zmin	0.0	m
	zmax	0.0	m
	Pressure	101325	Pa

	Temperature	298	K
	x-velocity	0.0	m/s
	y-velocity	0.0	m/s
	z-velocity	0.0	m/s
	q	0.001224745	m/s
	L	7.036989	m
	H_2	0.0	Mass Fraction
	H	0.0	
	O	0.0	
	O_2	0.2265	
	H_2O	0.0	
	H_2O_2	0.0	
	HO_2	0.0	
	OH	0.0	

Time Integration	
Is this a restart:	Yes
Simulation Strategy:	Transient
Integration Type:	Implicit
Number of global time steps for this run:	6000
Max. cumulative # of global time steps:	0
Turn on dual time-stepping:	Yes
Stop run at a given global time value:	No
Implicit scheme type:	Point-Implicit

Global time step based on Courant #:	No
Spatially varying local time step:	Yes
At restart, use Courant # for local time step from:	Values Below
Courant # for local time step ramped from:	10 to 10
Local Courant # ramped from global step number:	0 to 1
Local Max. Courant # adjustment factor:	0.95
Terminate run if adjusted local Courant # is <:	1.00E-04
Global time step size:	1.00E-06 s
Max. # of internal (local) iter. per global step:	20
Global step internal iter. Termination criterion:	0.1
Order of global time stepping:	2nd
Extrapolate using old dq/dt (1st iteration):	No
Local iteration convergence acceler.:	Multigrid (new)
Turn on temporal-smoothing:	Yes
Smoothing factor:	0.75
Turn on time-step spatial-smoothing:	No
Solution File Modification By Box	
Copy cdepsout.bin to cdepsin.bin before tool runs:	No

Copy cdepsout.bin to cdepsin.bin after tool runs:	No
xmin	-0.00005
xmax	0.0125
ymin	-0.00005
ymax	0.0875
zmin	0.0
zmax	0.0
Number of variables for this box:	15
Variable 1:	19286400
Variable 2:	3018.12
Variable 3:	882.2
Variable 4:	0.0
Variable 5:	0.0
Variable 6:	1.224745
Variable 7:	0.001871
Variable 8:	0.0022348
Variable 9:	0.00016446
Variable 10:	0.00088936
Variable 11:	0.0079392
Variable 12:	0.22568
Variable 13:	0.0
Variable 14:	0.0

Variable 15:	0.011434

B. DETONATION SIMULATION SETTINGS FOR 30 DEGREE INJECTION ANGLE

30 Degree Injection Angle			
Mesh Size	1142195		
Boundary Conditions			
Inlet	Multi-species Adiabatic Wall		
Outlet	Simple Back Pressure		
	Pressure	101325	Pa
Injinlet1, Injinlet2, and Injinlet3	Pressure Temperature and Normal Velocity Inflow		
	Pressure	167558	Pa
	Temperature	450	K
	Normal Velocity	50	m/s
	q	0.6123724	m/s
	L	0.01736194	M
	H_2	0.0	Mass Fraction
	H	0.0	
	O	0.0	
	O_2	0.2265	
	H_2O	0.0	
	H_2O_2	0.0	
	HO_2	0.0	

	OH	0.0	
Symmetry	Multi-species Adiabatic Wall		
Walls	Multi-species Adiabatic Wall		
Initial Conditions			
Box 1	xmin	-0.00005	m
	xmax	0.0125	m
	ymin	-0.00005	m
	ymax	0.0875	m
	zmin	0.0	m
	zmax	0.0	m
	Pressure	303975	Pa
	Temperature	450	K
	x-velocity	100	m/s
	y-velocity	0.0	m/s
	z-velocity	0.0	m/s
	q	1.224745	m/s
	L	0.006482519	m
	H_2	0.02833164	Mass Fraction
	H	0.0	
	O	0.0	
	O_2	0.2265	
	H_2O	0.0	
	H_2O_2	0.0	

	HO_2	0.0	
	OH	0.0	
Box 2	xmin	0.0125	m
	xmax	0.61	m
	ymin	-0.00005	m
	ymax	0.0875	m
	zmin	0.0	m
	zmax	0.0	m
	Pressure	303975	Pa
	Temperature	450	K
	x-velocity	100	m/s
	y-velocity	0.0	m/s
	z-velocity	0.0	m/s
	q	1.224745	m/s
	L	0.004785153	m
	H_2	0.0	Mass Fraction
	H	0.0	
	O	0.0	
	O_2	0.2265	
	H_2O	0.0	
	H_2O_2	0.0	
	HO_2	0.0	
	OH	0.0	

Box 3	xmin	0.695	m
	xmax	0.755	m
	ymin	-0.015	m
	ymax	0.02	m
	zmin	0.0	m
	zmax	0.0	m
	Pressure	167558	Pa
	Temperature	450	K
	x-velocity	50	m/s
	y-velocity	0.0	m/s
	z-velocity	0.0	m/s
	q	0.6123724	m/s
	L	0.01736194	m
	H_2	0.0	Mass Fraction
	H	0.0	
	O	0.0	
	O_2	0.2265	
	H_2O	0.0	
	H_2O_2	0.0	
	HO_2	0.0	
	OH	0.0	
Box 4	xmin	0.61	m
	xmax	0.695	m

	ymin	-0.00005	m
	ymax	0.0875	m
	zmin	0.0	m
	zmax	0.0	m
	Pressure	303975	Pa
	Temperature	450	K
	x-velocity	100	m/s
	y-velocity	0.0	m/s
	z-velocity	0.0	m/s
	q	1.224745	m/s
	L	0.004785153	m
	H_2	0.0	Mass Fraction
	H	0.0	
	O	0.0	
	O_2	0.2265	
	H_2O	0.0	
	H_2O_2	0.0	
	HO_2	0.0	
	OH	0.0	
Box 5	xmin	0.695	m
	xmax	0.755	m
	ymin	0.02	m
	ymax	0.0875	m

	zmin	0.0	m
	zmax	0.0	m
	Pressure	200000	Pa
	Temperature	450	K
	x-velocity	100	m/s
	y-velocity	0.0	m/s
	z-velocity	0.0	m/s
	q	1.224745	m/s
	L	0.005950135	m
	H_2	0.0	Mass Fraction
	H	0.0	
	O	0.0	
	O_2	0.2265	
	H_2O	0.0	
	H_2O_2	0.0	
	HO_2	0.0	
	OH	0.0	
Box 6	xmin	0.755	m
	xmax	1.25	m
	ymin	-0.12	m
	ymax	0.0875	m
	zmin	0.0	m
	zmax	0.0	m

	Pressure	101325	Pa
	Temperature	298	K
	x-velocity	0.0	m/s
	y-velocity	0.0	m/s
	z-velocity	0.0	m/s
	q	0.001224745	m/s
	L	7.036989	m
	H_2	0.0	Mass Fraction
	H	0.0	
	O	0.0	
	O_2	0.2265	
	H_2O	0.0	
	H_2O_2	0.0	
	HO_2	0.0	
	OH	0.0	

Time Integration	
Is this a restart:	Yes
Simulation Strategy:	Transient
Integration Type:	Implicit
Number of global time steps for this run:	6000
Max. cumulative # of global time steps:	0
Turn on dual time-stepping:	Yes
Stop run at a given global time value:	No

Implicit scheme type:	Point-Implicit
Global time step based on Courant #:	No
Spatially varying local time step:	Yes
At restart, use Courant # for local time step from:	Values Below
Courant # for local time step ramped from:	10 to 10
Local Courant # ramped from global step number:	0 to 1
Local Max. Courant # adjustment factor:	0.95
Terminate run if adjusted local Courant # is <:	1.00E-04
Global time step size:	1.00E-06 s
Max. # of internal (local) iter. per global step:	20
Global step internal iter. Termination criterion:	0.1
Order of global time stepping:	2nd
Extrapolate using old dq/dt (1st iteration):	No
Local iteration convergence acceler.:	Multigrid (new)
Turn on temporal-smoothing:	Yes
Smoothing factor:	0.75
Turn on time-step spatial-smoothing:	No
Solution File Modification By Box	
Copy cdepsout.bin to cdepsin.bin before	No

tool runs:	
Copy cdepsout.bin to cdepsin.bin after tool runs:	No
xmin	-0.00005
xmax	0.0125
ymin	-0.00005
ymax	0.0875
zmin	0.0
zmax	0.0
Number of variables for this box:	15
Variable 1:	19286400
Variable 2:	3018.12
Variable 3:	882.2
Variable 4:	0.0
Variable 5:	0.0
Variable 6:	1.224745
Variable 7:	0.001871
Variable 8:	0.0022348
Variable 9:	0.00016446
Variable 10:	0.00088936
Variable 11:	0.0079392
Variable 12:	0.22568
Variable 13:	0.0

Variable 14:	0.0
Variable 15:	0.011434

C. DETONATION SIMULATION SETTINGS FOR 60 DEGREE INJECTION ANGLE

60 Degree Injection Angle			
Mesh Size	1096640		
Boundary Conditions			
Inlet	Multi-species Adiabatic Wall		
Outlet	Simple Back Pressure		
	Pressure	101325	Pa
Injinlet1, Injinlet2, and Injinlet3	Pressure Temperature and Normal Velocity Inflow		
	Pressure	167558	Pa
	Temperature	450	K
	Normal Velocity	50	m/s
	q	0.6123724	m/s
	L	0.01736194	M
	H_2	0.0	Mass Fraction
	H	0.0	
	O	0.0	
	O_2	0.2265	
	H_2O	0.0	
	H_2O_2	0.0	

	HO_2	0.0	
	OH	0.0	
Symmetry	Multi-species Adiabatic Wall		
Walls	Multi-species Adiabatic Wall		
Initial Conditions			
Box 1	xmin	-0.00005	m
	xmax	0.0125	m
	ymin	-0.00005	m
	ymax	0.0875	m
	zmin	0.0	m
	zmax	0.0	m
	Pressure	303975	Pa
	Temperature	450	K
	x-velocity	100	m/s
	y-velocity	0.0	m/s
	z-velocity	0.0	m/s
	q	1.224745	m/s
	L	0.006482519	m
	H_2	0.02833164	Mass Fraction
	H	0.0	
	O	0.0	
	O_2	0.2265	
	H_2O	0.0	

	H_2O_2	0.0	
	HO_2	0.0	
	OH	0.0	
Box 2	xmin	0.0125	m
	xmax	0.61	m
	ymin	-0.00005	m
	ymax	0.0875	m
	zmin	0.0	m
	zmax	0.0	m
	Pressure	303975	Pa
	Temperature	450	K
	x-velocity	100	m/s
	y-velocity	0.0	m/s
	z-velocity	0.0	m/s
	q	1.224745	m/s
	L	0.004785153	m
	H_2	0.0	Mass Fraction
	H	0.0	
	O	0.0	
	O_2	0.2265	
	H_2O	0.0	
	H_2O_2	0.0	
	HO_2	0.0	

	OH	0.0	
Box 3	xmin	0.7	m
	xmax	0.755	m
	ymin	-0.02	m
	ymax	0.012	m
	zmin	0.0	m
	zmax	0.0	m
	Pressure	167558	Pa
	Temperature	450	K
	x-velocity	50	m/s
	y-velocity	0.0	m/s
	z-velocity	0.0	m/s
	q	0.6123724	m/s
	L	0.01736194	m
	H_2	0.0	Mass Fraction
	H	0.0	
	O	0.0	
	O_2	0.2265	
	H_2O	0.0	
	H_2O_2	0.0	
	HO_2	0.0	
	OH	0.0	
Box 4	xmin	0.61	m

	xmax	0.7	m
	ymin	-0.00005	m
	ymax	0.0875	m
	zmin	0.0	m
	zmax	0.0	m
	Pressure	303975	Pa
	Temperature	450	K
	x-velocity	100	m/s
	y-velocity	0.0	m/s
	z-velocity	0.0	m/s
	q	1.224745	m/s
	L	0.004785153	m
	H_2	0.0	Mass Fraction
	H	0.0	
	O	0.0	
	O_2	0.2265	
	H_2O	0.0	
	H_2O_2	0.0	
	HO_2	0.0	
	OH	0.0	
Box 5	xmin	0.7	m
	xmax	0.755	m
	ymin	0.012	m

	ymax	0.0875	m
	zmin	0.0	m
	zmax	0.0	m
	Pressure	200000	Pa
	Temperature	450	K
	x-velocity	100	m/s
	y-velocity	0.0	m/s
	z-velocity	0.0	m/s
	q	1.224745	m/s
	L	0.005950135	m
	H_2	0.0	Mass Fraction
	H	0.0	
	O	0.0	
	O_2	0.2265	
	H_2O	0.0	
	H_2O_2	0.0	
	HO_2	0.0	
	OH	0.0	
Box 6	xmin	0.755	m
	xmax	1.25	m
	ymin	-0.12	m
	ymax	0.0875	m
	zmin	0.0	m

	zmax	0.0	m
	Pressure	101325	Pa
	Temperature	298	K
	x-velocity	0.0	m/s
	y-velocity	0.0	m/s
	z-velocity	0.0	m/s
	q	0.001224745	m/s
	L	7.036989	m
	H_2	0.0	Mass Fraction
	H	0.0	
	O	0.0	
	O_2	0.2265	
	H_2O	0.0	
	H_2O_2	0.0	
	HO_2	0.0	
	OH	0.0	
Time Integration			
Is this a restart:		Yes	
Simulation Strategy:		Transient	
Integration Type:		Implicit	
Number of global time steps for this run:		6000	
Max. cumulative # of global time steps:		0	
Turn on dual time-stepping:		Yes	

Stop run at a given global time value:	No
Implicit scheme type:	Point-Implicit
Global time step based on Courant #:	No
Spatially varying local time step:	Yes
At restart, use Courant # for local time step from:	Values Below
Courant # for local time step ramped from:	10 to 10
Local Courant # ramped from global step number:	0 to 1
Local Max. Courant # adjustment factor:	0.95
Terminate run if adjusted local Courant # is <:	1.00E-04
Global time step size:	1.00E-06 s
Max. # of internal (local) iter. per global step:	20
Global step internal iter. Termination criterion:	0.1
Order of global time stepping:	2nd
Extrapolate using old dq/dt (1st iteration):	No
Local iteration convergence acceler.:	Multigrid (new)
Turn on temporal-smoothing:	Yes
Smoothing factor:	0.75
Turn on time-step spatial-smoothing:	No
Solution File Modification By Box	

Copy cdepsout.bin to cdepsin.bin before tool runs:	No
Copy cdepsout.bin to cdepsin.bin after tool runs:	No
xmin	-0.00005
xmax	0.0125
ymin	-0.00005
ymax	0.0875
zmin	0.0
zmax	0.0
Number of variables for this box:	15
Variable 1:	19286400
Variable 2:	3018.12
Variable 3:	882.2
Variable 4:	0.0
Variable 5:	0.0
Variable 6:	1.224745
Variable 7:	0.001871
Variable 8:	0.0022348
Variable 9:	0.00016446
Variable 10:	0.00088936
Variable 11:	0.0079392
Variable 12:	0.22568

Variable 13:	0.0
Variable 14:	0.0
Variable 15:	0.011434

APPENDIX E: CFD++ DETONATION SIMULATION RESULTING PLOTS

A. 30 DEGREE INJECTION ANGLE WITH BASELINE INJECTION MASS FLOW RATE

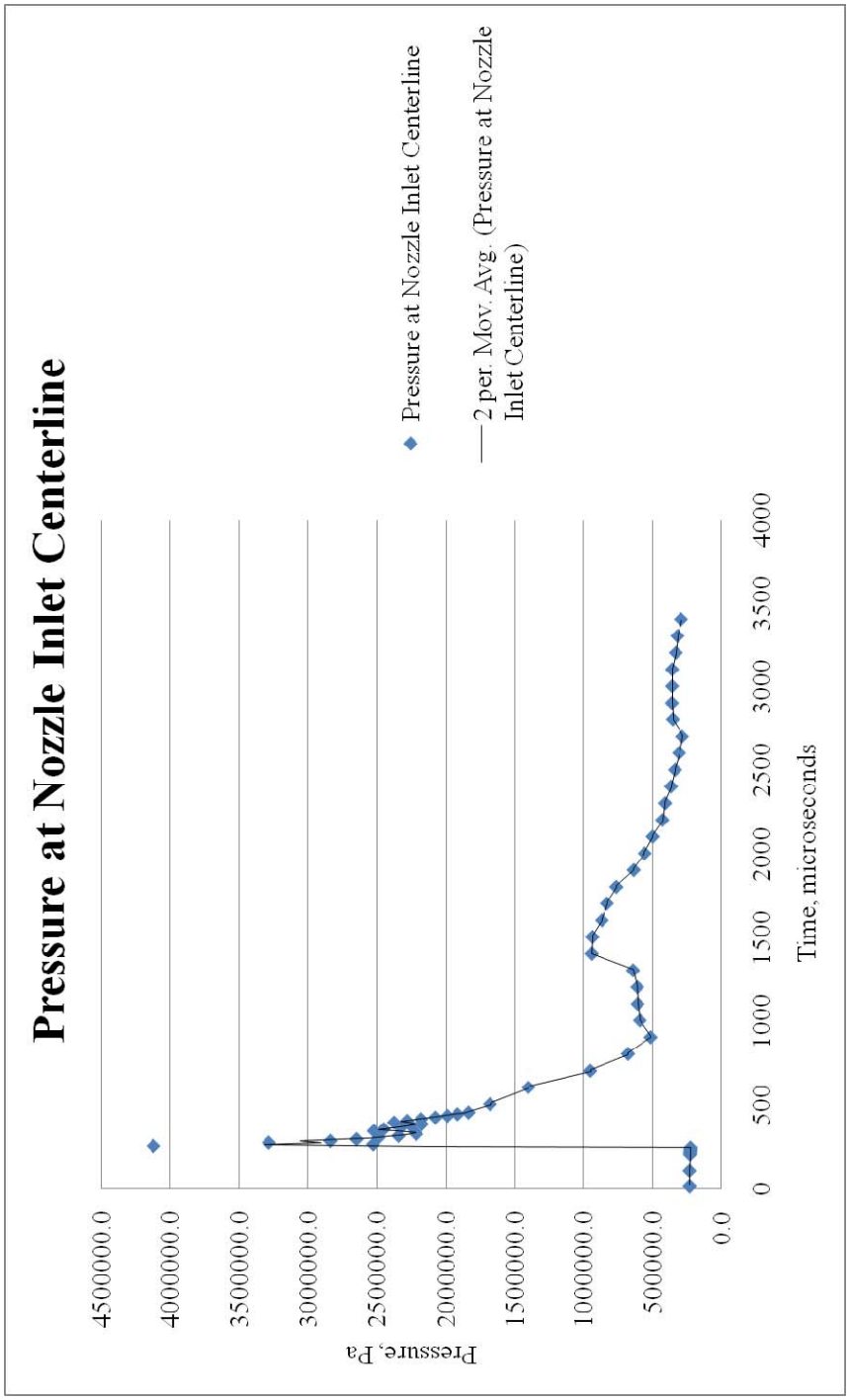

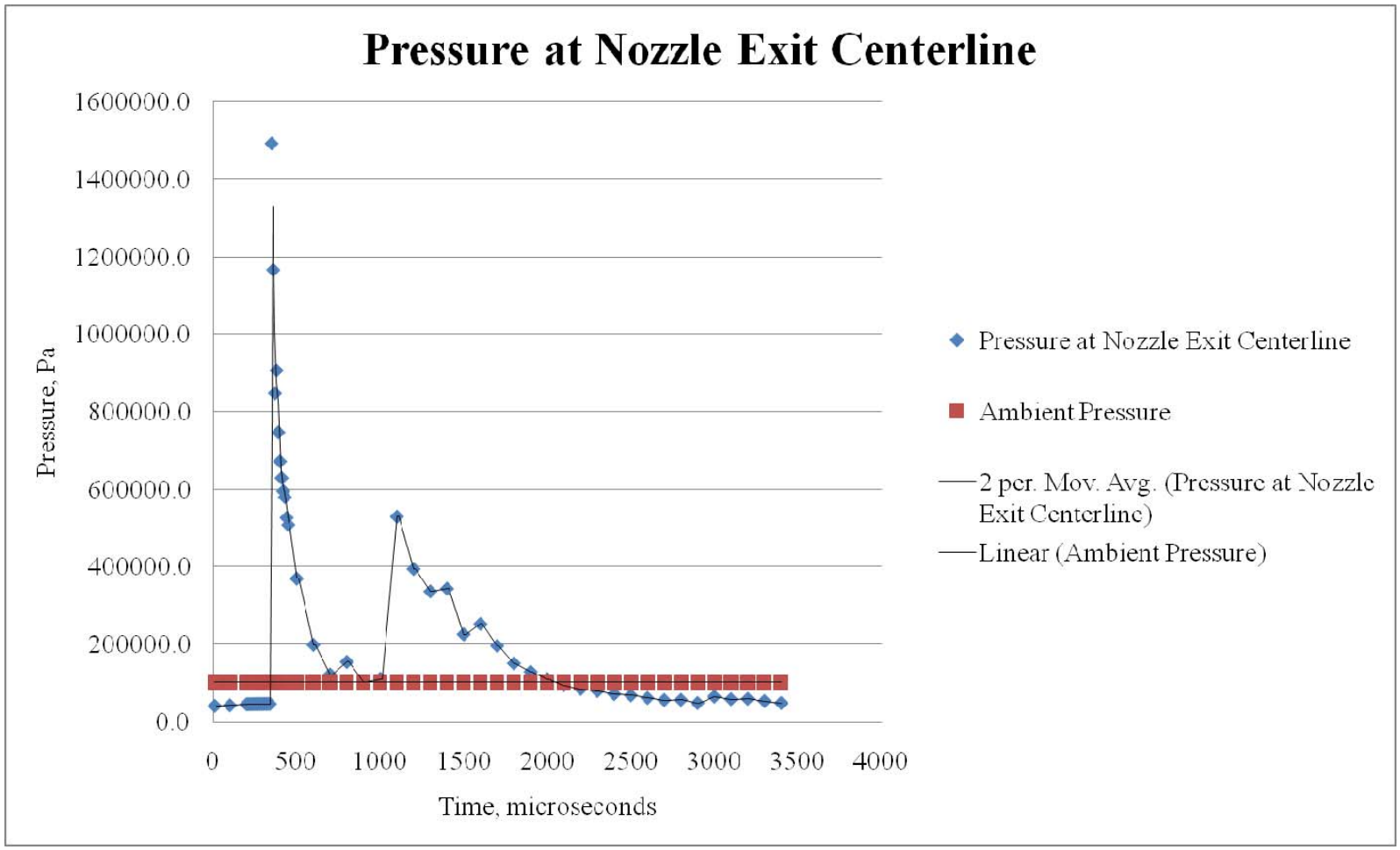
Pressure at Nozzle Exit Centerline
1600000.0
1400000.0
1200000.0
1000000.0
800000.0
600000.0
400000.0
200000.0
0.0
Pressure, Pa
0
500
1000
1500
2000
2500
3000
3500
4000
Time, microseconds
Pressure at Nozzle Exit Centerline
Ambient Pressure
2 per. Mov. Avg. (Pressure at Nozzle Exit Centerline)
Linear (Ambient Pressure)

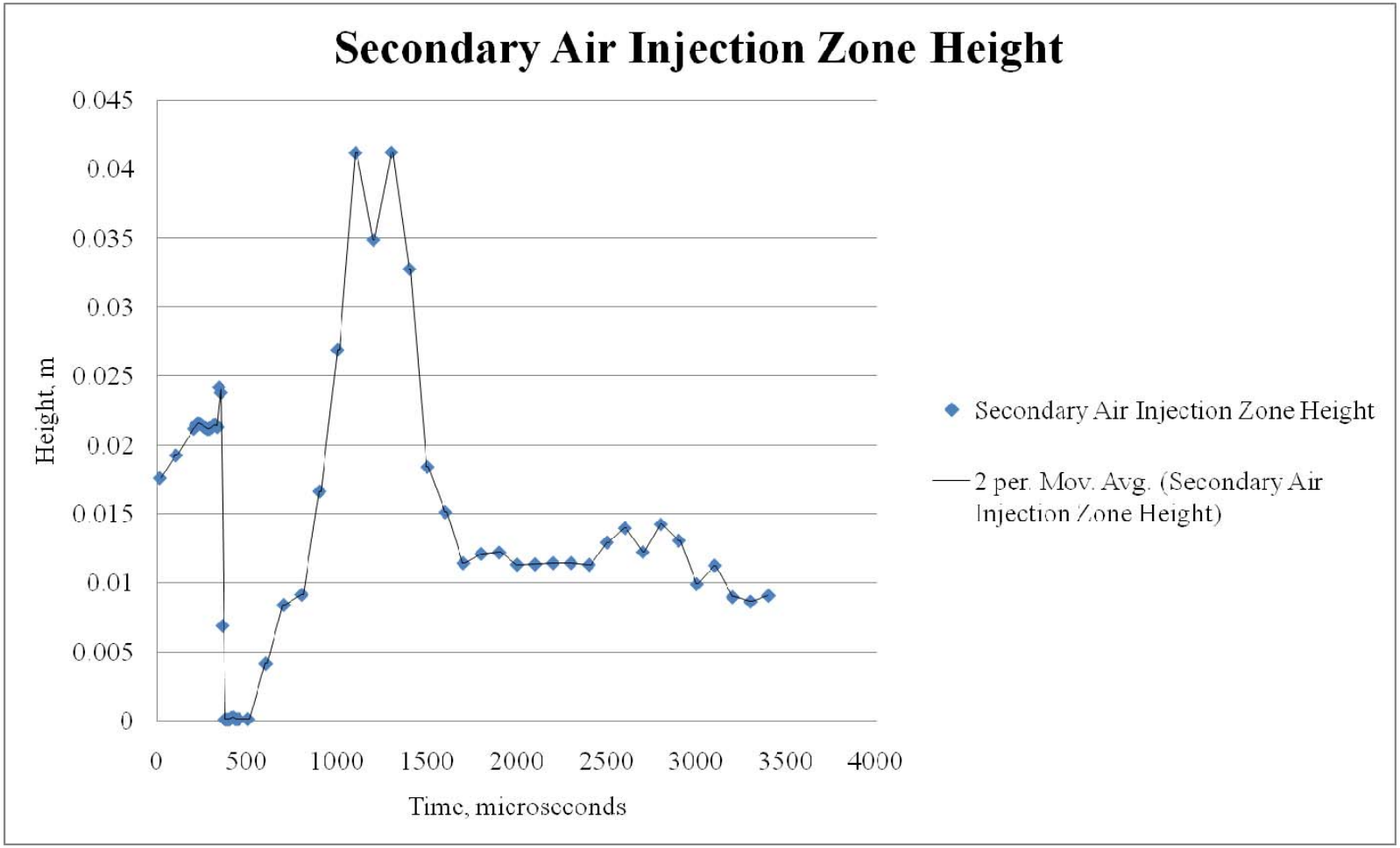
Secondary Air Injection Zone Height
0.045
0.04
0.035
0.03
0.025
0.02
0.015
0.01
0.005
0
Height, m
0
500
1000
1500
2000
2500
3000
3500
4000
Time, microseconds
Secondary Air Injection Zone Height
2 per. Mov. Avg. (Secondary Air Injection Zone Height)

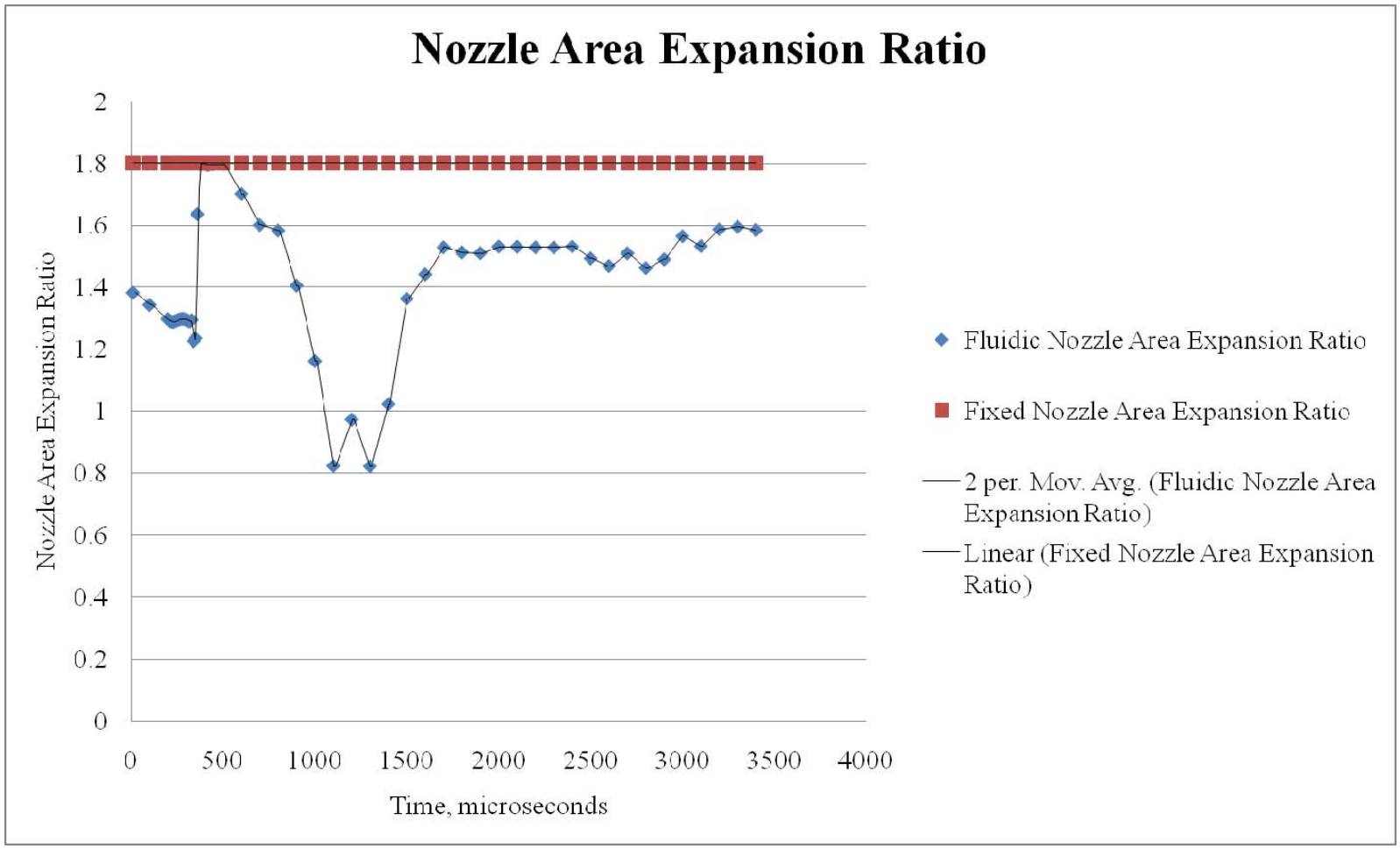
Nozzle Area Expansion Ratio
Nozzle Area Expansion Ratio
2
1.8
1.6
1.4
1.2
1
0.8
0.6
0.4
0.2
0
0
500
1000
1500
2000
2500
3000
3500
4000
Time, microseconds
Fluidic Nozzle Area Expansion Ratio
Fixed Nozzle Area Expansion Ratio
2 per. Mov. Avg. (Fluidic Nozzle Area Expansion Ratio)
Linear (Fixed Nozzle Area Expansion Ratio)

B. 45 DEGREE INJECTION ANGLE WITH BASELINE INJECTION MASS FLOW RATE

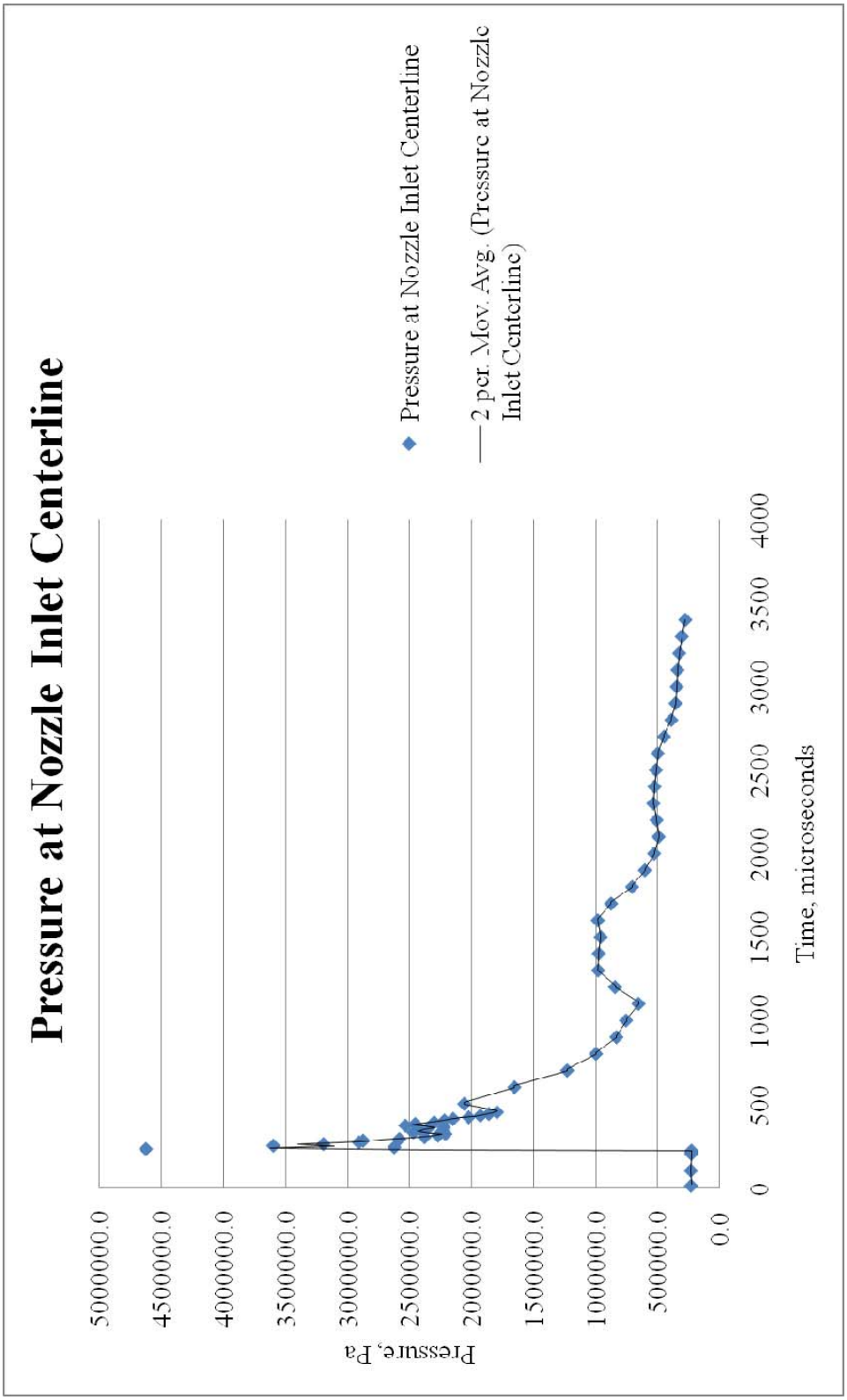

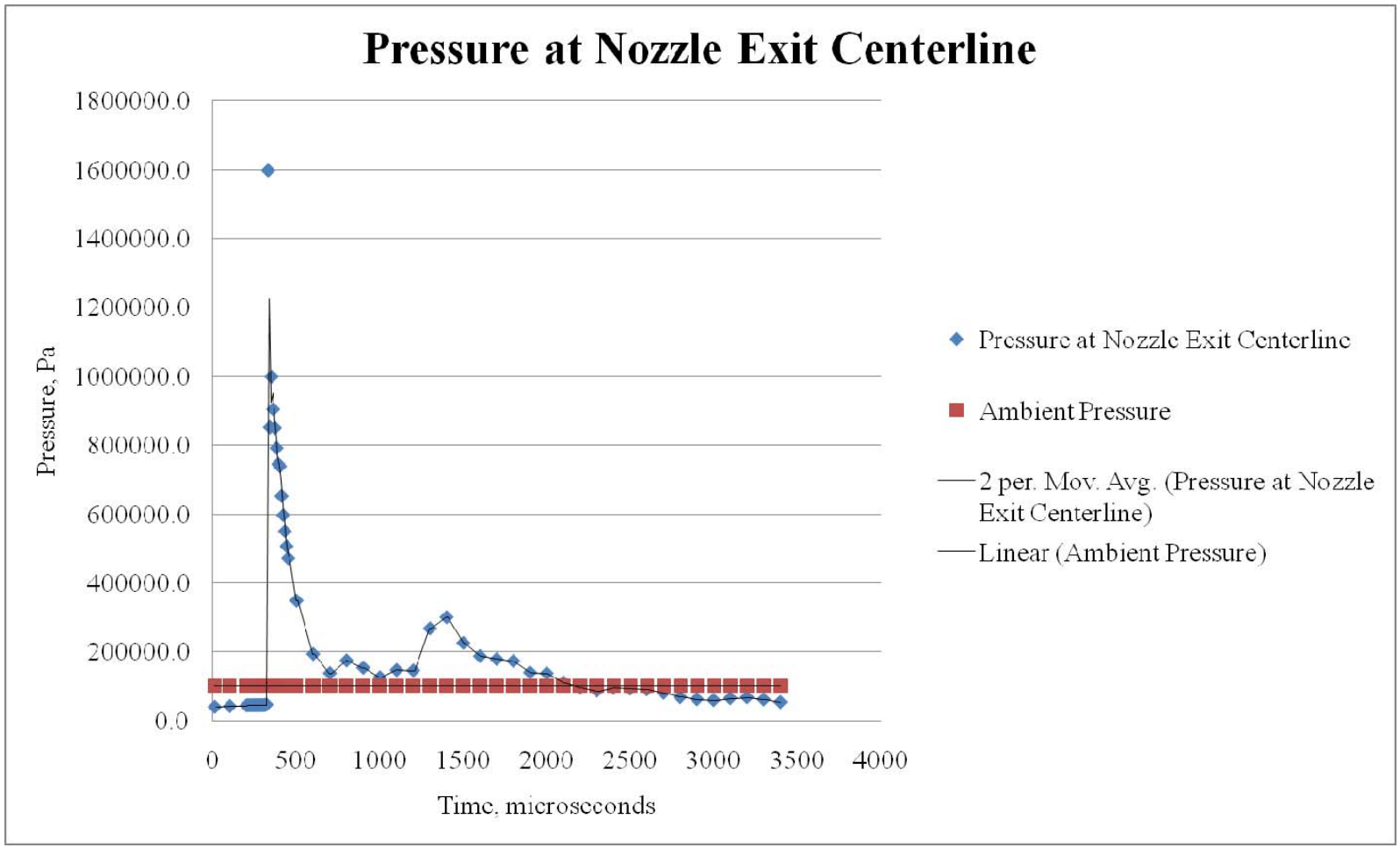
Pressure at Nozzle Exit Centerline
1800000.0
1600000.0
1400000.0
1200000.0
1000000.0
800000.0
600000.0
400000.0
200000.0
0.0
Pressure, Pa
0
500
1000
1500
2000
2500
3000
3500
4000
Time, microseconds
Pressure at Nozzle Exit Centerline
Ambient Pressure
2 per. Mov. Avg. (Pressure at Nozzle Exit Centerline)
Linear (Ambient Pressure)

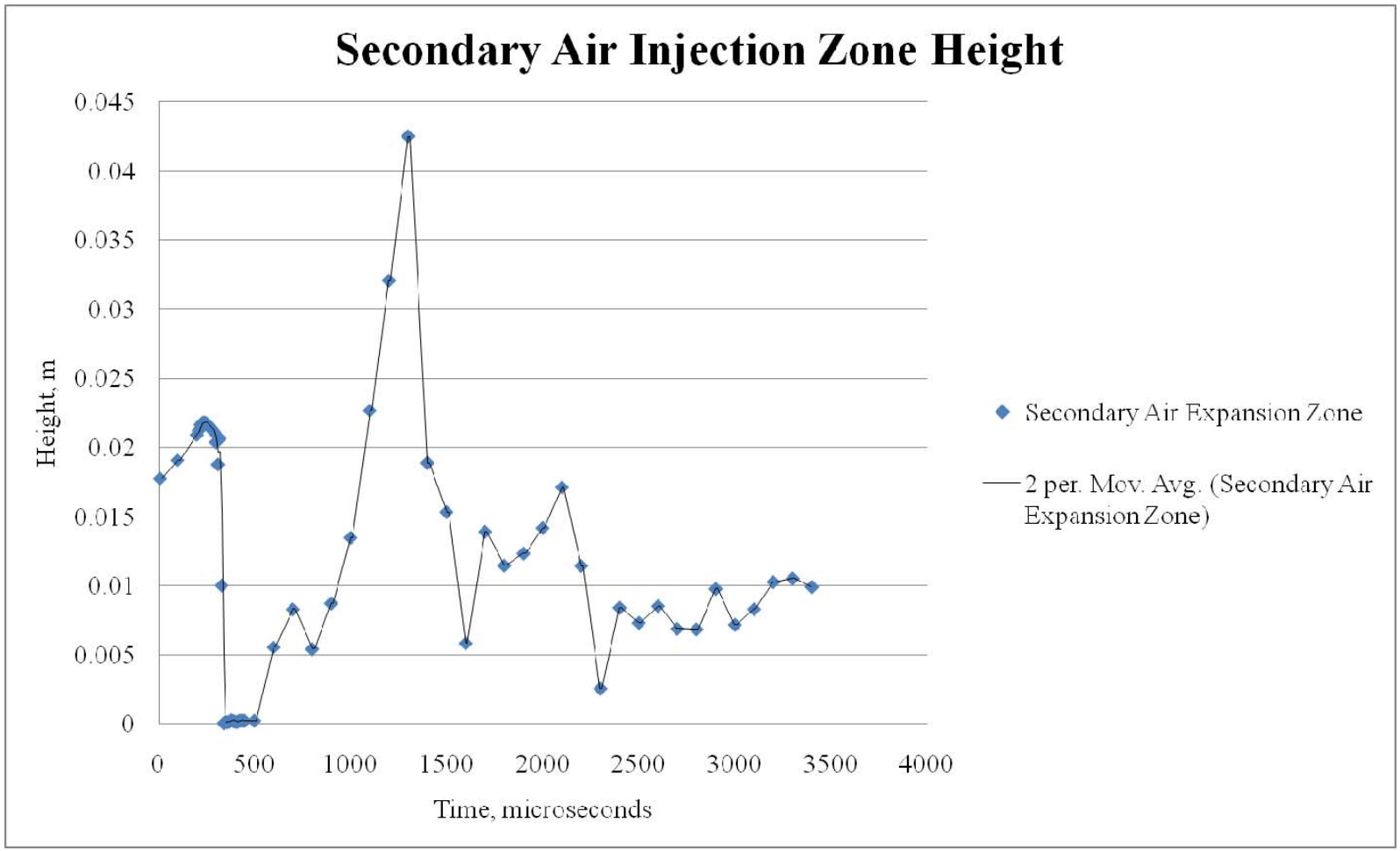
Secondary Air Injection Zone Height
0.045
0.04
0.035
0.03
0.025
0.02
0.015
0.01
0.005
0
Height, m
0
500
1000
1500
2000
2500
3000
3500
4000
Time, microseconds
Secondary Air Expansion Zone
2 per. Mov. Avg. (Secondary Air Expansion Zone)

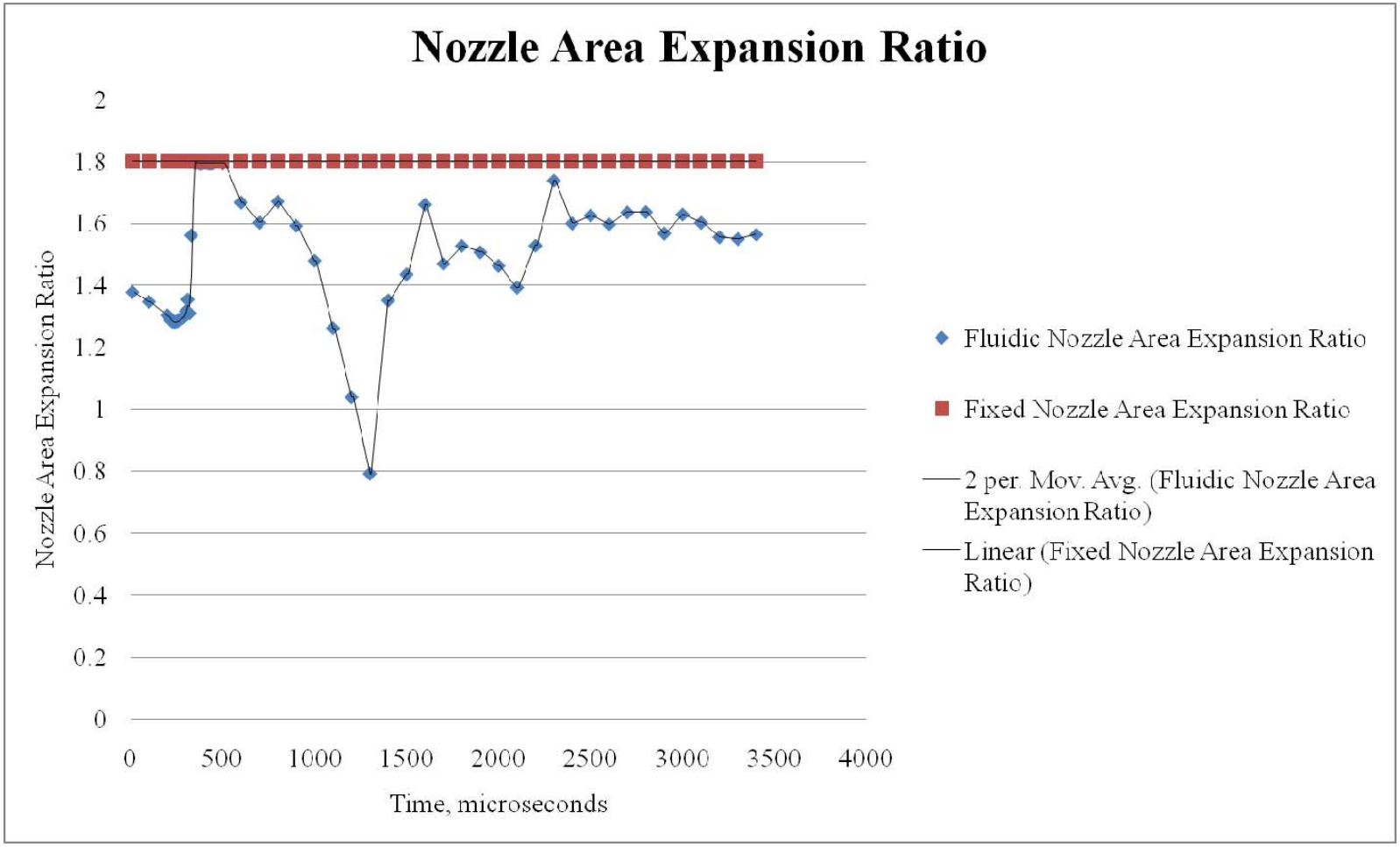
Nozzle Area Expansion Ratio
Nozzle Area Expansion Ratio
2
1.8
1.6
1.4
1.2
1
0.8
0.6
0.4
0.2
0
0
500
1000
1500
2000
2500
3000
3500
4000
Time, microseconds
Fluidic Nozzle Area Expansion Ratio
Fixed Nozzle Area Expansion Ratio
2 per. Mov. Avg. (Fluidic Nozzle Area Expansion Ratio)
Linear (Fixed Nozzle Area Expansion Ratio)

C. 60 DEGREE INJECTION ANGLE WITH BASELINE INJECTION MASS FLOW RATE

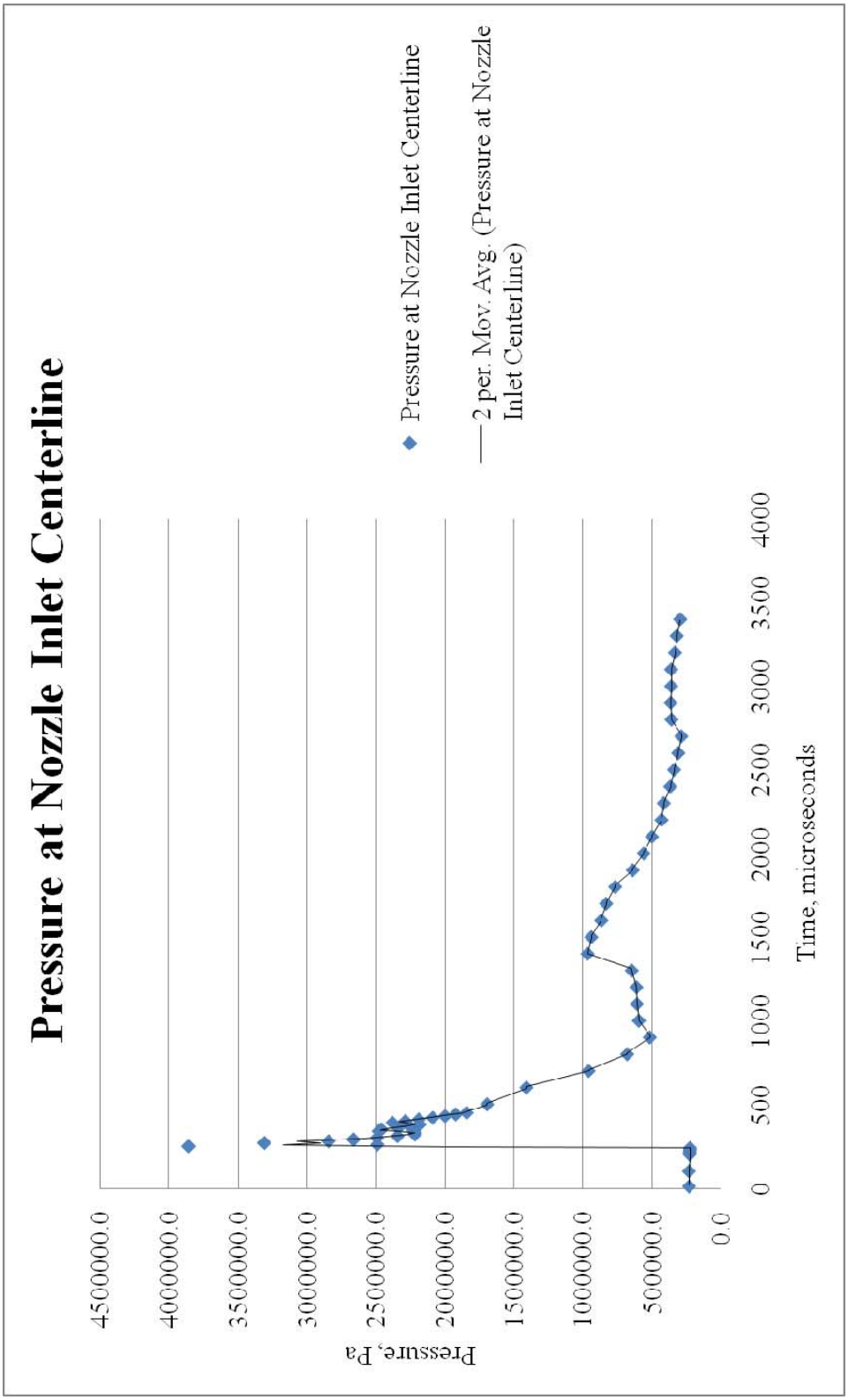

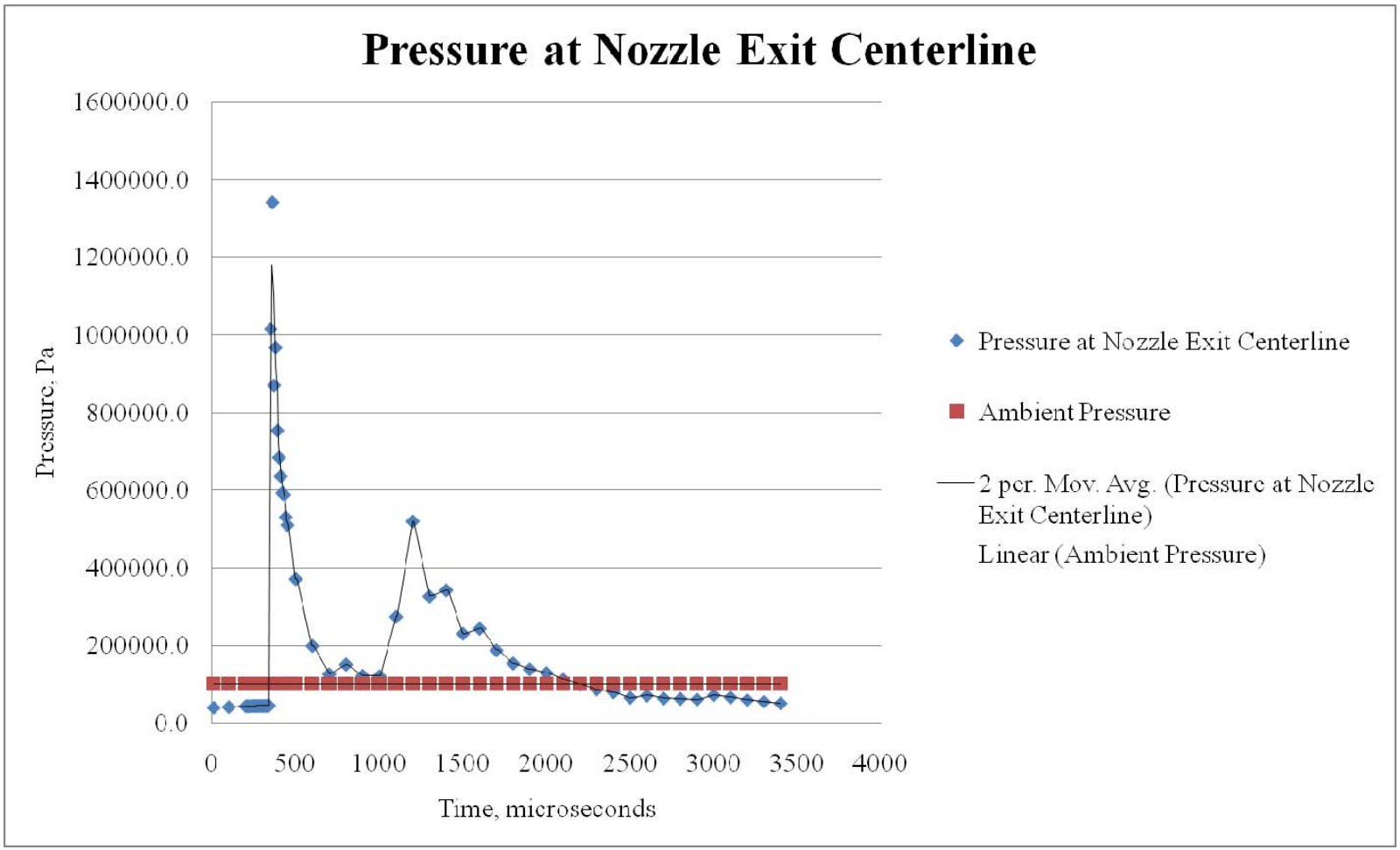
Pressure at Nozzle Exit Centerline
1600000.0
1400000.0
1200000.0
1000000.0
800000.0
600000.0
400000.0
200000.0
0.0
Pressure, Pa
0
500
1000
1500
2000
2500
3000
3500
4000
Time, microseconds
Pressure at Nozzle Exit Centerline
Ambient Pressure
2 per. Mov. Avg. (Pressure at Nozzle Exit Centerline)
Linear (Ambient Pressure)

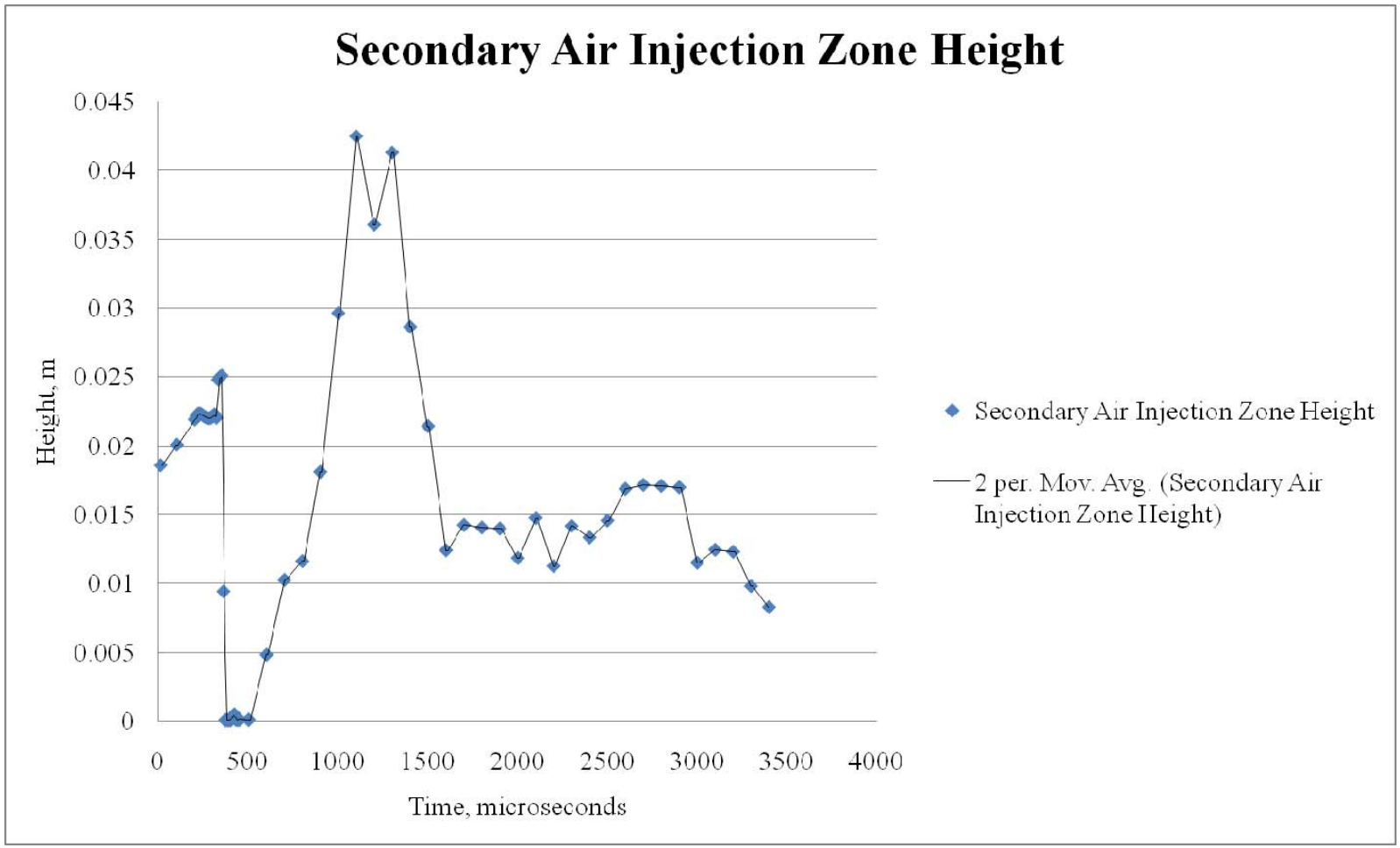
Secondary Air Injection Zone Height
0.045
0.04
0.035
0.03
0.025
0.02
0.015
0.01
0.005
0
Height, m
0
500
1000
1500
2000
2500
3000
3500
4000
Time, microseconds
Secondary Air Injection Zone Height
2 per. Mov. Avg. (Secondary Air Injection Zone HIeight)

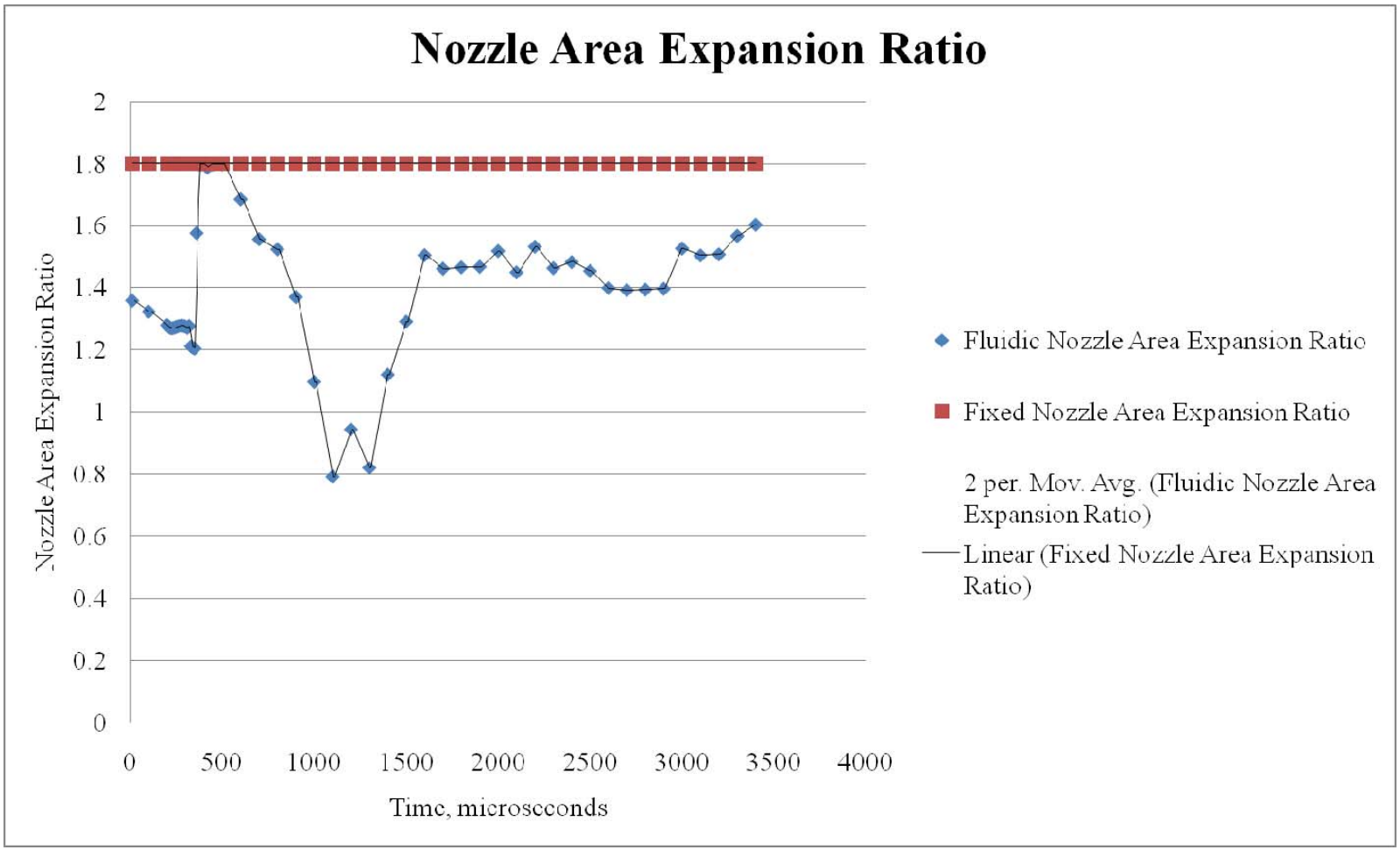
Nozzle Area Expansion Ratio
Nozzle Area Expansion Ratio
2
1.8
1.6
1.4
1.2
1
0.8
0.6
0.4
0.2
0
0
500
1000
1500
2000
2500
3000
3500
4000
Time, microseconds
Fluidic Nozzle Area Expansion Ratio
Fixed Nozzle Area Expansion Ratio
2 per. Mov. Avg. (Fluidic Nozzle Area Expansion Ratio)
Linear (Fixed Nozzle Area Expansion Ratio)

APPENDIX F: CFD++ DETONATION SIMULATION RESULTING PLOT DATA

A. 30 DEGREE INJECTION ANGLE WITH BASELINE INJECTION MASS FLOW RATE

30 Degree 100% Injection Mass Flow Rate					
Nozzle Exit Ymin (m)				0.0104645	
Time Step	Time	P1 (Pa)	P2 (Pa)	Secondary Air Injection Zone Y (m)	Secondary Air Injection Zone Height (m)
10	0.00001	228284.0	39932.5	0.0280782	0.0176137
100	0.00010	229958.0	41247.5	0.0297266	0.0192621
200	0.00020	225869.0	44098.4	0.0316531	0.0211886
210	0.00021	225042.0	44312.4	0.0319162	0.0214517
220	0.00022	224178.0	44397.1	0.0320439	0.0215794
230	0.00023	223299.0	44476.5	0.0320381	0.0215736
240	0.00024	222413.0	44567.8	0.0319580	0.0214935
250	0.00025	4119760.0	44650.1	0.0318358	0.0213713
260	0.00026	2528080.0	44712.1	0.0317394	0.0212749
270	0.00027	3283400.0	44781.5	0.0316471	0.0211826
280	0.00028	2838000.0	44848.9	0.0316288	0.0211643
290	0.00029	2646610.0	44918.8	0.0316471	0.0211826
300	0.00030	2485810.0	44983.4	0.0317661	0.0213016
310	0.00031	2341840.0	45028.1	0.0319309	0.0214664
320	0.00032	2214450.0	45085.7	0.0319674	0.0215029
330	0.00033	2218710.0	45121.6	0.0317703	0.0213058
340	0.00034	2523280.0	45191.5	0.0346604	0.0241959
350	0.00035	2448240.0	1492980.0	0.0342636	0.0237991
360	0.00036	2327220.0	1166380.0	0.0173846	0.0069201
370	0.00037	2253200.0	847781.0	0.0105840	0.0001195
380	0.00038	2173250.0	906774.0	0.0105893	0.0001248
390	0.00039	2373040.0	746794.0	0.0105787	0.0001142
400	0.00040	2281280.0	671838.0	0.0105870	0.0001225
410	0.00041	2177240.0	628910.0	0.0107143	0.0002498
420	0.00042	2075060.0	595107.0	0.0107352	0.0002707
430	0.00043	1989770.0	579101.0	0.0106092	0.0001447
440	0.00044	1913380.0	525869.0	0.0106026	0.0001381

450	0.00045	1833480.0	507561.0	0.0106153	0.0001508
500	0.00050	1678540.0	368722.0	0.0106071	0.0001426
600	0.00060	1400890.0	197770.0	0.0146316	0.0041671
700	0.00070	952473.0	120906.0	0.0188861	0.0084216
800	0.00080	678555.0	153606.0	0.0196318	0.0091673
900	0.00090	511850.0	102134.0	0.0271154	0.0166509
1000	0.00100	591818.0	110113.0	0.0373673	0.0269028
1100	0.00110	608517.0	528866.0	0.0516262	0.0411617
1200	0.00120	610672.0	393499.0	0.0453222	0.0348577
1300	0.00130	642461.0	335729.0	0.0516789	0.0412144
1400	0.00140	941420.0	342841.0	0.0432203	0.0327558
1500	0.00150	936537.0	224717.0	0.0288838	0.0184193
1600	0.00160	867063.0	251662.0	0.0255951	0.0151306
1700	0.00170	831062.0	195095.0	0.0219072	0.0114427
1800	0.00180	762077.0	149919.0	0.0225863	0.0121218
1900	0.00190	637380.0	128223.0	0.0226894	0.0122249
2000	0.00200	556263.0	109771.0	0.0218036	0.0113391
2100	0.00210	497317.0	93468.5	0.0218297	0.0113652
2200	0.00220	427593.0	83604.9	0.0219137	0.0114492
2300	0.00230	408188.0	78417.1	0.0219219	0.0114574
2400	0.00240	366313.0	70774.2	0.0217968	0.0113323
2500	0.00250	336030.0	67256.4	0.0234132	0.0129487
2600	0.00260	306329.0	60310.8	0.0244517	0.0139872
2700	0.00270	285090.0	55003.4	0.0227177	0.0122532
2800	0.00280	352816.0	55392.2	0.0247214	0.0142569
2900	0.00290	360012.0	47350.7	0.0235481	0.0130836
3000	0.00300	358419.0	63994.2	0.0203972	0.0099327
3100	0.00310	358490.0	57123.5	0.0217393	0.0112748
3200	0.00320	330511.0	58079.9	0.0194548	0.0089903
3400	0.00340	293017.0	47391.3	0.0195639	0.0090994

B. 45 DEGREE INJECTION ANGLE WITH BASELINE INJECTION MASS FLOW RATE

45 Degree 100% Injection Mass Flow Rate					
Nozzle Exit Ymin (m)				0.0104645	
Time Step	Time	P1 (Pa)	P2 (Pa)	Secondary Air Injection Zone Y (m)	Secondary Air Injection Zone Height (m)
10	0.00001	229384.0	39159.8	0.0282248	0.0177603
100	0.00010	230651.0	41314.2	0.0295395	0.019075
200	0.00020	227105.0	43345.4	0.0313819	0.0209174
210	0.00021	226352.0	43726.9	0.0317086	0.0212441
220	0.00022	225544.0	43716.2	0.0320982	0.0216337
230	0.00023	4627520.0	43699.8	0.0322600	0.0217955
240	0.00024	2623950.0	43795.7	0.0322936	0.0218291
250	0.00025	3600050.0	43806.1	0.0322200	0.0217555
260	0.00026	3195670.0	43793.6	0.0321002	0.0216357
270	0.00027	2909300.0	43825.7	0.0319271	0.0214626
280	0.00028	2875060.0	43888.2	0.0317588	0.0212943
290	0.00029	2582460.0	43993.5	0.0315944	0.0211299
300	0.00030	2379560.0	44112.0	0.0308431	0.0203786
310	0.00031	2271330.0	44239.8	0.0292383	0.0187738
320	0.00032	2210490.0	46260.0	0.0311149	0.0206504
330	0.00033	2469850.0	1598130.0	0.0204981	0.0100336
340	0.00034	2407900.0	851577.0	0.0105217	5.72E-05
350	0.00035	2356700.0	998521.0	0.0106264	0.0001619
360	0.00036	2225340.0	903986.0	0.0105946	0.0001301
370	0.00037	2534200.0	849778.0	0.0106295	0.000165
380	0.00038	2454890.0	791717.0	0.0107471	0.0002826
390	0.00039	2301630.0	745097.0	0.0106844	0.0002199
400	0.00040	2218960.0	738159.0	0.0106269	0.0001624
410	0.00041	2149030.0	652052.0	0.0106164	0.0001519
420	0.00042	2023730.0	596306.0	0.0106984	0.0002339
430	0.00043	1929070.0	549655.0	0.0107091	0.0002446
440	0.00044	1860200.0	505927.0	0.0107145	0.00025
450	0.00045	1794750.0	471441.0	0.0107038	0.0002393
500	0.00050	2058470.0	347959.0	0.0107091	0.0002446
600	0.00060	1653760.0	192923.0	0.0160185	0.005554
700	0.00070	1228350.0	137042.0	0.0187616	0.0082971

800	0.00080	996327.0	174094.0	0.0158883	0.0054238
900	0.00090	831167.0	152970.0	0.0191938	0.0087293
1000	0.00100	753861.0	125210.0	0.0239456	0.0134811
1100	0.00110	653434.0	146333.0	0.0331319	0.0226674
1200	0.00120	842744.0	144898.0	0.0425291	0.0320646
1300	0.00130	978997.0	267267.0	0.0529629	0.0424984
1400	0.00140	974356.0	299674.0	0.0293511	0.0188866
1500	0.00150	957981.0	225265.0	0.0258011	0.0153366
1600	0.00160	982080.0	186741.0	0.0163120	0.0058475
1700	0.00170	874459.0	178034.0	0.0243744	0.0139099
1800	0.00180	704976.0	172504.0	0.0219250	0.0114605
1900	0.00190	601922.0	139334.0	0.0227986	0.0123341
2000	0.00200	527313.0	136830.0	0.0246466	0.0141821
2100	0.00210	491411.0	110229.0	0.0275919	0.0171274
2200	0.00220	508554.0	95065.3	0.0219070	0.0114425
2300	0.00230	533766.0	86347.5	0.0130340	0.0025695
2400	0.00240	524307.0	94855.7	0.0188805	0.008416
2500	0.00250	513536.0	92330.8	0.0177888	0.0073243
2600	0.00260	498858.0	89921.3	0.0190016	0.0085371
2700	0.00270	447106.0	80268.3	0.0173592	0.0068947
2800	0.00280	388457.0	67837.6	0.0173172	0.0068527
2900	0.00290	354288.0	61840.9	0.0202461	0.0097816
3000	0.00300	345059.0	59324.2	0.0176498	0.0071853
3100	0.00310	338599.0	64755.6	0.0187747	0.0083102
3200	0.00320	324955.0	67356.2	0.0207419	0.0102774
3300	0.00330	304244.0	61065.5	0.0209980	0.0105335
3400	0.00340	275167.0	53265.1	0.0203880	0.0099235

C. 60 DEGREE INJECTION ANGLE WITH BASELINE INJECTION MASS FLOW RATE

60 Degree 100% Mass Flow					
Nozzle Exit Ymin (m)				0.0104645	
Time Step	Time	P1 (Pa)	P2 (Pa)	Secondary Air Injectio Zone Y (m)	Secondary Air Injection Zone Height (m)
10	0.00001	229438.0	40145.3	0.0290424	0.0185779
100	0.00010	230664.0	41721.7	0.0305404	0.0200759
200	0.00020	225970.0	43929.4	0.0323609	0.0218964
210	0.00021	225157.0	44018.4	0.0326323	0.0221678
220	0.00022	224323.0	44041.0	0.0328043	0.0223398
230	0.00023	223483.0	44138.5	0.0327970	0.0223325
240	0.00024	222653.0	44380.7	0.0327230	0.0222585
250	0.00025	3859770.0	44561.5	0.0326140	0.0221495
260	0.00026	2490710.0	44655.2	0.0325308	0.0220663
270	0.00027	3309950.0	44735.3	0.0324717	0.0220072
280	0.00028	2843430.0	44775.5	0.0324540	0.0219895
290	0.00029	2663610.0	44782.5	0.0324856	0.0220211
300	0.00030	2493480.0	44764.7	0.0325864	0.0221219
310	0.00031	2343750.0	44750.0	0.0327523	0.0222878
320	0.00032	2217700.0	44805.7	0.0324888	0.0220243
330	0.00033	2217090.0	45029.1	0.0352504	0.0247859
340	0.00034	2481440.0	45582.3	0.0354500	0.0249855
350	0.00035	2460940.0	1015520.0	0.0355589	0.0250944
360	0.00036	2338130.0	1341410.0	0.0198945	0.00943
370	0.00037	2257830.0	870184.0	0.0105533	0.0000888
380	0.00038	2181910.0	967558.0	0.0105623	9.78E-05
390	0.00039	2380700.0	753986.0	0.0105509	8.64E-05
400	0.00040	2286750.0	684325.0	0.0105555	9.1E-05
410	0.00041	2189750.0	636340.0	0.0108100	0.0003455
420	0.00042	2089410.0	593657.0	0.0109729	0.0005084
430	0.00043	1999470.0	588758.0	0.0105766	0.0001121
440	0.00044	1921850.0	531001.0	0.0105775	0.000113
450	0.00045	1842570.0	510421.0	0.0105856	0.0001211
500	0.00050	1693240.0	371466.0	0.0105773	0.0001128
600	0.00060	1409510.0	199233.0	0.0152964	0.0048319
700	0.00070	958566.0	126457.0	0.0207249	0.0102604

800	0.00080	677801.0	151442.0	0.0220872	0.0116227
900	0.00090	514674.0	122805.0	0.0285635	0.018099
1000	0.00100	593617.0	121446.0	0.0400881	0.0296236
1100	0.00110	607310.0	274558.0	0.0529285	0.042464
1200	0.00120	610845.0	520051.0	0.0465136	0.0360491
1300	0.00130	644972.0	326857.0	0.0517444	0.0412799
1400	0.00140	965748.0	342607.0	0.0390885	0.028624
1500	0.00150	938481.0	230863.0	0.0318885	0.021424
1600	0.00160	865749.0	243680.0	0.0228768	0.0124123
1700	0.00170	831162.0	188226.0	0.0247105	0.014246
1800	0.00180	765043.0	154093.0	0.0245294	0.0140649
1900	0.00190	638163.0	139015.0	0.0244543	0.0139898
2000	0.00200	558426.0	129650.0	0.0223199	0.0118554
2100	0.00210	499143.0	112839.0	0.0252221	0.0147576
2200	0.00220	429023.0	99814.5	0.0217279	0.0112634
2300	0.00230	413346.0	87319.6	0.0246460	0.0141815
2400	0.00240	365612.0	80160.9	0.0238097	0.0133452
2500	0.00250	338154.0	66068.6	0.0250324	0.0145679
2600	0.00260	307985.0	71673.1	0.0273390	0.0168745
2700	0.00270	285826.0	64020.4	0.0276237	0.0171592
2800	0.00280	357351.0	63135.5	0.0275566	0.0170921
2900	0.00290	362778.0	61372.0	0.0274489	0.0169844
3000	0.00300	358928.0	72325.5	0.0219718	0.0115073
3100	0.00310	359122.0	66699.1	0.0229163	0.0124518
3200	0.00320	331822.0	59925.7	0.0227679	0.0123034
3300	0.00330	319627.0	55851.5	0.0202768	0.0098123
3400	0.00340	293795.0	51376.5	0.0187541	0.0082896

APPENDIX G: STANDARD OPERATING PROCEDURE

Test Cell #1Standard Operating Procedures (S.O.P)
Combustor Start Up
(Modification Date 26 Feb 2010)

INITIAL PREPARATIONS

1. Notify all lab personnel of intention to make test cell 1 live.
2. Turn **ON** control console
3. Turn **ON** warning lights
4. Cell #1 EMERGENCY SHUTDOWN BUTTON (Control Room)- **VERIFY IN**
5. Notify the Golf Course (x2167) (Only Required during Detonation Experiments)
6. Open Test Cell Door
7. Igniter Control (Test Cell)-**VERIFY OFF** (Red Button Out)
8. PXI-1000B Rack (Test Cell)-**VERIFY ON**
9. Shop Air-**VERIFY > 100 PSI**
10. Shop Air Valve (Test Cell)-**VERIFY OPEN**
11. 115 VAC Control/Cell #1 Switch (Control Room)-**ON** (Only Required during Detonation Experiments or when Ethylene is Being Used)
12. 28VDC Power Supply/Cell #1 Switch (Control Room)-**ON** (Only Required during Detonation Experiments or when Ethylene is Being Used)
13. Open LABVIEW (Only Required during Detonation Experiments or when Ethylene is Being Used)

TESTING SET-UP

1. Kistler Amplifier Power-**ENSURE OFF**
2. Kistler Leads-**CONNECT** (Only Required during Detonation Experiments)
3. Exhaust Tube-**VERIFY PROPER POSTION**
4. Notify all personnel that gasses and TESCOM will be enabled.
5. Test Cell #2 and #3 Node 1 Air Isolation Valve (Test Cell #2)-**VERIFY CLOSED**

****NOTE: This valve maybe left open only if Test Cell #2 or #3 is configured for active testing****

6. Turn on Optical Sensor. (Only Required during Detonation Experiments)
7. TRANSDUCER and TESCOM Power Switch (Test Cell #2)-**ON**
8. Set **0 (Zero)** pressures on ER3000 (Control Room) for the following:
    a. **Node 3 (Ethylene)**
    b. **Node 1 (Main Air)**
    c. **Node 4 (Injection Air)**
9. Main HP Air Jamesbury Valve (Outside Test Cell)-**OPEN SLOWLY**

10. Power Strip (above PXI-1000B)-**VERIFY ON**
11. Igniter Control Light (Red LED upper left on CRYDOM in PX-1000B Rack)-**VERIFY OUT** (Only Required during Detonation Experiments)

****DANGER: IF RED LIGHT IS ENERGIZED, MUST CLEAR USING LABVIEW BEFORE CONTINUING TO PREVENT PREMATURE IGNITION****

12. Igniter Control (Test Cell)-**PUSH RED BUTTON IN** (Only Required during Detonation Experiments)
13. Igniter Control Startup Diagnostics-**OBSERVE COMPLETION OF DIAGNOSTICS** (Verify energy level setting reads 2.03 J) (Only Required during Detonation Experiments)
14. Injection Air Isolation Valves (2) (Located in Test Cell)-**OPEN SLOWLY**
15. Main HP Air Isolation Valves (2) (Located in Test Cell)-**OPEN SLOWLY**

****DANGER: OPEN VALVES SLOWLY TO PREVENT RAPID PRESSURIZTION OF DOWNSTREAM LINES****

16. Node 3 (Ethylene) Shop Air Valve (Above Bottle in Bottle Room)-**OPEN** (Only Required during Detonation Experiments or when Ethylene is Being Used)
17. Ethylene Bottle Isolation Valve (On Bottle)-**OPEN SLOWLY** (Only Required during Detonation Experiments or when Ethylene is Being Used)

**** VERIFY ADEQUATE ETHYLENE PRESSURE FOR TESTING ON DOWNSTREAM GAGE LOCATED IN BOTTLE ROOM****

LASER SET-UP

1. Laser Warning Lights-**TURN ON**
2. Remove All Covers from Mirrors
3. Water Supply to Laser (Located in Test Cell)-**OPEN**
4. Laser-**VERIFY SHUTTER IS CLOSED**
5. Laser Control Box-**VERIFY LASER POWER SETTING 10 WATTS**
6. Laser Control Box-**VERIFY LASER CURRENT SETTING 50 AMPS**
7. Laser Control Box-**VERIFY CONTROL SELECTOR SET TO CURRENT**
8. Laser Control Box-**VERIFY CURRENT CONTROL KNOB FULLY COUNTER-CLOCKWISE**
9. Laser Control Box-**LINE POWER BREAKER ON**
10. Laser Control Box-**VERIFY LINE (3) AND FUSE (3) LIGHTS ENERGIZE**
11. Laser Control Box-**KEY CONTROL ON**
12. Laser Control Box-**VERIFY COVERS, WATER TEMP, WATER FLOW, REQ TEMP, AND INTLK LIGHTS ENERGIZE**
13. Laser Control Box-**PRESS POWER ON**
14. Laser Control Box-**VERIFY POWER LIGHT ENERGIZES**
15. Laser Control Box-**WAIT FOR READY LIGHT TO ENERGIZE**

16. Don Laser Protective Goggles
17. Laser-**OPEN SHUTTER**
18. Laser Control Box-**PRESS LASER START**
19. Laser Control Box- **TURN CURRENT CONTROL KNOB FULLY CLOCKWISE**
20. Remove Laser Protective Goggles upon Leaving Test Cell

PRE-TESTING

1. Lightning RDT 2000 Camera-**VERIFY COMPUTER IN TEST CELL ON**
2. Start MIDAS Software from Control Room
3. Determine Desired Fuel and Air Pressures
4. Set Required Pressures on ER3000
    a. **Node 3 (Ethylene)** (Only Required during Detonation Experiments or when Ethylene is Being Used)
    b. **Node 1 (Main Air)**
    c. **Node 4 (Injection Air)**
5. Insert Tape into VCR
6. Switch Monitor to B (Test Cell #1)

TESTING

1. Clear All Test Cells and Verify with Head Count
2. Verify Golf Course is **CLEAR**
3. Flashing Red Lights and Siren-**ENERGIZE**
4. VCR-**RECORD**
5. In LABVIEW Enable Facility Button-**ON**
6. Test Cell #1 Emergency Shutdown Button-**TURN CLOCKWISE** (Only Required during Detonation Experiments or when Ethylene is Being Used)
7. Camera-**RECORD**
8. Toggle Node 3 to **Desired Pressure** (Only Required during Detonation Experiments or when Ethylene is Being Used)
9. Toggle Node 4 to **Desired Pressure**
10. Toggle Node 1 to **Desired Pressure**
11. In LABVIEW Start Button-**CLICK TO START** (Only Required during Detonation Experiments or when Ethylene is Being Used)

WHEN TESTING COMPLETE

12. Set Node 1 Pressure to **0 (Zero)**
13. Set Node 4 Pressure to **0 (Zero)**
14. Set Node 3 Pressure to **0 (Zero)** (Only Required during Detonation Experiments or when Ethylene is Being Used)
15. Camera-**STOP RECORDING**

16. In LABVIEW Turn Off Button-**CLICK TO SECURE** (Only Required during Detonation Experiments or when Ethylene is Being Used)
17. In LABVIEW Enable Facility Button-**VERIFY OFF** (Only Required during Detonation Experiments or when Ethylene is Being Used)
18. Test Cell #1 Emergency Shutdown Button-**PUSH IN** (Only Required during Detonation Experiments or when Ethylene is Being Used)
19. Siren-**OFF**
20. VCR-**Stop/Pause**
21. Save Camera Image

****NOTE: If Further Testing is Required, re-perform steps 1-21 of the Testing Section****

SECURING LASER

1. Don Laser Protective Goggles Prior to Entering Test Cell
2. Laser Control Box-**TURN CURRENT CONTROL KNOB FULLY COUNTER-CLOCKWISE**
3. Laser Control Box-**PRESS POWER OFF**
4. Laser-**CLOSE SHUTTER**
5. Remove Laser Protective Goggles
6. Laser Control Box-**KEY CONTROL OFF**
7. Laser Control Box-**LINE POWER BREAKER OFF**
8. Water Supply to Laser (Located in Test Cell)-**CLOSE**
9. Install Covers on All Mirrors
10. Laser Warning Lights-**TURN OFF**

POST-TESTING

1. Verify pressures on ER3000 are set to 0 (Zero) on the following:
    a. **Node 3 (Ethylene)**
    b. **Node 1 (Main Air)**
    c. **Node 4 (Injection Air)**
2. Main HP Air Isolation Valves (2) (Located in Test Cell)-**CLOSE**
3. Injection Air Isolation Valves (2) (Located in Test Cell)-**CLOSE**
4. Main HP Air Jamesbury Valve (Outside Test Cell)-**CLOSE**
5. Ethylene Bottle Isolation Valve (On Bottle)-**CLOSE** (Only Required during Detonation Experiments or when Ethylene is Being Used)
6. Igniter Control (Test Cell)-**PUSH RED BUTTON OUT** (Only Required during Detonation Experiments)
7. TRANSDUCER and TESCOM Power Switch (Test Cell #2)-**OFF**
8. Close Test Cell Door
9. Node 3 (Ethylene) Shop Air Valve (Above Bottle in Bottle Room)-**CLOSE** (Only Required during Detonation Experiments or when Ethylene is Being Used)

10. Secure Bottle Room (Only Required during Detonation Experiments or when Ethylene is Being Used)
11. Exit out of MIDAS
12. EXIT out of LABVIEW (Only Required during Detonation Experiments or when Ethylene is Being Used)
14. 28VDC Power Supply/Cell #1 Switch (Control Room)-**OFF** (Only Required during Detonation Experiments or when Ethylene is Being Used)
15. 115 VAC Control/Cell #1 Switch (Control Room)-**OFF** (Only Required during Detonation Experiments or when Ethylene is Being Used)

THIS PAGE INTENTIONALLY LEFT BLANK

LIST OF REFERENCES

[1] R. Friedman, "American Rocket Society," Vol. 24, p. 349, November 1953.

[2] Patrick D. Hutcheson, *Design, Modeling and Performance of a Split path JP-10/Air Pulse Detonation Engine*, M.S. Thesis, Naval Postgraduate School, Monterey, CA, December 2006.

[3] Daniel M. Juillet, et al., *ME 4704 Missile Design Final Report 2009*, Thesis, Naval Postgraduate School, CA, December 2009.

[4] Ethan A. Barbour, *Modeling and Laser-based Sensing of Pulsed Detonation Engines*, Doctoral Dissertation, Stanford University, Palo Alto, CA, April 2009.

[5] George P. Sutton, *Rocket Propulsion Elements: An Introduction to the Engineering of Rockets*, 6th ed., John Wiley & Sons, Inc., 1992.

[6] G. S, Settles, *Schlieren and Shadowgraph Techniques: Visualizing Phenomena in Transparent Media*, Springer-Verlag Berlin Heidelberg New York, 2001.

[7] Charles B. Myers IV, *Initiation Mechanisms of Low-loss Swept-Ramp Obstacles for Deflagration to Detonation Transition in Pulse Detonation Combustors*, M.S. Thesis, Naval Postgraduate School, Monterey, CA, December 2009.

[8] Michael A. Fludovich Jr., *Investigation of Detonation Wave Diffraction Interaction with Reactive Transpiration*, M.S. Thesis, Naval Postgraduate School, Monterey CA, September 2002.

[9] Carlos A. Medina, *Evaluation of Straight and Swept Ramp Obstacles on Enhancing Deflagration to Detonation Transition in Pulse Detonation Engines*, M.S. Thesis, Naval Postgraduate School, Monterey, CA, December 2006.

[10] John A. Anderson, *Deflagration-to-Detonation Transition Enhancement Using Low-Loss Obstacle Fields*, M.S. Thesis, Naval Postgraduate School, Monterey, CA, December 2007.

[11] DRS Technologies, *DRS's Lightning RDT High-speed Digital Camera*, Tech Imaging: High-speed Imaging Experts, DRS Data & Imaging Systems, Inc., 06 March 2010, http://www.techimaging.com/Web%20Suff/specsheets/lightning.pdf.

[12] Michael J. Zehe, *Chemical Equilibrium with Applications*, Glenn Research Center, NASA, 20 January 2010, http://www.grc.nasa.gov/WWW/CEAWeb/ceaRequestForm.htm

[13] Neil C. Hawkes, *Characterization of Transient Plasma Ignition Flame Kernel Growth for Varying Inlet Conditions*, M.S. Thesis, Naval Postgraduate School, Monterey, CA, December 2009.

INITIAL DISTRIBUTION LIST

1. Defense Technical Information Center
   Ft. Belvoir, Virginia

2. Dudley Knox Library
   Naval Postgraduate School
   Monterey, California